Experimental study of passive scalar mixing in swirling jet flows

by

Ramis Örlü

September 2006
Technical Reports from
Royal Institute of Technology
KTH Mechanics
SE-100 44 Stockholm, Sweden

Akademisk avhandling som med tillstånd av Kungliga Tekniska Högskolan i Stockholm framlägges till offentlig granskning för avläggande av teknologie licentiatsexamen den 26 oktober 2006 kl 10.30 i Seminarierrummet S40, Teknikringen 8, Kungliga Tekniska Högskolan, Stockholm.

Universitetsservice US–AB, Stockholm 2006

Ramis Örlü 2006, **Experimental study of passive scalar mixing in swirling jet flows**

Linné Flow Centre
KTH Mechanics
SE–100 44 Stockholm, Sweden

Abstract

Despite its importance in various industrial applications there is still a lack of experimental studies on the dynamic and thermal field of swirling jets in the near-field region. The present study is an attempt to close this lack and provide new insights on the effect of rotation on the turbulent mixing of a *passive scalar*, on turbulence (joint) statistics as well as the turbulence structure.

Swirl is known to increase the spreading of free turbulent jets and hence to entrain more ambient fluid. Contrary to previous experiments, which leave traces of the swirl generating method especially in the near-field, the swirl was imparted by discharging a slightly heated air flow from an axially rotating and thermally insulated pipe (6 m long, diameter 60 mm). This gives well-defined axisymmetric streamwise and azimuthal velocity distributions as well as a well-defined temperature profile at the jet outlet. The experiments were performed at a *Reynolds* number of 24000 and a swirl number (ratio between the angular velocity of the pipe wall and the bulk velocity in the pipe) of 0.5.

By means of a specially designed combined X-wire and cold-wire probe it was possible to simultaneously acquire the instantaneous axial and azimuthal velocity components as well as the temperature and compensate the former against temperature variations. The comparison of the swirling and non-swirling cases clearly indicates a modification of the turbulence structure to that effect that the swirling jet spreads and mixes faster then its non-swirling counterpart. It is also shown that the streamwise velocity and temperature fluctuations are highly correlated and that the addition of swirl drastically increases the streamwise *passive scalar* flux in the near field.

Descriptors: Fluid mechanics, swirling jet, turbulence, passive scalar, mixing, hot-wire anemometry, cold-wire.

Part of this work have been presented and accepted for presentation at:

Programkonferens Energirelaterad Strömningsmekanik STEM,
30 November – 1 December 2004, *Piteå, Sweden*

6th World Conference on Experimental Heat Transfer, Fluid Mechanics, and Thermodynamics,
17 – 21 April 2005, *Matsushima, Miyagi, Japan*

6th Euromech Fluid Mechanics Conference,
26 – 30 June 2006, *Stockholm, Sweden*

59th Annual Meeting of the American Physical Society - Division of Fluid Dynamics,
19 – 21 November 2006, *Tampa Bay, Florida, USA*

Contents

CHAPTER 1

Introduction

I always wondered what my former supervisor found so fascinating about tea (or coffee) with milk (or cream), when we had our occasional coffee breaks and where he drew our attention to the milk traces in our cup.[1] Now, after a couple of years and a few *eureka* moments, the mystery might be solved.

If we slice a very small hole in a milk carton and squeeze it strongly, milk will be forced out of the opening under pressure and thus a *jet* will be formed. We can observe a regular, smooth, and hence *laminar* stream of milk near the opening, which then due to *hydrodynamic instabilities*, introduced at the orifice and the interface between the jet and the ambient air, will start to lose its regular shape. We have reached the *transition region* where the perturbations originating from the orifice as well as the interface most likely grow and develop into a stream of milk covering a wide range of *temporal* and *spatial scales*, characterised by high *diffusivity* and *dissipation* as well as *chaotic three-dimensional vorticity*. These are few characteristics of a *turbulent* flow in general. Riveted to the instability mechanism the jet will probably impinge on the table near to our cup forming a *free jet* near the orifice, an oblique *impinging jet* where it hits the surface of the table and an evolving *wall jet* along the table.

After a little while the milk carton is empty and instead we slide a highly viscous cream along the inner surface of our cup into the coffee. We clean the table and continue our conversation and later on we grab our cup and intend to move it towards our mouth, but then we stop. The surface of the cup is still too hot and furthermore the drop of cream has still its initial shape and drifts slowly on the surface of the coffee with which it is entirely unmixed. Intuitively we grab a spoon and stir the coffee (and most probably we impart a *swirling* motion by rotating the spoon along the inner surface of the cup), because experience (as a part of knowledge) has taught us that *molecular diffusivity* needs too much time (approximately a dozen of hours or days depending on the fat content of the cream) to create a well-mixed fluid composed of cream and coffee. Hence to our displeasure the coffee would become cold.

[1] Of course it depends on our perspective how we view and ponder about that what concerns the cup of coffee or on the amount of caffeine we have to consume in order to stimulate our nervous system as well as our imagination.

Lets rewind to the beginning and observe carefully what actually happened during the regular and slow stirring process of the coffee: The single droplet of milk starts to follow the rotating motion of the coffee and thereby elongates along the rotational direction and becomes thinner normal to it. At certain very thin positions within the droplet of cream we observe separation into smaller droplets and this continuous like a *cascade process* where the *large scale* droplet of the order of magnitude comparable to the size of the cup fractionates continuously into smaller and smaller droplets down to the order of magnitude comparable with the *viscous scale*. What we have accomplished is that an larger interface between the cream and the coffee has been formed, thus increasing the *mixing* of both fluids on a molecular basis.

Up to here we have only increased the *diffusive flux* in terms of an increased surface area. However if we stir the spoon faster (or stir the coffee with the inner surface normal to the rotational direction in order to increase the surface area of the stirring spoon) the fluid motion will resemble a much more irregular structure than observed for the slow and regular stirring process, and it seems as we have had increased the diffusivity of our fluid mixture. Nevertheless this is not the case, rather a new mechanism, *turbulent mixing*, has come into play. Finally we recognise that we have accomplished our goal, i.e. to prepare a well-mixed fluid mixture at a drinkable temperature, within seconds.

We have learned a lot just by analysing a daily procedure and there is still much more to gain just by continuing to think about a so familiar process. So for instance it occurs to us, that a continuous supply of energy is needed to overcome viscosity, which tries to slow down the rotation. And that a wide range of length scales are involved (just within our small cup) ranging from the size of the cup down to viscous scales. Most important we noticed that various opposing and cooperating processes are involved and that we, as engineers, have to find a specific solution for a special demand within certain geometrical and temporal restrictions. Combustion chambers for instance demand air and fuel to be well-mixed within the chamber in order to maximise the combustion efficiency and to minimise harmful emissions. Hence the objective is to burn all of the mixture as completely as possible, which is mostly done by imparting an azimuthal velocity component to the mixture in order to improve mixing and combustion.

At this point it seems appropriate to depict the importance of experiments: The exact equations governing the turbulent motion in our small cup are not solved up to this day and we are even not sure whether a set of solutions satisfying the initial and boundary conditions exist and whether they are unique[2].

[2]This problem is one of the seven 'Millennium problems' named by *The Clay Mathematics Institute of Cambridge, Massachusetts* and allocated with $1 million for the solution of the problem.

This has brought fluid dynamicists quite early to a statistical approach to turbulence. The possibility to involve computers to assist turbulence researchers[3] in terms of *direct numerical simulations* (DNS) of the governing equations has become a promising tool, however the bounds are clearly seen within our cup of coffee. If we just consider the number of grid points needed to simulate the flow physically realistic we have to divide the fluid in our cup in a three-dimensional mesh with more grid points than tractable by the best supercomputers if we are aiming for a solution before our cup of coffee is completely covered with mildew.

However if we consider only the large-scales of the flow and cut off the smallest scales (this would lead us to the less expensive *large-eddy simulation* (LES)), then on average, the gross motion can be captured satisfactory for engineering purposes. The more of the detailed structure we skip and instead model, the faster we will find a solution and at the same time the more our solution will lack on a physical basis. Nevertheless turbulence models (implemented in *computational fluid dynamics* (CFD)) serve a great deal for many industrial applications where DNS and experiments may cost too much time and hence money. But here we see that the last mentioned methods need validations with reality and recalling that the DNS (even though it simulates the governing equations without models) is restricted by computational limits, experiments are highly demanded.

This brief excursion introduced a part of the terminology we will frequently use during the next sections and furthermore it illustrated figuratively with what we are concerned. The aforementioned research field goes beyond the scope of the present work and here we will solely concentrate on the near-field region of a *fully developed turbulent jet*. More precisely we will mainly focus on *how* the *dynamic* and *thermal fields* are affected by the addition of swirl. Furthermore we will assume that the thermal field has a negligible effect on the dynamic field, which can be imagined as if the concentration of milk or cream in the coffee serves as a tracer.

As evident from figure 1.1 jets can be of many types (among others are *free*, *confined*, *compressible* and *chemically reacting* jets) and occur in numerous technical applications and natural phenomena. The water jet from our kitchen tap or a windscreen washer system as well as the hot air jet from a pressure cooker or an exhaust are just few examples of ordinary occurrences. Besides these household examples, jets occur under various circumstances in aircraft jets (as in the *F-15 Eagle* fighter in figure 1.1(c)), propulsion, combustion, drying and cooling/heating as well as ventilation technologies. Swirl is in many of these applications either facilitated to manipulate the flow field as it is done

[3]Some believe that they even compete with us experimentalist, however *Moorse' law* (CPU power doubles every 18–24 month) reassures us at least for more than a half century.

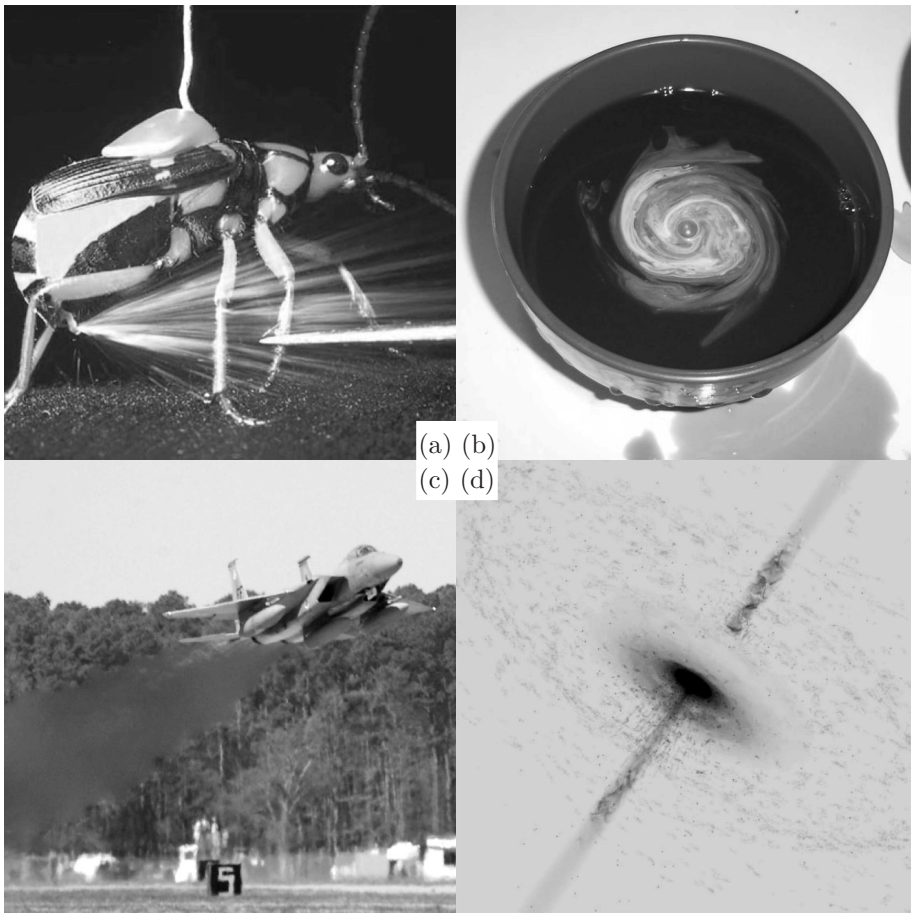

FIGURE 1.1. Ordinary and extraordinary occurrences of jets, stirring, mixing, impingement, and swirl as well as their combinations. (a) Bombardier beetle defending itself by squirting predators with a high-pressure jet of boiling liquid in a rapid-fire action. (b) Coffee with cream. (c) *F-15 Eagle* fighter during a steep takeoff. (d) Swirling radio jet originating from an accretion disk in an active galaxy. [(a) Courtesy of Thomas Eisner and Daniel Aneshansley, Cornell University. (c) Courtesy of Staff Sgt. Verlin Levi Collins, U.S. Air Force. (d) Courtesy of Wolfgang Steffen, Instituto de Astronomía, UNAM, Mexico.]

for instance in cyclone separators or it is a byproduct as for instance in flows through turbomachineries.

Certain insects utilise jets as a defence mechanism. The *cerura vinula* (a butterfly) for instance sprays formic acid from its head, whereas the *scytodidae* (a spider) sprays a sticky substance to subdue its prey. Under certain conditions in the 'tubing system'[4] or the 'nozzle' within the insects swirl could be induced upon the jet. A more complex defence mechanism is situated in the abdomen of the *stenaptinus insignis* (commonly known as a bombardier beetle), where two chemicals are stored separately (Eisner & Aneshansley 1999). Under attack the liquids are mixed in a mixing chamber and a boiling toxicant ejects from a 'swirl nozzle facility' near the abdominal tip of the beetle (McIntosh & Forman 2004). Figure 1.1(a) shows a bombardier beetle defending itself (not against its natural preys ants, frogs and spiders, but rather a forceps) by squirting a high-pressure jet of boiling liquid in a rapid-fire action. The design of the mixing chamber as well as the 'nozzle' became recently of interest to engineers. McIntosh & Forman believe that the shape of the bombardier beetle's tiny mixing chamber is very important in maximising the amount of material ejected for each explosion (about 300 explosions per second).

Few orders of magnitude larger occurrences of jets can be found in different water animals like octopuses, squids and cuttlefishes, which move by jet propulsion. Dust devils and tornadoes are just two other examples of natural occurring swirling flows. The by far the largest swirling jets are probably observable in galaxies. Astronomers have observed that quasars, young galaxies with supermassive black holes (with masses millions to billions times that of our sun), fire jets with nearly the speed of light aligned through magnetic fields to the black holes accretion disc (see e.g. Gómez *et al.* 2000). Such a swirling radio jet emanating from an *active galactic nuclei* (AGN) is illustrated in figure 1.1(d).

As the brief overview suggests swirling jets are of interest to a wide audience. Engineers aim to understand the underlying physics of these flows to control, i.e. promote or prevent, the generation of swirl in order to modify the turbulence structure and hence the flow field for the sake of maximised efficiency. The interest in these flows, in particular for fluid dynamicists, is perceptible through the availability of experimental databases as for instance the ones by Morse (1980) and Mehta (1991), which are both well known test and validation cases for turbulence modellers.

The present work is part of a larger project, which aims to study the effect of swirl on an impinging jet, where the impinging plate is close to the orifice. This let us concentrate on the momentum and heat transfer processes in the near-field of the developing jet emanating from a fully developed heated turbulent pipe flow, a situation less well-studied than the case of laminar initial

[4]It is for instance known that certain pipe bend combinations induce swirl (Fiedler 1997).

conditions. The thesis is organised as follows: The governing equations are introduced in chapter 2 including simplified relations for free swirling jet flows. A review on previous work done in this area is presented in chapter 3 followed by a detailed description of the experimental setup and the measurement technique in chapter 4. The results and the analysis of the measurements of the velocity and *passive scalar* field are presented in chapter 5, whereas chapter 6 summarises and concludes the work.

CHAPTER 2

Basic equations

"Everything should be made as simple as possible,
but not simpler."

Albert Einstein (1879–1955)

We will first give a short overview over the governing equations to both make the reader acquainted with the quantities that will be used and analysed within the next chapters and to provide a physical background to which we can go back when trying to interpret the experimental results. The first two sections introduce the equations of motion for the velocity field as well as the advection-diffusion relation governing the *passive scalar*, while the remaining section presents simplified integral relations regarding the swirling jet.

2.1. The velocity field

The starting point concerning fluid motion is in general the *Navier-Stokes*[1] equation. Exact analytical solutions of this equation is in general impossible, except for a few simple cases. The equation is derived by applying the physical principle of conservation of mass and *Newton*'s[2] second law to a continuum medium. Specialising the equation for incompressible flow and *Newtonian* fluid, i.e. a specific constitutive law relating viscous stresses to the rate of deformation of a fluid element, the incompressible *Navier-Stokes* equation simplifies to

$$\frac{D\tilde{\mathbf{u}}}{Dt} = \frac{\partial \tilde{\mathbf{u}}}{\partial t} + (\tilde{\mathbf{u}} \cdot \nabla)\tilde{\mathbf{u}} = -\frac{1}{\rho}\nabla\tilde{p} + \nu\nabla^2\tilde{\mathbf{u}} \tag{2.1}$$

where $\tilde{\mathbf{u}}(\mathbf{x}, t)$ and $\tilde{p}(\mathbf{x}, t)$ represents the velocity and pressure[3] field at a point in three-dimensional space coordinates, $\mathbf{x}$, and time, t, respectively. The tilde over the symbol indicates that an instantaneous quantity is being considered. Furthermore the density of the fluid is denoted by ρ and the kinematic viscosity

[1] Claude-Louis Marie Henri Navier (1785–1836), French engineer and physicist and George Gabriel Stokes (1819–1903), Irish mathematician and physicist.
[2] Isaac Newton (1643–1727), English polymaths.
[3] It is worth noting that $\tilde{p}$ may contain a hydrostatic pressure which acts contrary to the gravitational force. However as long as density changes are negligible, i.e. temperature differences are small, gravitational body forces can be considered insignificant.

of the fluid by ν, whereas both are considered to be constant in our case. The conservation of mass reduces in the absence of sources or sinks of mass for incompressible flows, to the so-called *continuity* equation,

$$\nabla \cdot \tilde{\mathbf{u}} = 0. \tag{2.2}$$

The acceleration of a fluid element is the *convective* or *substantive* derivative of the velocity field and thereby denoted by $D\tilde{\mathbf{u}}/Dt$. It is written in equation (2.1) in terms of its components to emphasise the nonlinear character of the *Navier-Stokes* equation, which causes the *closure problem* of turbulence.

For many particular problems and especially for jets emanating from cylindrical orifices it is convenient to use the aforementioned equations in cylindrical polar coordinates rather then in Cartesian ones. Even though the use of rotating frames of reference in the study of rotating flows, above all in the turbomachinery literature, is of widespread use here we will content ourselves with a stationary frame of reference as presented in figure 2.1.

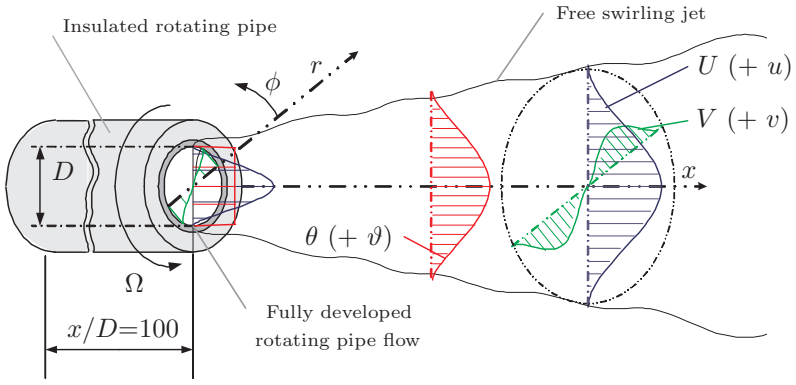

FIGURE 2.1. Schematic of the cylindrical coordinate system of the free developing swirling jet emanating from a fully developed rotating pipe flow.

The velocity vector, $\tilde{\mathbf{u}}$, is decomposed into its three cylindrical components, namely its radial ($\tilde{w}$), azimuthal ($\tilde{v}$), and axial velocity ($\tilde{u}$) components. Thus the *continuity* equation becomes,

$$\frac{1}{r}\frac{\partial}{\partial r}(r\tilde{w}) + \frac{1}{r}\frac{\partial \tilde{v}}{\partial \phi} + \frac{\partial \tilde{u}}{\partial x} = 0\,, \tag{2.3}$$

whereas the *Navier-Stokes* equation can be rewritten in its cylindrical components,

$$\begin{aligned}\frac{\partial \tilde{w}}{\partial t} + \tilde{w}\frac{\partial \tilde{w}}{\partial r} + \frac{\tilde{v}}{r}\frac{\partial \tilde{w}}{\partial \phi} + \tilde{u}\frac{\partial \tilde{w}}{\partial x} - \frac{\tilde{v}^2}{r} = \\ -\frac{1}{\rho}\frac{\partial p}{\partial r} + \nu\left(\nabla^2\tilde{w} - \frac{\tilde{w}}{r^2} - \frac{2}{r^2}\frac{\partial \tilde{v}}{\partial \phi}\right)\end{aligned} \tag{2.4}$$

$$\begin{aligned}\frac{\partial \tilde{v}}{\partial t} + \tilde{w}\frac{\partial \tilde{v}}{\partial r} + \frac{\tilde{v}}{r}\frac{\partial \tilde{v}}{\partial \phi} + \tilde{u}\frac{\partial \tilde{v}}{\partial x} + \frac{\tilde{w}\tilde{v}}{r} = \\ -\frac{1}{\rho r}\frac{\partial \tilde{p}}{\partial \phi} + \nu\left(\nabla^2\tilde{v} - \frac{\tilde{v}}{r^2} + \frac{2}{r^2}\frac{\partial \tilde{w}}{\partial \phi}\right)\end{aligned} \tag{2.5}$$

$$\begin{aligned}\frac{\partial \tilde{u}}{\partial t} + \tilde{w}\frac{\partial \tilde{u}}{\partial r} + \frac{\tilde{v}}{r}\frac{\partial \tilde{u}}{\partial \phi} + \tilde{u}\frac{\partial \tilde{u}}{\partial x} = \\ -\frac{1}{\rho}\frac{\partial \tilde{p}}{\partial x} + \nu\nabla^2\tilde{u}\,.\end{aligned} \tag{2.6}$$

Hereby ∇^2 denotes the *Laplace*[4] *operator* in cylindrical coordinates, which is defined as

$$\nabla^2 = \frac{1}{r}\frac{\partial}{\partial r}\left(r\frac{\partial}{\partial r}\right) + \frac{1}{r^2}\frac{\partial^2}{\partial \phi^2} + \frac{\partial^2}{\partial x^2}\,. \tag{2.7}$$

Equations (2.3)–(2.6) govern the instantaneous flow regardless of its state, whether it is of laminar or turbulent nature. For a turbulent flow it is convenient to reduce the overwhelming amount of information at any instant of time, by analysing the flow in two parts, a mean and a fluctuating component. In order to find an expressions for the mean flow the *Reynolds*[5] *decomposition* is introduced,

$$\begin{aligned}\tilde{w} &= W + w \\ \tilde{v} &= V + v \\ \tilde{u} &= U + u \\ \tilde{p} &= P + p\end{aligned} \tag{2.8}$$

where uppercase letters represent the mean, and lowercase letters the fluctuating motion, respectively.[6] Substitution of equations (2.8) into the *continuity* and *Navier-Stokes* equations in cylindrical coordinates, equations (2.3)–(2.6), and taking the mean value of it, which in statistically stationary turbulence

[4]Pierre-Simon (Marquis de) Laplace (1749–1827), French mathematician and astronomer.
[5]Osborne Reynolds (1842–1912), Irish fluid dynamics engineer
[6]It should be noted that if the averages are defined as ensemble instead of time averages, they are, in general, time-dependent.

is equivalent to take the time average (denoted by an overbar), leads to the *Reynolds averaged continuity* and *Reynolds averaged Navier-Stokes* (RANS) equations. Assuming a steady and axisymmetric mean flow, i.e.

$$\frac{\partial}{\partial t} = 0, \quad \frac{\partial}{\partial \phi} = 0\,, \tag{2.9}$$

the *Reynolds averaged continuity* equation,

$$\frac{1}{r}\frac{\partial}{\partial r}(rW) + \frac{\partial U}{\partial x} = 0\,. \tag{2.10}$$

as well as the *Reynolds averaged Navier-Stokes* equations,

$$\begin{aligned} W\frac{\partial W}{\partial r} + U\frac{\partial W}{\partial x} + \frac{\partial \overline{w^2}}{\partial r} + \frac{\partial \overline{uw}}{\partial x} - \frac{1}{r}(V^2 + \overline{v^2} - \overline{w^2}) = \\ -\frac{1}{\rho}\frac{\partial P}{\partial r} + \nu\left(\nabla^2 W - \frac{W}{r^2}\right) \end{aligned} \tag{2.11}$$

$$\begin{aligned} W\frac{\partial V}{\partial r} + U\frac{\partial V}{\partial x} + \frac{VW}{r} + \frac{\partial \overline{uv}}{\partial x} + \frac{1}{r^2}\frac{\partial}{\partial r}(r^2\overline{vw}) = \\ \nu\left(\nabla^2 V - \frac{V}{r^2}\right) \end{aligned} \tag{2.12}$$

$$\begin{aligned} W\frac{\partial U}{\partial r} + U\frac{\partial U}{\partial x} + \frac{\partial \overline{u^2}}{\partial x} + \frac{1}{r}\frac{\partial(r\overline{uw})}{\partial r} = \\ -\frac{1}{\rho}\frac{\partial P}{\partial x} + \nu\nabla^2 U \end{aligned} \tag{2.13}$$

in cylindrical polar coordinates are found. A quick glance at the *continuity* equation for both the instantaneous and averaged motion, equations (2.3) and (2.10), reveals that they satisfy the same form of mass conservation equations, due to its linear character. On the other hand the nonlinear character of the advective term in the *Navier-Stokes* equation has given rise to contributions to the *Reynolds averaged Navier-Stokes* equations involving turbulent quantities. These are the so-called *Reynolds* stresses, which represent the mean momentum fluxes induced by the turbulence.[7] Thus they do not really represent stresses, but act like those on the mean flow.

It will be shown in section 2.3 that these equations can be further simplified under certain assumptions and moreover they will serve as a very useful tool especially in free jets in stagnant surroundings.

[7]The transport equations for the *Reynolds* stresses are reported in Appendix A.

2.2. The scalar field

We are investigating both isothermal and non-isothermal swirling jets and thus, besides the velocity and pressure field, interest in the influence of the turbulence on a scalar quantity, viz. temperature or a concentration, arises. In section 2.1 we restricted ourselves to incompressible flows and stated that the density as well as the viscosity is being considered constant, whereas here interest in the temperature distribution, due to a non-isothermal jet, is manifested. To neutralise the incompatibility in those statements it is emphasised that only small temperature variations are allowed, such that the density and viscosity can indeed be considered as constant, but that at the same time variations in temperature are still large enough to detect them and distinguish them from unavoidable deviations in the ambient temperature. As a consequence of this the passive contaminant, i.e. the temperature, has no influence on the turbulence and on the dynamics of the flow and we refer to it as a *passive scalar*.

The *passive scalar* obeys an advection-diffusion equation of the form,

$$\frac{D\tilde{\vartheta}}{Dt} = \frac{\partial\tilde{\vartheta}}{\partial t} + (\tilde{\mathbf{u}}\cdot\nabla)\tilde{\vartheta} = a\nabla^2\tilde{\vartheta} \tag{2.14}$$

where $\tilde{\vartheta}$ is the instantaneous temperature and a the thermal diffusivity.[8] Following the procedure for the velocity field, first the equation governing the *passive scalar* is given in cylindrical coordinates,

$$\frac{\partial\tilde{\vartheta}}{\partial t} + \tilde{w}\frac{\partial\tilde{\vartheta}}{\partial r} + \frac{\tilde{v}}{r}\frac{\partial\tilde{\vartheta}}{\partial\phi} + \tilde{u}\frac{\partial\tilde{\vartheta}}{\partial x} = a\nabla^2\tilde{\vartheta} \tag{2.15}$$

then in analogy with the *Reynolds decomposition* the instantaneous scalar field is divided into a mean and fluctuating part,

$$\tilde{\vartheta} = \theta + \vartheta \tag{2.16}$$

and finally the transport equation for the mean *passive scalar* in steady and axisymmetric flow is obtained by introducing the decomposition into equation (2.15) and taking the time average,

$$W\frac{\partial\theta}{\partial r} + U\frac{\partial\theta}{\partial x} + \frac{\partial\overline{u\vartheta}}{\partial x} + \frac{1}{r}\frac{\partial(r\overline{w\vartheta})}{\partial r} = a\nabla^2\theta\,. \tag{2.17}$$

[8] Recalling that equation (2.14) is derived from the first law of thermodynamics and *Fourier*'s law it becomes clear that the thermal diffusivity, a, is defined as the ratio of the thermal conductivity, k, to the heat capacity, $\rho\, c_p$, where c_p denotes the specific heat capacity at constant pressure.

The scalar or heat flux terms emanating from the nonlinear advection term in equation (2.14) are referred to as *Reynolds* fluxes in analogy to the *Reynolds* stresses.[9]

The *Peclet* as well as the *Reynolds* number are known to appear inversely in front of the diffusive terms in the dimensionless form of the governing equations for the transport of momentum and a *passive scalar*, equations (2.1) and (2.14). Thus the definition of the *Reynolds* number, Re, as the ratio between inertia forces and viscous forces,

$$Re = \frac{UL}{\nu} \tag{2.18}$$

and the definition of the *Peclet* number, Pe, as the ratio of the thermal energy convected to the fluid and the thermal energy conducted within the fluid,

$$Pe = \frac{UL}{a} = \frac{UL}{\nu}\,\frac{\nu}{a} = Re\,Pr\,. \tag{2.19}$$

In the latter equation Pr is known as the *Prandtl*[10] number, and it relates the diffusion of vorticity to the diffusion of heat. For the present study the outer parameters given by the pipe flow will be used for the characteristic length and velocity, i.e. $L = D$ and $U = U_b$, where D denotes the pipe diameter and U_b the bulk velocity.

It is worth mentioning that the derived equations and the results which will follow in chapter 5 for the temperature are also valid for any other passive contaminant like pollutants, small-particle smoke, or ink as long as the similarity parameters are of the same order of magnitude. Thus the temperature and thermal diffusivity can easily be replaced by the concentration and the mass diffusivity, respectively, leading to a new non-dimensional number, namely the *Schmidt*[11] number, Sc. Analogous to the *Prandtl* number the *Schmidt* number expresses the ratio between the vorticity and mass diffusivities.

2.3. Specialisation to free swirling jet flows

The theoretical description of steady, axisymmetric and non-isothermal[12] free swirling jets can further be simplified, by taking advantage of a thin shear layer approximation similar to *Prandtl*'s *boundary layer approximation*. Moreover the molecular and thermal diffusivity can safely be neglected at high *Reynolds*

[9] The transport equations for the *Reynolds* fluxes are reported in Appendix B.
[10] Ludwig Prandtl (1875–1953), German fluid dynamicist.
[11] Ernst Heinrich Wilhelm Schmidt (1892–1975), German thermodynamicist.
[12] As mentioned in section 2.2 we refer to non-isothermal conditions even though the changes in temperature are restricted in such a way that the density as well as the viscosity are considered constant and thus the dynamics of the flow are unaffected.

and *Peclet*[13] numbers compared with the *Reynolds* stresses and fluxes in the absence of solid surfaces, which is the case for all free jets.

To find simple integral equations for the governing equations, we assume that the jet covers a very narrow regime in the direction of its axis and therefore the *Reynolds averaged continuity* equation yields $U \gg W$,[14] which with the mentioned thin shear layer approximation further simplifies equations (2.11–2.13), so that the *Reynolds averaged Navier-Stokes* equation in radial direction becomes:

$$\frac{1}{\rho}\frac{\partial P}{\partial r} = -\frac{\partial \overline{w^2}}{\partial r} + \frac{1}{r}\left(V^2 + \overline{v^2} - \overline{w^2}\right). \tag{2.20}$$

Neglecting the radial gradient of the radial turbulence intensity and anticipating that the azimuthal and radial turbulence intensities are comparable, the simple radial equilibrium relation,

$$\frac{\partial P}{\partial r} \approx \rho\frac{V^2}{r} \tag{2.21}$$

can be derived as shown by Reynolds (1961), which demonstrates the existence of a radial pressure gradient induced by the swirling motion, i.e. the azimuthal velocity component. Therefore, for non-swirling flows ($V = 0$) the radial pressure gradient is negligible, whereas swirling flows ($V > 0$) exhibit a positive radial pressure gradient.

Following Chigier & Chervinsky (1967) and multiplying equations (2.20) with r, integrating it across the jet, i.e. from the centreline ($r = 0$) to a radial position, where the presence of the jet is not detectable ($r \to \infty$), and applying the boundary conditions corresponding to a free axisymmetric jet issuing into a quiescent environment at $r = 0$,

$$W = V = 0\,; \quad \frac{\partial U}{\partial r} = 0\,; \quad \frac{\partial \overline{uw}}{\partial r} = \frac{\partial \overline{vw}}{\partial r} = 0 \tag{2.22}$$

and at $r \to \infty$

$$V = U = 0\,; \quad \overline{uw} = \overline{vw} = 0\,; \quad \frac{\partial U}{\partial r} = \frac{\partial V}{\partial r} = 0\,; \quad \frac{\partial \overline{uw}}{\partial r} = \frac{\partial \overline{vw}}{\partial r} = 0 \tag{2.23}$$

the following relation is obtained

[13] Jean Claude Eugène Péclet (1793–1857), French physicist.

[14] This assumption holds only as long as the swirl strength is below swirl numbers associated with reverse flow, i.e. the vortex breakdown regime, as experimentally evidenced by Farokhi, Taghavi & Rice (1989), who observed strong radial inflows with amplitudes reaching half the axial velocity component.

$$\int_0^\infty r(P - P_\infty)\, dr = -\frac{1}{2}\rho \int_0^\infty r \left(V^2 + \overline{v^2} + \overline{w^2}\right) dr\,. \tag{2.24}$$

In an analogous manner equation (2.13) can be simplified to obtain

$$\frac{d}{dx}\int_0^\infty r \left[(P - P_\infty) + \rho\left(U^2 + \overline{u^2}\right)\right] dr = 0\,. \tag{2.25}$$

Substitution of equation (2.24) into the latter expression the following momentum integral relation to second order can be formulated:

$$\frac{d}{dx}M_x = \frac{d}{dx}\,2\pi\rho \int_0^\infty r \left(U^2 - \frac{V^2}{2} + \overline{u^2} - \frac{\overline{v^2} + \overline{w^2}}{2}\right) dr = 0\,. \tag{2.26}$$

As pointed out by Hussein, Capp & George (1994) the integral relation for M_x is not the axial or streamwise momentum flux[15], since it includes the contribution from the radial momentum equation (2.24) to eliminate the streamwise pressure gradient. Rather the integral conservation in equation (2.25) is a direct consequence of the axial momentum balance equation.

An integral expression for the conservation of the axial flux of angular (or swirl) momentum can be derived by multiplying equation (2.12) with $r\,dA$, where $dA = 2\pi r\,dr$, and integrating it under the same conditions as in the previous derivation,

$$\frac{d}{dx}M_\phi = \frac{d}{dx}\,2\pi\rho \int_0^\infty r^2\,(UV + \overline{uv})\, dr = 0\,. \tag{2.27}$$

The ratio of angular momentum, M_ϕ, to the momentum integral expressed through equation (2.26), M_x, times the radius of the orifice, R, is one of the common ways to quantify the swirl intensity (e.g. Gupta, Lilley & Syred 1985). Thus an integral swirl number, $S_{\phi x}$, can be defined as

$$S_{\phi x} = \frac{M_\phi}{RM_x}\,. \tag{2.28}$$

It is common for a first-order analysis to discuss the integral swirl number in terms of the contribution due to the streamwise and azimuthal mean velocities only. Assuming that the algebraic relation of the squared fluctuating velocity components in equation (2.26) as well as the turbulent shear stress in

[15] However various publications starting from the early work by Chigier & Chervinsky (1967) kept this misleading notation.

the streamwise-azimuthal direction in (2.27) are negligible with respect to the squared mean components the swirl intensity reduces to an expression identical to the one in laminar flow,

$$S_{\phi x} = \left[\int_0^\infty r^2 UV\, dr\right]\left[R\int_0^\infty r(U^2 - \frac{1}{2}V^2)\, dr\right]^{-1}. \tag{2.29}$$

It should be noted that the aforementioned assumptions have been confirmed experimentally by Pratte & Keffer (1972) and will also be shown in the present measurements. Assets and drawbacks of this definition and others will be discussed in section 3.2.

Finally the transport equation for the mean *passive scalar*, equation (2.17), can be multiplied by r and integrated to give a relation for the conservation of the axial flux of heat,

$$\frac{d}{dx}M_\theta = \frac{d}{dx}\,2\pi\rho\, c_p \int_0^\infty r(U\theta + \overline{u\vartheta})\, dr = 0\,, \tag{2.30}$$

whereas for a first-order approximation the turbulent streamwise heat flux term can be neglected at least in the near-field.

CHAPTER 3

Review of swirling jet studies

"We are like dwarfs standing [or sitting] upon the shoulders of giants, and so able to see more and see farther than the ancients."

Bernard of Chartres (twelfth-century)

"If I have not seen as far as others, it is because giants were standing on my shoulders."

Hal Abelson (1922–)

Some historians assume that *Newton* may have cleverly employed the phrase "on the shoulders of giants" to ridicule *Hooke*'s[1] lack of physical stature and imply that he lacked intellectual stature as well.[2] Nevertheless both phrases show the possibilities, which are offered to us. Alternatively one may contribute to the insight of "dwarfs" and "giants" by providing them with compound pieces of a puzzle. Reviews of previous works and their main contributions are one kind of building blocks on which one can start on to begin a personal journey. A background on swirling jets, their main parameters and generation methods follows and concludes with a summary on previous works.

The present study deals with turbulent free jets, where an azimuthal velocity is superimposed on the streamwise flow, thus the reader is referred to monographs of Abramovich (1963) and Rajaratnam (1976) for an general account on jets.

3.1. Background

Turbulent jets with rotation exhibit distinctive characters absent in their non-rotating counterparts. A subsonic jet experiences theoretically no static pressure gradient in the axial or radial direction, hence the mechanism for jet spread is dominated by the turbulence mixing at the interface between the jet and the ambient fluid. A swirling jet however, exceeding a certain degree of swirl in the

[1] Robert Hooke (1635–1703), English polymaths.

[2] For the traces of *Newton's* aphorism see for instance *On the Shoulders of Giants*, by R. K. Merton.

near-field, is affected by the static pressure gradients in both axial and radial direction (Farokhi & Taghavi 1990).

The effect of rotation on jets is well known and for instance exploited in compressible and/or reacting swirling jets in furnace flows and burners as well as in combustion system, due to the increased turbulent mixing of fuel with air. Another phenomenon observed at high swirl intensities is the reverse flow in the vicinity of the orifice, which may lead to vortex breakdown, i.e. an abrupt structural change forming a free stagnation point or recirculation zone on the axis of the mean flow, if a certain swirl strength is exceeded. Although this phenomenon is utilised to stabilise flames in combustion chambers and furnaces, it will be left out of count in the present investigation, due to our primary interest in low and moderate swirl intensities far below the onset of reverse flow along the centreline and the inaccessibility through the present measurement technique.[3]

To sum up, we restrict ourselves here to incompressible, non-reacting and fully developed turbulent free swirling jets with swirl strengths below the occurrence of reverse flow at the central region of the jet, and refer the interested reader to the review articles of Syred & Beér (1974) and Lilley (1977) concerning swirling flows and jets in combustion, to Lucca-Negro & O'Doherty (2001) regarding the vortex breakdown phenomenon in swirling flows and jets and to Billant, Chomaz & Huerre (1998), Loiseleux & Chomaz (2003) and Gallaire & Chomaz (2003) for an account on instability of swirling jets. A good overview on both theoretical and experimental work is given in the classical book by Gupta, Lilley & Syred (1985).

Although we have restricted our study to small swirl rates the remaining research field is still full of industrial applications. The addition of mild degrees of swirl to a jet is for instance known to intensify the processes of mass, momentum and heat transfer, to spread, entrain and mix faster and to reduce noise production in the near-field of a jet exhaust. Furthermore swirling jet flows are byproducts of flows through turbomachinery and flows over wings and are utilised in separators. Even though we profit from the mentioned features, for most of the cases we still do not know for sure *why* and *how* swirl embeds all these features. A selection on previous experimental work is given in table 1 on page 18 and 19 evidencing the interest and search for an understanding of the underlying physics.

Before going over to a more detailed review on the results of previous works of interest the parameters defining the swirling jet as well as the techniques to impart the swirl on the axial mean flow will be presented in the next two sections.

[3]Reverse flow itself is an instantaneous phenomenon of turbulent jets issuing into stagnant fluid at the interface between the jet and its irrotational environment. This is one of the major difficulties for the application of stationary *hot-wire anemometry* in the outer edge of the jet and will be discussed in section 4.2.4.

Author(s) (year)	Swirl generator	Measurement technique(s)	Range of $Re \cdot 10^3$	Range of $S_{\phi x}$	Range of x/D	Presented quantities
Rose (1962)	rotating pipe	single hot-wire (SW)		0–0.23	0.235–15	U, V, W & $\overline{u_i u_i}$
Chigier & Beér (1964)	tang. injection	impact probe (IP)		0–0.6	0.39–1.43	U & V
Kerr & Fraser (1965)	passive vanes	impact probe		0–0.72	11.7–19	U, V & W
Chigier & Chervinsky (1967)	tang. injection	impact probe	24–260	0.066–0.64	0.2–15	U, V & P
Pratte & Keffer (1972)	rotating pipe	SW, IP	2.3	0–0.3	1–30	U, V & $\overline{u_i u_j}$
Wooten *et al.* (1972)	straw inserts	X-wire (XW)		(G=)0.08		U, V, u' & v'
Morse (1980)	see section 3.4	SW	56	(S=)0.48	0–6	U, V, W & $\overline{u_i u_j}$
Fujii *et al.* (1981)	passive vanes	LDV	100	0.69–1.5	0.5–5	U, V, W & $\overline{u_i u_j}$
Sislian & Cusworth (1986)	passive vanes	LDV	11.5	0.79	0.125–5	U, V, W & $\overline{u_i u_j}$
Samet & Einav (1988)	tang. injection	impact probe		(G=)0–0.49	2–20	U & V
Farokhi *et al.* (1989)	tang. nozzles	IP, SW	375	0.48	0–6	U, V, W, & P
Mehta *et al.* (1991)	rotating honeycomb	SW, XW		0–0.2	0–2.31	U, V & $\overline{u_i u_j}$
Park & Shin (1993)	swirl burner	Schlieren visualization	13–20.5	0–1.87	0–5	images & entrainment rates
Feyedelem & Sarpkaya (1998)	tang. injection	3D-LDV	18	0–0.52	0.14–32	U, V, W & $\overline{u_i u_j}$

TABLE 1. Previous experimental studies on isothermal and heated swirling jets.

Author(s) (year)	Swirl generator	Measurement technique(s)	Range of $Re \cdot 10^3$	Range of $S_{\phi x}$	Range of x/D	Presented quantities
Oljaca *et al.* (1998)	rotating paddle	XW, ultrasound scattering	10	0–0.24	0.25–3	U, V
Gilchrist & Naughton (2005)	tang. injection	impact probe	100	0–0.23	0–20	U, V
Facciolo (2006)	rotating pipe	XW, 2D-LDV, 2D-PIV	12–33.5	(S=)0–0.5	0–8	U, V, W, $\overline{u_i u_i}$ & $\overline{vw}$
Craya & Darrigol (1967)	tang. injection	SW, cold-wire (CW), thermocouple (TC)		0–1.58	1–15	U, V, W, θ, ϑ' & $\overline{u_i u_j}$
Ogawa *et al.* (1979, 1981, 1982)	tang. injection	IP, TC	11.2–105.3	0–0.616	0–20	U, V, P & θ
Grandmaison & Becker (1982)	passive vanes	nephelometry	100	0–0.68	0–60	θ & ϑ'
Komori & Ueda (1985)	rotating nozzle	LDV, CW	4.92	0–0.53	0–10	U, V, W, θ, $\overline{u_i u_i}$, $\overline{uw}$, $\overline{u\vartheta}$ & $\overline{w\vartheta}$
Elsner & Kurzak (1987, 1989)	passive vanes	XW, CW, temp. compensated SW	80	0–0.42	1–15	U, V, W, θ, $\overline{u_i u_j}$ & $\overline{u_i \vartheta}$
Toh *et al.* (2005)	tang. injection	PIV, PLIF	3.9	(S_{m_0}=)0.06–0.15	0–5.8	images
Present study	rotating pipe	XW-CW	24	(S=)0–0.5	0–6	U, V, θ, $\overline{u_i u_i}$, $\overline{uv}$, $\overline{u\vartheta}$ & $\overline{v\vartheta}$

3.2. Parameters of a swirling jet

A free jet is characterised through its *Reynolds* number and its initial conditions. The latter can be characterised by a large numbers of non-dimensional parameters: the initial mean streamwise velocity profile (and hence the momentum thickness of the inner boundary layer at the exit), its state (laminar or turbulent, as defined by their shape factors and fluctuation intensities), and the spectra (informing about the frequency content of the flow) of the exit jet (see e.g. Buresti, Talamelli & Petagna 1994). For fully developed turbulent conditions at the orifice however, as is the case in the present investigation, the (unforced) free jet is characterised by the *Reynolds* number and the streamwise velocity profile.

Classical theory (see e.g. Townsend 1976 or Pope 2000) assumes that a turbulent wake or jet with increasing downstream position forgets about its origin, so that the actual shape of the orifice and thus the initial velocity profile does not effect the shape of the velocity profile in the far-field if properly scaled. Here we can not contribute on this issue, due to our interest in the near-field evolution, but for the near-field the initial conditions do matter and they even determine the flow field vigourously.

Coming to the swirling jet a third quantity becomes important, namely the swirl, which for instance can be quantified through its rotation number introduced in equation (2.28). However the exact radial profile of the azimuthal velocity component does have influence (at least) in the near-field of the jet. In the following the three aforementioned parameters will be discussed separately.

3.2.1. *The Reynolds number*

There are mainly two different characteristic velocities used in the literature to express the *Reynolds* number, Re, concerning free jets with and without swirl. For swirling jets emanating from rotating pipes one usually selects the cross-sectional mean velocity, the so-called bulk velocity, U_b, at the outlet of the orifice as the characteristic velocity. Whereas the majority utilises the exit centreline velocity for the non-swirling jet, $U_{0,S=0}$. As evident from table 1 not much care was given by the authors to mention the *Reynolds* number, which probably is due to the classical assumption that ones the jet is fully turbulent the *Reynolds* number does not strongly affect the dynamics of the flow. However Pitts (1991) and Richards & Pitts (1993) report that the *Reynolds* number does matter at least for jets emanating from long pipes below a threshold of approximately $Re = 25000$. Ricou & Spalding (1961) in an early study concerning the entrainment rate of axisymmetric jets have shown that the effect of *Reynolds* number diminishes for $Re > 25000$. It is worth mentioning that *laser-Doppler*[4] *velocimetry* measurements performed by the author along the centreline of the jet in the range of $0 \leqslant x/D \leqslant 10$ showed that at least for

[4] Johann Christian Andreas Doppler (1803–1853), Austrian mathematician and physicist.

the mean axial velocity component as well as its turbulence intensity the flow tends to become independent of the *Reynolds* number in the higher end of the range from $Re = 6000$ to 34000. The *Reynolds* numbers reported in table 1 are either the ones mentioned in the respective paper or are recalculated.

3.2.2. *The swirl number*

The non-dimensional parameter describing the swirl strength in a free jet, but also in internal flows, is the integrated swirl number, $S_{\phi x}$, defined through equation (2.28). Inserting the invariants of the jet, M_x and M_ϕ, into the integrated swirl number including the *Reynolds* stress components gives

$$S_{\phi x} = \frac{\int_0^\infty r^2 (UV + \overline{uv})\, dr}{R \int_0^\infty r \left[U^2 + \overline{u^2} - \frac{1}{2}(V^2 + \overline{v^2} + \overline{w^2})\right] dr} \,. \tag{3.1}$$

Feyedelem & Sarpkaya (1998), who used three-component *laser-Doppler velocimetry*, expressed the swirl number though this relation, whereas most of the researchers computed the swirl number without the *Reynolds* stresses as given in equation (2.29), due to the assumed negligible effect of these terms. Furthermore not all investigations provide these components. An additional simplification is often introduced for the far-field of the swirling jet by neglecting the mean azimuthal velocity component in M_x. It will be shown in section 5.1.1 that the azimuthal velocity component will rather quickly reduce to less then 10 % of its initial value just after 6 pipe diameters, justifying this simplification.

It will become apparent throughout section 4.2.4, where we will discuss the difficulties in acquiring reliable measurements in the outer edge of the jet by means of *hot-wire anemometry*, that the integral swirl number is rather difficult to compute. This also holds true for non-intrusive measurement techniques such as *laser-Doppler velocimetry* and *particle image velocimetry* unless the ambient air is continuously seeded without introducing arbitrary disturbances. Because of these difficulties other measures have been introduced.

Chigier & Chervinsky (1967), who imparted the swirl through tangential slots, showed that for the case of a solid-body rotation plug flow at the orifice a much more convenient swirl number,

$$S_{m_0} = \frac{G/2}{1 - (G/2)^2} \,, \tag{3.2}$$

could be introduced, where G is the ratio of maximal angular velocity, V_{m_0}, to maximal axial velocity, U_{m_0}. Good agreement between both swirl numbers were found up to $S_{\phi x} = 0.2$. This definition was for instance used by Toh, Honnery & Soria (2005) with a more or less uniform axial velocity profile with solid-body rotation in the core region. Wooten, Wooldridge & Amaro (1972)

and Samet & Einav (1988), however, used G as their swirl number, whereas Billant, Chomaz & Huerre (1998) employed a more arbitrary swirl number by taking the ratio between the azimuthal velocity at the half radius of their nozzle and the centreline velocity at an axial distance where measurements were possible.

Other frequently used definitions are related to the vane angle when swirl is generated by guide vanes or spirally shaped vanes. Several definitions are mentioned by Bilen *et al.* (2002). However, for jets emanating from long rotating pipes there exist another possibility, namely the ratio between the azimuthal velocity at the wall, V_w, and the bulk velocity, U_b, at the pipe outlet,

$$S = \frac{V_w}{U_b}\,. \tag{3.3}$$

This definition is quite convenient since the wall velocity is directly obtained through the rotational speed of the pipe.

The list of swirl numbers presented here is of course not complete, but it covers all the previous investigations, which will be reviewed in section 3.4.

3.2.3. *The initial boundary conditions*

We already raised the importance of initial conditions and we retain to exclude here the more fundamental quest whether or not turbulent shear flows in the far-field, the region where certain quantities such as mean velocity components or *Reynolds* stresses, become self-similar when scaled properly. A large variety of mean axial as well as azimuthal velocity profiles, due to different swirl generating methods, can be produced and it is obvious that a integrated quantity like $S_{\phi x}$ will fail to contain all the information which characterises the azimuthal velocity component. Besides S the other introduced swirl numbers have the same shortcoming, because they express only information about the velocity components at a certain radial (and axial) position. Contrary the fully developed turbulent pipe flow possesses a well-defined axial as well as azimuthal velocity profile making it possible to express the whole flow field at the pipe exit by means of S and Re.

This deficit was recognised right from the beginning (Chigier & Beér 1964 and Pratte & Keffer 1972) and was studied by Farokhi, Taghavi & Rice (1989) and quite recently by Gilchrist & Naughton (2005) pointing out that threshold values for the onset of reverse flow or vortex breakdown do not make sense if decoupled from the exact velocity profiles. This explains why two different types of swirling jet behaviours can exist with both the same swirl number and *Reynolds* number. In conclusion it becomes clear that besides the *Reynolds* number and the swirl number also the initial condition has to be quantified in order to facilitate any comparison between experimental results among themselves or with computations.

3.3. Swirl generating methods

Throughout the previous sections different methods for introducing the swirl onto the free jet were mentioned without further explanation. We already saw that different swirl generating methods (for a summary of different swirl generating methods see also Facciolo 2006) will most likely lead to different azimuthal, but also axial velocity profiles. Following the description of these methods will be given and the reader is referred to table 1 for a list of previous works and their swirl generating methods.

3.3.1. *Rotating methods*

In the present investigation the swirling jet emanates from a fully developed axially rotating pipe flow. This method was used by Rose (1962) and Pratte & Keffer (1972) among others and is known to produce well-defined outlet conditions regardless the individual facility provided that the flow is fully developed, i.e. sufficiently high *Reynolds* number and large enough length-to-diameter ratio. Hence it provides an optimal benchmark for comparisons with turbulence models for the near-field of swirling jets. Pratte & Keffers length-to-diameter ratio of the pipe was just half as large as the one by Rose, hence they implemented a dividing strip of 70 % of the total pipe length into the pipe in order to impart a strong enough azimuthal velocity component. However they had to accept a certain asymmetry in the vicinity of the pipe outlet.

A honeycomb placed inside the rotating pipe may help to overcome this restriction as for instance done by Mehta *et al.* (1991) who placed a honeycomb at the beginning of a rotating pipe (followed by a stationary pipe). A similar technique was employed by Komori & Ueda (1985) who rotated a convergent nozzle producing rather uniform radial profile of the axial velocity component. Rotating four-bladed paddles upstream of a nozzle were used by Oljaca *et al.* (1998), so that 'top-hat' axial velocity profiles were generated in the absence of swirl, whereas for the swirling case the axial velocity profile became pointed at the centre. A similar behaviour was observed by Billant *et al.* (1998), who used a motor driven rotating honeycomb upstream a nozzle. Gore & Ranz (1964) imparted rotation to axial pipe flow by means of a rotating perforated plate in which holes were drilled.

3.3.2. *Tangential injection*

Tangential injection methods are widely used in swirling jet experiments and they are known to be capable to generate high degrees of swirl enabling the study of reverse flow and vortex breakdown along the centreline in the near vicinity of the orifice. Chigier & Chervinsky (1967) injected a portion of the fluid peripherally into a nozzle and controlled the flow field by varying the ratio of axial to tangential air. These axial-plus-tangential entry swirl generators are available in a variety of geometrical shapes changing in the number of supply

pipes and tangential inlet slots. A different approach was followed by Ogawa & Hatakeyama (1979) who injected secondary flow into the pipe upstream the output nozzle. Asymmetric azimuthal velocity profiles were observed down to 12 pipe diameters downstream (Ogawa *et al.* 1981).

By introducing secondary flow through a large amount of nozzles ordered along circular rings Farokhi *et al.* (1989) was able to produce different initial swirl distributions.

3.3.3. *Passive methods*

A rather simple method to deflect the flow into curved streamlines is by means of deflecting or guiding vanes which are mounted upstream the orifice or nozzle. Different sets of shaped profiles were for instance used by Elsner & Kurzak (1987) and Sislian & Cusworth (1986) enabling the study of reverse flow. The necessity of a nozzle downstream the swirl vanes was recognised by Gore & Ranz, who found that the flow was not axisymmetric and in addition to it secondary flows were induced.

Other passive methods to introduce helical streamlines are for instance found in the study of Rahai & Wong (2002) and Wooten *et al.* (1972). The former used coil inserts mounted at the wall while the latter used a circular bundle of soda straws bound together and twisted to a proper angle generating solid-body rotation of the flow.

3.4. Experimental studies on swirling jets

The first experimental investigation on turbulent swirling jets is probably the one by Rose (1962). By means of *hot-wire anemometry* he determined radial profiles of all mean velocity components as well as turbulence intensities from the vicinity of the pipe outlet up to 15 diameters downstream. Additionally the centreline decay of the streamwise mean velocity as well as the turbulence intensity up to 70 diameters downstream were determined. One interesting result obtained was, that in the case of a turbulent pipe flow the mean azimuthal velocity—even after 100 pipe diameters—deviates clearly from the solid body rotation, which is observable in laminar pipe flows. He assumed that a solid-body rotation could be obtained with an even longer pipe, but his successors Kikuyama *et al.* (1983) and Imao, Itoh & Harada (1996) among others showed experimentally that a fully developed rotating pipe flow has indeed a parabolic profile, regardless how long the pipe might be.[5] Major features of the addition of rotation to a free jet were observed by him, namely the larger spreading angles, the enhanced entrainment rates, the more rapid decay of the centreline velocity as well as the increased turbulence intensities.

[5]Orlandi & Fatica (1997), through *direct numerical simulations* and Oberlack (1999), by means of theoretical scaling laws fitted to experimental results, confirm the existence of a parabolic profile for the azimuthal velocity component.

Mean velocity components and static pressure distributions for swirl numbers corresponding to weak, moderate and strong swirl, including the case of the onset of reverse flow in the central region of the jet, were conducted by Chigier & Chervinsky (1967). They found that the swirling motion had more or less completely vanished already at about 10 diameters downstream. For moderate swirl numbers and beyond 4 nozzle diameters downstream their results fitted very well to the integral relations derived in section 2.3. For high swirl numbers a shift of the mean axial velocity from the centreline outwards is observed. However 10 pipe diameters downstream the peak value moved back to the centreline from which point the flow could be described by their semi-empirical relations, which are based on the aforementioned integral relations.

Pratte & Keffer (1972) investigated the streamwise decay by means of a single hot-wire probe, which could be rotated in order to determine all velocity components. Similar to Chigier & Chervinsky they utilised boundary layer assumptions and self-similarity arguments showing that the maximum axial and swirling velocity components in a region beyond the initial formation region should vary asymptotically as x^{-1} and x^{-2}, respectively. These decay rates were confirmed by their experiments.

Since the invention of the jet engine and the continuously increasing air traffic noise production in turbulent jets became an annoying byproduct. Besides the effect of grids and water droplets to reduce the noise production in the near-field of a jet Wooten *et al.* (1972) investigated the effect of swirl upon the structure of the jet mixing region. Their results indicate that even with a very low degree of swirl ($G = 0.08$) a change in the noise production can be expected. The noise in the initial portion of the jet was higher while noise was substantially reduced in the far-field resulting in an overall noise reduction.

Morse (1980) investigated the near-field of a swirling jet emanating from a pipe by means of *hot-wire anemometry*. He provided all mean and *Reynolds* stress values to validate *Reynolds* stress closure models (see e.g. Launder & Morse 1979 and Gibson & Younis 1986). As mentioned in the introductory chapter the experimental study by Morse is well known among turbulence modellers and serves as a validation case. However, in the same time, neither the details of the experimental set-up (e.g. swirl generating method or length of the pipe) nor the measurement technique are accessible from the experimental database, which makes it difficult to classify his work.[6]

Fujii, Eguchi & Gomi (1981) applied *laser-Doppler velocimetry* in the near-field of a swirling jet with reverse flow to acquire all velocity and six *Reynolds* stress components under isothermal and combustion conditions. They found

[6]Experimental data of Morse (1980) are for instance available in the *ERCOFTAC "Classical Collection" Database* and in *"Collaborative testing of turbulence models"* funded by AFOSR, Army research office, NASA and ONR (see Bradshaw, Launder & Lumley 1996).

that the virtual origin of radial spread moves upstream under combustion conditions indicating lesser spread of axial velocity, whereas the turbulence levels where increased as a consequence of combustion.

Other studies in strongly swirling jets with reverse flow were performed by Sislian & Cusworth (1986) and Park & Shin (1993). The latter investigated the entrainment characteristics of the near-field of an isothermal swirling jet for swirl intensities of moderate and strong strength, in which the jet is dominated by the azimuthal component causing up to five times higher entrainment rates. Schlieren flow visualisation was utilised to study the *Reynolds* number dependence on the entrainment enhancement as well as to explore the role of the *precessing vortex core* (PVC), which induces large-scale periodic motion in the jet boundary regions near the nozzle exit.[7] A *Reynolds* number dependence was found for swirl intensities causing vortex breakdown, whereas no dependence was found for $S_{\phi x} < 0.6$.

The presence of swirl activates extra production terms in the transport equations causing the shear stresses to be more affected by swirl than the normal stresses as shown by Mehta *et al.* (1991).[8] They report an increase in *all* the peak *Reynolds* stresses as well as in the shear layer thickness within the mixing layer with increasing swirl number. The otherwise negligible secondary *Reynolds* shear stresses, $\overline{uv}$ and $\overline{vw}$, reach values around half the value of the primary *Reynolds* shear stress, $\overline{uw}$.

Feyedelem & Sarpkaya (1998) investigated a swirling jet submerged in water with both a 5-hole pressure tube and three-component *laser-Doppler velocimetry*. They observed stagnation without vortex breakdown at a critical swirl number of $S_{\phi x} = 0.5$ and vortex breakdown for $S_{\phi x} \geqslant 0.51$. Farokhi, Taghavi & Rice (1989) detected an even lower value for the occurrence of vortex breakdown ($S_{\phi x} = 0.48$) in their study concerning the effect of initial swirl distributions on the evolution of a turbulent jet. Their unique swirl generator system with 54 elbow nozzles mounted on three concentric rings enabled them to produce different azimuthal velocity profiles by keeping the swirl number constant at $S_{\phi x} = 0.48$. Both of the previous studies query the 'critical value' of $S_{\phi x} = 0.6$ (see e.g. Gupta, Lilley & Syred 1985) as a threshold for the occurrence of vortex breakdown and conclude that the characteristics of swirling flows are highly complex to be described by only the swirl and *Reynolds* numbers. This is due to the strong influence of the pre-exit history upstream the orifice and the conditions at the orifice itself, which was anticipated already in section 3.2.3. Using the same experimental setup Taghavi & Farokhi (1988)

[7] The role of the precessing vortex core in swirl combustion systems was recently reviewed by Syred (2006).

[8] Compare this to the transport equations for the *Reynolds* stresses in Appendix A.

additionally studied the effect of acoustic excitation as well as the effect of screens upstream the nozzle.[9]

The study of Farokhi *et al.* was recently picked up by Gilchrist & Naughton (2005) who generated swirling jets resembling solid-body and q vortex (solid-body core with a free vortex outer region) type azimuthal velocity components. They found that regardless the swirl generation mechanism, the centreline decay rate seems to be accurately predicted by the swirl number. Contrary as swirl levels sufficient for vortex breakdown are approached, the tangential velocity distribution will play an important role. While Chigier & Chervinsky (1967) believed that the growth rate for low and moderate swirl numbers increases linearly with $S_{\phi x}$, they found enhanced growth rates only when the swirl number exceeded a certain value as did Mehta *et al.* (1991) for the near-field region. Gilchrist & Naughton infers that there appears to be three regions of swirl-enhanced jet growth rates: A region without enhancement effects ($S_{\phi x} < 0.1$), a region were enhancement scales with the swirl number ($0.1 < S_{\phi x} < 0.3$) and a region were the swirl strength is sufficiently high to cause vortex breakdown. This however is lower than the previously mentioned values of 0.48 and 0.6 by Farokhi *et al.* (1989) and Gupta *et al.* (1985), respectively.

As seen in table 1 most of the early investigations were conducted by means of impact probes, single-wire and/or X-wire probes and were later on supported by one-dimensional *laser-Doppler velocimetry*. Within the last decade a trend towards 'modern' techniques is recognisable. Oljaca *et al.* (1998) for instance mentions that there is a linear relationship between the *Fourier*[10] component of the scattered acoustic pressure and the *Fourier* transform of the vorticity component. They exploited this relationship to compute the power spectra of the pressure field by propagating acoustic waves through a swirling jet and showed the potential of the technique as a non-intrusive spectral probe.

Using X-wire, two-dimensional *laser-Doppler velocimetry* as well as stereoscopic *particle image velocimetry* the near-field of the swirling jet was examined by Facciolo (2006) and the data constitutes a well-defined database for a complex flow field. Besides an encountered counter-rotating core at a downstream position around 6 pipe diameters, which was observed with all measurement techniques involved and through *direct numerical simulations* (DNS) (reported in Facciolo, Orlandi & Alfredsson 2005), the time resolved PIV measurements show interesting differences between the non-swirling and swirling jet.

Besides the small amount of experimental studies on swirling jets generated by different mechanisms few review articles as well as book chapters have been provided for topics related to combustion and mixing. The review articles by Syred & Beér (1974) and Lilley (1977) give an overview on swirling flows

[9] It is interesting to note that the interest in studying the effect of screens on non-swirling round jets arose much later (Burattini *et al.* 2004).

[10] Jean Baptiste Joseph Fourier (1768–1830), French mathematician and physicist.

in the field of combustion in general. Rajaratnam (1976) in his book about turbulent jets provides a theoretical background and discusses the turbulence statistics obtained by Chigier & Chervinsky (1967) and Pratte & Keffer (1972). The book chapter by Schetz (1980) reviews briefly the aforementioned works, whereas the classical book by Gupta *et al.* (1985) gives a good overview over experimental as well as theoretical work done on swirling flows in general. A short review over experimental studies in relation to turbulence modelling is given in Piquet (2001).

The above review on previous works on the dynamics of swirling jets shows a wide range of measurement techniques and swirl generating methods, which makes it difficult to compare results in the near-field of the jet. Despite the studies of Rose (1962) and Facciolo (2006) in jets emanating from rotating pipe facilities most of the jets in the near outlet region of the orifice contain traces of the swirl generating method[11] and make impossible any general conclusion. Due to the interest in the recirculation zone by the combustion community there is a scarcity of data on nonrecirculating swirling jets. As pointed out by Mehta *et al.* (1991) this complicates the interpretation of the results by the presence of both, a stabilising region around the axis of rotation and an unstable region farther outwards.

The lack on experimental data regarding the *passive scalar* mixing in swirling jets is even more scarce. Craya & Darrigol (1967) were probably the first ones who determined the mean temperature as well as the root mean square value of the temperature fluctuations with the help of thermocouples and a slightly heated wire.

Using *Pitot*[12]-tubes and thermistor thermometers the mean dynamic and thermal field of swirling jets for a large variety of *Reynolds* numbers and swirl numbers were investigated by Ogawa, Hatakeyama & Fujita (1979, 1981 and 1982).

In a rather unique investigation Grandmaison & Becker (1982) used marker nephelometry to study the fluid concentration field of a free swirling turbulent jet with and without internal reverse flow in the self-preserving region up to 60 nozzle diameters downstream including its turbulence intensity. The effect of swirl on the axial decay, the spreading as well as the correlation functions and the spectra of the concentration were accessed. They conclude that the addition of swirl has a small effect on the flow structure, although it increases the rates of entrainment and spreading.

The results by Komori & Ueda (1985) in a weakly heated swirling jet with moderate to strong swirl show that in a strongly swirling jet the ambient fluid is rapidly entrained into the jet in the region near the nozzle exit. They linked the

[11] The study of Pratte & Keffer (1972) is not listed here, due to the asymmetry in the vicinity of the pipe outlet caused by their long dividing strip in the pipe (see section 3.3.1).
[12] Henri Pitot (1695–1771), French hydraulic engineer.

rapid entrainment to the large negative static pressure induced by the strong centrifugal forces. The turbulent kinetic energy was found to exhibit a large peak in the vicinity of the nozzle showing that strong turbulence is generated by the rapid mixing encountered in strongly swirling jets with reverse flow. For a weakly swirling flow the maximum moves further downstream.

The study by Elsner & Kurzak (1987 and 1989) extends the work by Komori & Ueda by means of an X-wire, cold-wire and temperature compensated single-wire in a slightly heated swirling jet. All velocity components, *Reynolds* stresses and heat flux terms were determined giving a full description of the dynamic and thermal flow field.

Quantitative velocity and scalar measurements of the flow flied of low swirl intensity jets were obtained by Toh, Honnery & Soria (2005) using *multi-grid cross correlation digital particle image velocimetry* (MCCDPIV) and *planar laser induced fluorescence* (PLIF). The findings are consistent with known gross effects of swirl.

Most of the previous studies concerning the concentration or temperature field were restricted to strong swirl intensities, the self-preserving and far-field region. There is clearly a lack of experimental results concerning the effect of rotation on the *passive scalar* behaviour in the near-field of a free turbulent jet, which justifies the need for the present study. The present swirling jet facility makes it moreover possible to access the effect of rotation on the dynamic and thermal field without traces or asymmetric distributions of velocity components as well as temperature, which, in regard of the previous experimental works, is to be emphasised.

CHAPTER 4

Experimental methods

"If you can not measure it, you can not improve it."

William Thomson, aka Lord Kelvin (1824–1907)

"A theory is something nobody believes, except the person who made it. An experiment is something everybody believes, except the person who made it."

Albert Einstein (1879–1955)

As engineers we are seeking to improve every process around us and to do this we need *to measure*. To measure is still associated with experimentation and the present investigation can be seen in this context. As Einstein's quote suggests, the confidence in experiments by "everybody" is high and even though the author of the present work intends to go through the experimental setup and the applied measurement technique thoroughly trusting that *he* as well gains trust in the way the measurements were accomplished.

4.1. Experimental apparatus

The experiments are performed at the *Fluid Physics Laboratory* of *KTH Mechanics* in a specially designed setup, consisting of a 100 pipe diameters long axially rotating pipe. The rotating pipe apparatus, shown in figure 4.1, was designed, built and taken into operation in connection with the licentiate thesis of Facciolo (2006), in order to investigate the effect of rotation on turbulent pipe and jet flows. Few modifications on the experimental facility made it possible to extend the focus of investigation from the dynamics of the flow to include the mixing of a passive contaminant.

Figure 4.2 shows the modified experimental apparatus schematically. Air at ambient temperature is provided by a centrifugal fan (A) with a butterfly valve for flow rate adjustment, which is monitored through the pressure drop across an orifice plate (B) inserted in the air supply pipe. A distribution chamber (D) to reduce the transmission of vibrations generated by the fan follows. From there the air stream is distributed into three different spiral pipes, which are symmetrically fed into the stagnation chamber (E), consisting of a honeycomb,

FIGURE 4.1. Experimental setup showing the pipe mounted within the triangular shaped framework and fed into the stagnation chamber covered by an elastic membrane.

in order to distribute the air evenly. One end of the cylindrical stagnation chamber is covered with an elastic membrane in order to further reduce the pressure fluctuations as apparent from figure 4.1. A bell mouth shaped entrance first leads the air into a one meter long stationary section, which is connected to the rotating pipe (K) through a rotating coupling (F). In the first section of the rotating part of the pipe a 12 cm long honeycomb (G), consisting of drinking straws of a diameter of 5 mm, is mounted which brings the flow into more or less solid body rotation. The inner diameter of the pipe amounts 60 mm whereas the wall thickness is 5 mm. The pipe 6 m long pipe is made of seamless steel and has a honed inner surface with a roughness of less than 5 micron, according to manufacturer specifications. It is supported along its full length by 5 ball bearings (J), which are mounted within a rigid triangular shaped framework. The pipe is belt driven via a feedback controlled DC motor (H), which is capable to run the pipe up to rotational speeds of 2000 rpm. The pipe flow emanates as a free (swirling) jet (M) 1.1 m above the floor into the ambient air at rest. By placing the apparatus in a large laboratory with a large ventilation opening far downstream of the pipe outlet it is ensured that the jet can develop far away from any physical boundaries. In the present measurements the pipe ends with a 30 cm diameter circular end plate (L).

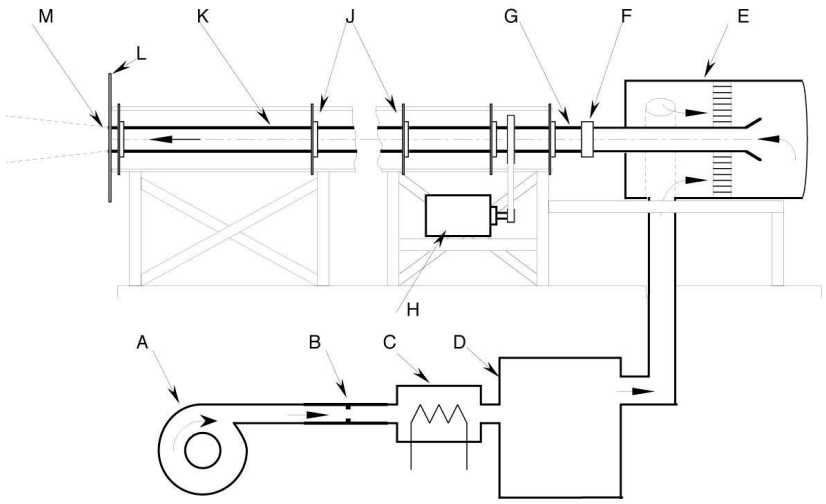

FIGURE 4.2. Schematic of the experimental setup. A) Centrifugal fan. B) Flow meter, C) Electrical heater, D) Distribution chamber, E) Stagnation chamber, F) Coupling between stationary and rotating pipe, G) Honeycomb, H) DC motor, J) Ball bearings, K) Rotating pipe, L) Circular end plate, M) Pipe outlet.

It is worth mentioning that many previous experimental studies (among others the often cited work by Wygnanski & Fiedler (1969), which became a benchmark and standard reference for both turbulence modellers as well as experimentalists) failed to fulfil the equations believed to govern the flow (see e.g. George 1990). As evinced by Hussein, Capp & George (1994) the discrepancies between existing experimental results concerning the far field are more facility-related and not mainly due to the measurement techniques involved. They showed e.g. that for Wygnanski & Fiedler's data the jet is rather a *confined jet* in a finite environment, for which conservation of mass demands that a return flow be set up around the outer edge of the facility. The effect of this return flow is to steal momentum from the jet so that the experiment no longer simulates a jet in a free environment. Here, however, we are only interested in the near field of the jet, so that despite the moderate distance to the floor ($\sim$ 18 pipe diameters) the jet can be safely considered to be a *free jet*.

As mentioned above an orifice flow meter is used to monitor the pipe flow rate. The pressure difference across the orifice is measured by a pressure transducer, which was calibrated against hot-wire measurements performed with a single-wire probe in the cold jet at different mass flow rates. Thus the voltage of

the pressure transducer is directly related to the axial bulk velocity and hence the *Reynolds* number, which is based on the bulk velocity and pipe diameter. Such an extensive calibration is not needed for the aim of the investigation presented here, because only measurements at a certain *Reynolds* number ($Re_D \simeq 24000$) were acquired. Nevertheless it was beneficial to know the deviation from the desired *Reynolds* number for changes due to variations in the thermophysical quantities. Furthermore the effect of *Reynolds* number on the axial decay of mean and root mean square values of the streamwise fluctuation was studied by means of *laser-Doppler velocimetry* (results are not shown here) in collaboration with Facciolo (2006).

To introduce a *passive scalar* in laboratory shear flows the jet or the pipe wall has to be heated weakly. To heat and maintain a heated rotating pipe at a certain temperature difference above ambient temperature would be an elaborate task. The related boundary conditions of either a uniform surface heat flux or a uniform surface temperature would also yield a 'saddle-back' temperature profile (i.e. the highest temperature would be at the pipe wall rather then in the centre of the pipe) of the jet which is evolving contrary to the streamwise velocity component in the near-field of the jet. Thus it is more advantageous to heat the air before entering the rotating pipe, which is done by placing an electrical heater (C) in the flow upstream of the distribution chamber. The heater power can be regulated and is typically around 800 W, which in consideration of the heat losses determines the temperature at the pipe outlet to be around 12 K above ambient temperature at the pipe outlet. This corresponds to approximately 250 W and the rest is heat losses to the environment. To check furthermore that the installation of the electrical heater does not alter the flow field and its turbulent structure the virtual identity of power spectral density of the streamwise velocity fluctuations were demonstrated at the pipe outlet.

Preliminary measurements of the temperature profile with thermocouples showed that to reach and maintain a steady temperature difference of 12 K between the flow in the centre of the pipe and the ambient air requires approximately three hours. By insulating the entire outer pipe surface with a 15 mm foam material the time to reach steady state conditions was drastically reduced as can be evinced through figure 4.3. To reduce the time needed to reach the desired operation temperature the heater was operated at 1000 W until the temperature at the centre of the pipe outlet corresponds nearly the desired temperature and then reduced to 800 W, which yields an excess temperature of approximately 12 K. Due to the ventilation far away from the pipe outlet the ambient temperature remains quite stable. Deviations of the order of 0.1 K occur hardly within an operational time of 24 hours. The temperature evolution at the pipe outlet (solid line) on the other hand clearly emphasises the quality of the experimental setup, i.e. it provides a constant temperature

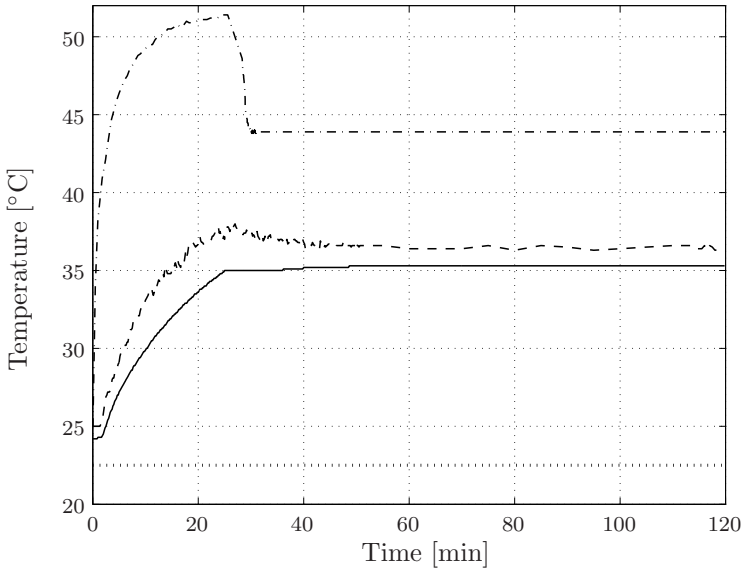

FIGURE 4.3. Thermocouple measurements of the temperature evolution during the heating procedure at different locations for the non-rotating pipe: ambient (dotted line), heater box (dash-dot line), pipe inlet (dashed line) and centre of the pipe outlet (solid line).

(within the measurement resolution of the thermocouples of 0.1 K) after approximately one hour, whereas the flow at the pipe inlet is highly turbulent upstream the honeycomb, as can be evinced from the dashed line in figure 4.3.

An additional advantage of the insulation is that it flattens the radial temperature profile compared with the uninsulated case and provides a wide area of the pipe outlet with a constant temperature and low temperature fluctuations, which will be exploited as a calibration jet for the temperature sensitive measurement probe.

To ensure that effects due to free convection can safely be neglected the *Grashof*[1] number,

$$Gr_D = \frac{g\beta\theta D^3}{\nu^2} \tag{4.1}$$

indicating the ratio of buoyancy force to the viscous force, has to satisfy the

[1]Franz Grashof (1826–1893), German engineer.

inequality $(Gr_D/Re_D^2) \ll 1$.[2] With a maximal excess temperature of 12 K the left hand side of the inequality is less than one percent and hence the temperature can be assumed to act only as a passive contaminant.

4.2. Hot-wire anemometry

The flow field was mainly examined by means of *hot-wire anemometry* (HWA), whereas preliminary measurements with *laser-Doppler velocimetry* (LDV) and stereoscopic *particle image velocimetry* (PIV) were initiated. The following paragraphs provide a deeper look into *hot-wire anemometry* and its application to the present flow case to both, make the reader acquainted with the applied measurement technique and provide details about the difficulties which arise during the acquisition of measurement data from a free jet emanating into quiescent air. The latter is of importance, because it provides crucial background information needed for the analysis of the measurements.

In spite of the fact that *hot-wire anemometry* is mainly dated back to King (1914), many scientists before him were familiar with the fact that a heated wire with temperature dependent resistance exposed in an air flow can be exploited to measure the fluid velocity.[3] Especially the research on cooling methods for conductors with their immense high temperatures due to the induced heating (see e.g. Oberbeck 1895) may have given the clue for the practical application of a conductor as a measurement instrument. The detecting element of a *hot-wire anemometer* consists of a very tiny tungsten or platinum (or its alloys) wire acting as the fourth arm of a *Wheatstone*[4] bridge, heated by an electrical current, which responds to changes in velocity and temperature of the fluid around the wire. The first practically functioning *hot-wire anemometers* consisted of about 10 cm long wires with diameters of a few tenths of a millimetre, whereas today platinum wires down to 0.25 micron in diameter in form of *Wollaston*[5] wires are available. However due to robustness reasons standard probe sizes around 1 mm in length and 5 micron in diameter are common in turbulence measurements.

Given a brief description of *what* a hot-wire is, the subsequent steps from the probe manufacturing over to the calibration of the used single and combined X-wire and cold-wire probes (from now on denoted as triple-wire probe) will now be presented in detail including the encountered problems during the application in the present flow investigation.

---

[2] If density variations are due to temperature variations only, which is assumed in the present case, the volumetric thermal expansion coefficient, β, can—for ideal gases—be expressed as the inverse of the absolute film temperature.

[3] According to Comte-Bellot (1976) King himself in a 1915 issued paper mentions preliminary experiments conducted by Shakespear in 1902.

[4] Sir Charles Wheatstone (1802-1875), British inventor.

[5] William Hyde Wollaston (1766-1828), English chemist.

4.2.1. *Probe manufacturing*

The hot-wire probes were built in house by following the steps outlined in Alfredsson & Tillmark (2005). The probe bodies are cylinders of ceramic tubes, which are used for insulating thermocouples, and consist of four and six holes for the single and combined X-wire and cold-wire probe, respectively. Piano wires with diameters of 0.4 mm and 0.3 mm were used as prongs for the single and triple-wire probe. The thinner diameter was chosen to reduce the spatial resolution as well as the thermal interference of the 6 prongs of the triple-wire probe, due to much thinner diameters and lengths needed for temperature measurements in order to minimise the thermal inertia and get access to the highest frequency fluctuations of the flow temperature.

As apparent from figure 4.4 the measurement cube was reduced by etching more than just the tip of the prongs in order to fit them into a thinner ceramic tube. This was necessary because piano wires thinner then 0.3 mm were not available. The tip of the prongs were etched using Nitric acid in order to obtain a conical shape with diameters around 50 micron and 20 micron for the single and triple-wire probe, respectively. These dimensions were selected to avoid prong vibrations, to reduce blockage of the flow as well as the development of the thermal boundary layers around the temperature sensor as much as possible. Especially in the present study, where high velocity gradients can be encountered near the pipe wall and in the region of the annular shear layer, the separation of the prongs has not only to be small to reduce the spatial resolution, but also as pointed out by Sandborn (1976) to ensure that the sensing elements are not subjected to large velocity gradients. A too small separation between the prongs however, would result in a not negligible sensor and prongs interference and thus the final design is a compromise. In the present study approved constructions of previous studies, like those of Wikström (1998) or Vukoslavčević & Wallace (2002), were taken as presettings and small adjustments due to outer prevailing conditions, viz. the relative position of the holes in the ceramic tubes, were made.

Platinum wire with a diameter of 1.27 micron is used for all sensors of the triple-wire, whereas the single-wire probe was equipped with a 2.54 micron wire. As shown in figure 4.4 the X-probe with sensor-planes parallel to the probe-stem consists of 0.8 mm long wires, whereas a 1 mm and 1.1 mm long wire was used for the single-wire probe and temperature sensor of the triple-wire, respectively. The parallel stem orientation was preferred instead of the X-probe with the sensor plane perpendicular to the probe-steam, due to the larger flow-angles the former is able to handle (see Bruun 1995, chap. 7). The resulting length-to-diameter ratio for the cold-wire was chosen in order to reduce end effects due to the heat loss through the prongs and to the development of thermal boundary layers around the prongs which in turn, see e.g. Paranthoën, Petit & Lecordier (1982), affect the temperature variance measurements. Antonia & Mi (1993)

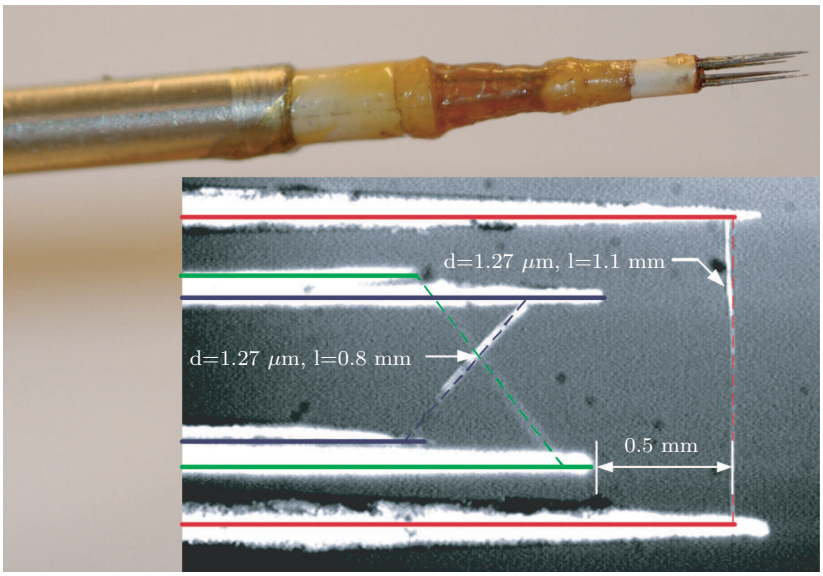

FIGURE 4.4. Combined X-wire and cold-wire probe with close-up of probe and wire constellation. The picture was taken several months after the performed measurements, which explains the traces of corrosion on the prongs. All wires are soldered to the tip of the prongs, which is not apparent from the two-dimensional microscopic picture.

recommend a wire with a length-to-diameter ratio greater then 700 to reduce these effects. A wire length-to-diameter ratio above 400, a low overheat ratio as well as a thinner hot-wire were experimentally shown to be more advantageous for measurements in near-wall regions and thus for low velocities by Chew, Khoo & Li (1998) as well as Durst, Zanaoun & Pashtrapanska (2001). The latter showed further that the wall becomes influential due to additional heat losses to the wall at $y^+ \leqslant 4$ giving rise to apparent higher velocities. We will tie in to near-wall effects and other restrictions in section 4.2.4.

Pure platinum wires were chosen due to their small diameters available in our laboratory[6], consequently they suffer in robustness compared with their rhodium or iridium alloys and especially with tungsten, but serve with a higher flow sensitivity, due to a higher temperature coefficient of electrical resistance. A small current was let through the sensing elements which was enough for the

[6]For the single hot-wire a 2.54 micron platinum + 10 % rhodium wire was used, which has a twice as high value for its tensile strength and serves very well as a temperature insensitive velocity probe, due to its less then half as large temperature coefficient of electrical resistance compared to its pure platinum counterpart.

wire to glow. This procedure is normally applied to burn away any contaminants from the etching and soldering processes, but it was found to increase the robustness of the sensing elements.

One of the main problems for multiple probes for the measurement of both velocity and temperature is their mutual thermal interference. In their search for a suitable position for a cold-wire relative to an X-wire Vukoslavčević & Wallace (2002) conclude that especially for high turbulence levels the cold sensor should be positioned upstream of the X-wire. This conclusion sounds anachronistic when earlier investigators (see e.g. Bremhorst & Bullock 1970 or Bourke & Pulling 1970) with similar motives placed the temperature sensitive wire likewise upstream the hot-wires, however the authors quantified and presented the error induced by the thermal wake of the hot-wires upon the cold-wire. Hishida & Nagano (1978) tested several probe configurations for a combined single hot-wire/cold-wire probe and demonstrated that the fluid velocity measured by the downstream hot-wire started to deviate significantly from the true velocity when the cold-wire was placed closer than 150 wire diameters. Bearing this in mind the cold-wire was placed 0.5 mm upstream and parallel between the two hot-wires of the X-probe.

4.2.2. *Basics of hot-wire anemometry*

There is a vast amount of scientific publications about *hot-wire anemometry* and its applications to various flow situations. Thus it would be redundant to repeat what has been published. Here, however, we will mention only what has relevance to the present investigation. For more details one is referred to classical books, like Hinze (1975), Perry (1982), Lomas (1986) and Bruun (1995) or to Vukoslavčević & Petrovic (2000) for multiple hot-wire probes.

The principle of a *hot-wire anemometer* is quite simple: We immerse for instance a wire with a temperature dependent resistance, $R(T)$, in an isothermal flow normal to the mean flow direction and let a current, I, through it, which results in a heated wire with a heating power of $P = I^2R$. Finally the heat loss through forced convection can be related to the effective cooling velocity, which one wishes to determine. If measurements with hot-wires were really as simple as outlined here, there were no need for thousands of publications[7] and 'plug and play' probes would rescue young scientists from sleepless nights.

The already mentioned heat loss due to conduction through the prongs as well as the natural convection, which becomes important at very low velocities, are two problems, which were neglected in our simple thought experiment. Fluid velocity and its direction will effect the cooling of the wire as will the thermophysical properties of the fluid. The latter can safely be assumed to be a constant in incompressible and isothermal flows, whereas our aim is to

[7]Fingerson & Freymuth (1996) mentions a number of over 2500 publications up to 1992 related to thermal anemometry techniques.

determine the former, i.e. the fluid velocity and its direction. Furthermore there are many other unstated assumptions in the abstract relations, which relate the cooling of the wire to the velocity components acting on the wire.

The first method and simplest way to utilise a *hot-wire anemometer* is by feeding the probe with a constant electrical current and then measuring the decreasing voltage, E, with increasing effective cooling velocity. This is commonly referred to as the *constant current anemometry* (CCA) and it is mainly restricted to low turbulence levels. Due to its poor frequency response it is nowadays mainly used for resistance thermometers as done in the present study. Ziegler (1934) integrated a feedback amplifier in the anemometer circuit to keep the resistance of the sensing element constant. The so obtained *constant temperature anemometer* (CTA) is the most common mode of operation and a frequency response up to several hundred kilohertz can be obtained.[8] In the present experimental investigation both the single wire as well as the X-wire were operated in the CTA mode. Exposing the hot-wire in a flow with increasing velocity would hence cause the wire to cool down, which in turn would lead the feedback amplifier to increase the voltage across the sensing elements in order to increase the current and thereby keep its temperature constant. Hence the relation between cooling velocity and voltage is opposite to what is observable in the CCA mode.

For the materials used normally in *hot-wire anemometry* the relation between the resistance of the heated wire, $R(T_h)$, and its averaged temperature, T_h, can be assumed to be a linear function, such that

$$R(T_h) = R(T_{ref})[1 + \alpha_{el}(T_h - T_{ref})], \tag{4.2}$$

unless the wire temperature exceeds 250 $^\circ C$, where higher order temperature terms become significant. Here T_{ref} is a reference temperature and α_{el} the temperature coefficient of electrical resistivity of the wire's material. Assuming that all heat transfer from the wire to the environment is due to forced convection the heating power can be related to *Newton*'s law of cooling

$$I^2 R(T_h) = Nu_d \, k_f \pi L(T_h - T_f), \tag{4.3}$$

where Nu_d denotes the *Nusselt*[9] number based on the diameter of the wire, k_f the heat conductivity of the fluid, L the length of the sensitive area of the

[8] Actually both modes of operation, i.e. the CCA and CTA mode, were already described by Simmins and Bailey in 1927 as reported in the review article by Comte-Bellot (1976). She also mentions publications by Riabouchinsky and Morris dating back to 1909 and 1912 describing the concepts of the CCA and CTA, respectively.

[9] Wilhelm Nusselt (1882–1957), German engineer.

hot-wire and T_f the temperature of the fluid to which the wire is exposed. To examine temperature effects the King's law[10]

$$Nu = A' + B'\, Re^n\,, \tag{4.4}$$

where A' and B' are calibration constants for a given ambient temperature, in combination with the heat balance, equation (4.3), can be utilised to obtain:

$$I^2 R(T_h) = E^2/R(T_h) = (A + BU^n)(T_h - T_f) = f(U)(T_h - T_f). \tag{4.5}$$

Hereby A, B and n are the constants of King's law. The right hand side of relation (4.5) is frequently utilised to compensate against temperature drifts of the ambient air as well as against changes in the fluid temperature itself as will be shown in the next paragraph.

An important quantity, which can be set by the user of the probe, is the temperature overheat ratio, a_T, and resistance overheat ratio, a_R, defined as

$$a_T = \frac{T_h - T_{ref}}{T_{ref}} \quad \text{and} \tag{4.6}$$

$$a_R = \frac{R(T_h) - R(T_{ref})}{R(T_{ref})}, \tag{4.7}$$

respectively. Hereby T_{ref} is a reference temperature normally chosen to be the ambient temperature during the velocity calibration. Attention should be paid to different definitions of the overheat ratio in the literature. Relations (4.6)–(4.7) as well as the ratio $R(T_h)/R(T_{ref})$ used by Bruun (1995) are all found in various publications and they are solely introduced as the overheat ratio. The selection of a certain resistance overheat ratio will thus determine the desired temperature overheat ratio, $a_T = a_R/(\alpha_{el}\, T_f)$, and determine the wire temperature under operation.

For the present measurements the resistance overheat ratio for the hot-wires of the triple-wire probe were set to 0.3, whereas the single-wire probe was operated at $a_R = 0.5$. The constant current of the cold-wire during operation was set to 0.3 mA. These values were found to be a good compromise between several requirements which will be mentioned during the next two sections.

[10] Although Collis & Williams (1959) extended relation (4.4) with n instead of one half it is usually still referred to as King's law. Furthermore they extended King's law to account for the temperature overheat ratio.

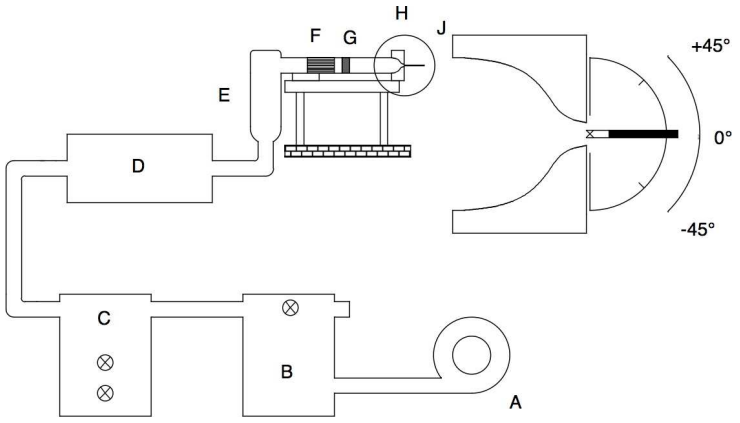

FIGURE 4.5. Schematic of the calibration jet setup. A) Fan, B) Settling chamber with seven valves, C) Settling chamber with two valves, D) Large stagnation chamber, F) Small stagnation chamber, G) Sponge, H) Contraction, J) Angular traversing mechanism for the X-probe.

4.2.3. *Calibration procedures*

In the present experiment, the scalar field of the jet was marked by a passive temperature differential, with the air in the jet slightly heated relative to the surrounding ambient air. In order to get simultaneous acquisition of the instantaneous velocity and temperature signals, a specific home made probe as described in section 4.2.1 has been designed and built. Two slanted wires yielding an X-probe, operated in the constant temperature (CTA) mode, to measure the streamwise and azimuthal velocity components are combined with a cold-wire, operated in the constant current (CCA) mode, positioned on the same probe for temperature measurements.

Due to the inherent turbulence intensity at the pipe outlet the velocity sensing wires are preferably not calibrated *in situ*, viz. in the centre of the pipe outlet. Moreover, a small deviation from the physical centre of the pipe would expose the wires to a nonzero streamwise velocity gradient and thus falsify the calibration. Hence the probe was calibrated for velocities in a special designed calibration jet facility.[11] The calibration device was used by Facciolo

[11] Antonia & Zhao (2001) calibrated their X-probe among a potential core of a contraction jet also at the exit of a fully developed turbulent pipe flow, which makes it difficult to compare results from both calibrations in situations where small differences in the measured variances are important. It is generally suggested to place the probe in a low turbulence intensity ($u_{rms}/U \lesssim 0.5\,\%$) flow (see e.g. Bruun 1995, chap. 4), due to the occurrence of squared mean averaged fluctuations in the relation to determine the effective cooling velocity as well as its *root mean square* (r.m.s.) value.

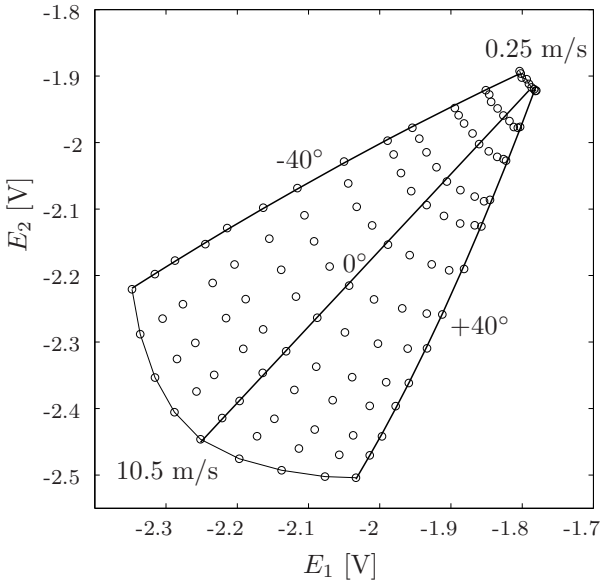

FIGURE 4.6. Example of a calibration plot for the X-wire consisting of 9 yaw-angles between $\pm 40°$ and 13 velocities between 0.25 m/s and 10.5 m/s.

(2006) and is sketched in figure 4.5. The probe was positioned in the potential core of a contraction jet, which was used to produce a 'top-hat' velocity profile and to achieve a laminar flow state at the nozzle exit. The two velocity sensing wires were calibrated according to the *look-up inversion method* (see e.g. Bruun 1995, chap. 5). The *look-up matrix method* for X-wire probes is a direct extension of the *look-up table method* for single-wire probes and was proposed by Cheesewright (1972), who calibrated the velocity vector and yaw angle against different velocities and angular positions, thus obtaining a unique voltage pair (E_1, E_2) for each velocity vector/yaw-angle pair $(\mathbf{U}, \alpha)$. Hereby it was ensured that the probe is oriented such that the third velocity component, the binormal or radial velocity component (W), equals zero. The measured velocity, the yaw angle and their corresponding voltages from the two CTA channels were registered for yaw-angles from $-40°$ to $40°$ in $10°$ intervals and more than 7 different velocities in the expected range. Figure 4.6 shows an example of such a calibration plot for the X-probe with 13 different velocities ranging from 0.25 m/s to 10.5 m/s.

Similar to Österlund (1999) the calibration data were curve-fitted using separate fifth-order polynomials for the sums and differences of E_1 and E_2 related to the velocity vector, $\mathbf{U}$, and the ratio of the azimuthal to axial velocity

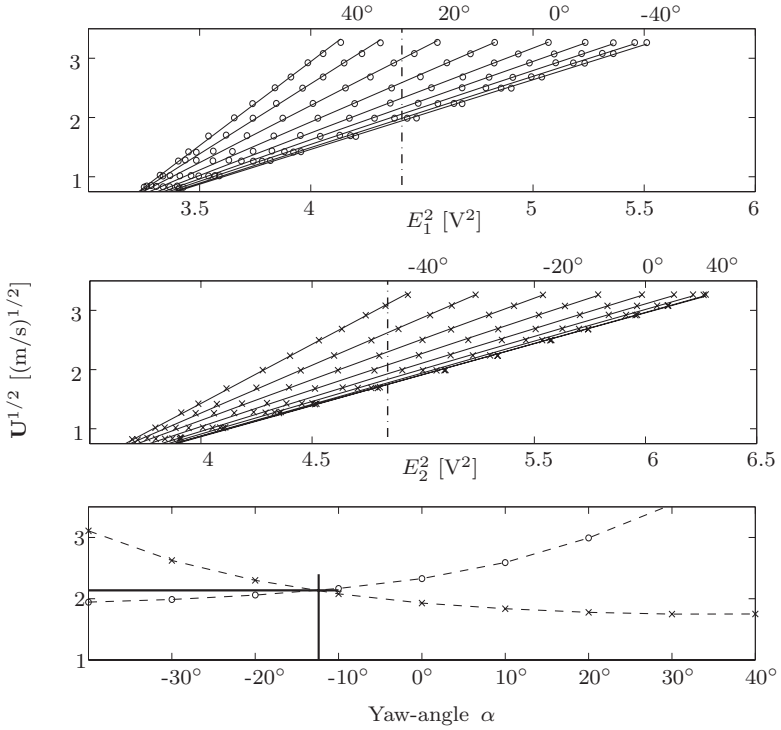

FIGURE 4.7. Illustrative method for the determination of the velocity vector **U** and the yaw-angle α for a voltage pair E_1 and E_2 using King's law.

component, $\tan\alpha = V/U$. Thereafter the 21 polynomial coefficients for **U** and $\tan\alpha$ were determined by a least-square method and stored for the evaluation programs.

To illustrate the computation for the determination of the axial and azimuthal velocity component a first-order polynomial based on King's law was utilised. A line corresponding to a set of two measured voltage pairs ($E_1 = -2.1$ V, $E_2 = -2.2$ V) is drawn into the calibration curves for the two hot-wires as illustrated in figure 4.7(a,b) and their crossing points with the individual calibration curves are determined. Plotting the obtained points in a separate diagram, figure 4.7(c), the value for the corresponding velocity vector and its yaw angle is obtained through their point of intersection. Finally the values for U and V can be evaluated from $(\mathbf{U}, \alpha)$ as

$$U = \mathbf{U}\cos\alpha \qquad V = \mathbf{U}\sin\alpha\,. \tag{4.8}$$

As pointed out by Moro, Vukoslavčević & Blet (2003) many researches report that the accuracy of the aforementioned relations becomes critical at low velocities and for small probes with limited length-to-diameter ratios. This can also be observed by the dense agglomeration of the calibration points and curves in the calibration plots for low velocities, figure 4.6 and 4.7.

Under conditions were the temperature of the calibration is the same as the isothermal flow of interest the aforementioned procedure would be sufficient to extract the velocity components from the X-probe measurements. This can easily be seen through relation (4.5), which states that the velocity signal is solely coupled to a velocity dependent function, *if* the wires are operated in the CTA mode, i.e. T_h is fixed, and the fluid temperature, T_f, is kept constant. However in temperature variable flows and even due to temperature drifts in the ambient air between the calibration procedure and the actual measurements the voltage output for the hot-wires must be compensated against changes in fluid temperature.

The voltage signals from the *hot-wire anemometer* channels were compensated for temperature changes through the well known relation

$$E_{out}(T_{ref})^2 = E_{out}(T)^2 \left(\frac{T_h - T_{ref}}{T_h - T} \right), \tag{4.9}$$

which was derived by considering the right hand side of equation (4.5) for both the temperature during the calibration of the X-probe and an elevated temperature to which the probe is exposed. The velocity dependency, $f(U)$, for both cases is assumed to be equal, due to the unchanged dynamics of the flow field.[12] $E_{out}(T_0)$ is the hot-wire response obtained for the same velocity under isothermal ($T = T_0$) conditions and $E_{out}(T)$ is the measured response from the anemometer output. Hence relation (4.9) provides the anemometer signal which would have been measured if the fluid around the hot-wire would have had the same temperature T_{ref} as during its calibration, whereas in reality it had temperature T. Combining the overheat ratios defined through relation (4.6) and (4.7) the wire temperature, T_h, and thus the compensated *hot-wire anemometer* voltage can be expressed though the resistance overheat ratio and the temperature coefficient of electrical resistivity,

$$E_{out}(T_{ref})^2 = E_{out}(T)^2 \left(1 - \frac{T - T_{ref}}{a_R/\alpha_{el}} \right)^{-1}. \tag{4.10}$$

The actual temperature is available as an instantaneous signal from the cold-wire and the resistance overheat ratio is default set by the user. Apparently the

[12] Recall that a *passive scalar* does not affect the turbulent velocity field while an *active scalar* affects the flow field.

temperature compensation can be performed without any complications, *if* the temperature coefficient of electrical resistivity is known. But exactly here lies the crux of the matter. As pointed out by van Dijk & Nieuwstadt (2004*a* and 2004*b*) in their detailed study concerning temperature and velocity calibration methods for (multi-) hot-wire probes most literature based estimates for the temperature coefficient of electrical resistivity are too high causing the heated wire temperature to appear lower and hence leading to an overcorrection of the *hot-wire anemometer* signal. Furthermore, even a small impurity of the level as small as 0.3 % iridium or rhodium, which can be found in 'pure platinum' used in *Wollaston* wires, is enough to cause a reduction of approximately 7 % in the value of α_{el} as found by Bradbury & Castro (1972).

The crystal structure of a raw hot-wire material will become less ordered every time it is going through tormenting processes, like during the process of making a spool of thin wire or through welding or soldering the wire to the prongs as well as the glowing for cleaning or strengthening reasons. The mentioned series of operations will lead to an increased resistance for electrons as reported by van Dijk (1999) and causes the value of the thermal coefficient of electrical resistance to lower remarkable. In an earlier attempt to apply a temperature compensation with values found in the literature (Bruun 1995, table 2.1) the measured axial velocity component in the heated swirling jet were overcompensated up to 40 % for the highest occurring temperature difference of 12 K.[13]

Many temperature compensation methods have been proposed over the years (see Bruun, chap. 7, for a review of methods for the measurement of temperature fluctuations as well as for correction methods for drifts in the fluid temperature, and Lekakis (1996), van Dijk & Nieuwstadt or Moro *et al.* (2003) among others for more recent accounts), but none of them were applied here. On the one hand the velocity calibration jet was not built for temperature calibrations, whereas the centre of the pipe outlet was not eligible for velocity calibrations due to its persistent velocity fluctuations as well as the fact that the velocity profile at the pipe outlet is not known *a priori*. In this experiment an iterative approach was followed in order to determine the value of the temperature coefficient of electrical resistivity.

In the evaluation process the coefficient to determine was decreased until the measured streamwise velocity profile of the triple-wire probe coincided with results from the single-wire probe in the cold jet, which are confirmed by the results from *laser-Doppler velocimetry* conducted by Facciolo (2006). The value for the temperature coefficient of electrical resistivity was tested at different radial and axial positions in the range of interest and it was confirmed that

[13]This high overcorrection is of course partially caused by the low resistance overheat ratio of 0.3 of the hot-wires.

even large changes in velocity and temperature are indeed insignificant for the determined value.

Before going over to describe the calibration of the resistance thermometer it is necessary to ensure that the temperature sensing wire is (within certain conditions) indeed insensitive to velocity variations. By partially differentiating the heat balance relation (4.5),

$$dE = \frac{\partial E}{\partial U}\, dU + \frac{\partial E}{\partial \theta}\, d\theta = e_U\, dU + e_\theta\, d\theta\,, \tag{4.11}$$

the variation in the *hot-wire anemometer* voltage can be decomposed into a velocity and temperature dependent term. Hereby e_U represents the velocity sensitivity and e_θ the temperature sensitivity. For a temperature sensing wire it is desirable to maximise e_θ and minimise e_U, whereas for a velocity sensing wire the opposite is aspired. The velocity and temperature sensitivity for a wire operated in the CCA mode can be shown to be (see e.g. Bruun 1995, chap. 2):

$$e_U^{\mathrm{CCA}} = -\frac{nBU^{n-1}R(T_h)^2\, I^3}{R(T_f)(a+BU^n)^2}\,, \tag{4.12}$$

$$e_\theta^{\mathrm{CCA}} = \frac{\alpha_{el}R(T_h)R_0\, I}{R(T_f)}\,. \tag{4.13}$$

Recalling that for the temperature measurements the current, I, is set to a very low value ($I = 0.3$ mA in the present case) it follows that $T_h \simeq T_f \simeq T_{ref}$ and hence $R(T_h) \simeq R(T_f) \simeq R_0$, so that the velocity sensitivity of the cold-wire ($e_U^{\mathrm{CCA}} \sim I^3$) is practically zero in the range of interest. On the other hand the temperature sensitivity ($e_\theta^{\mathrm{CCA}} \simeq \alpha_{el}R_0\, I \sim I$) for a constant current can safely be assumed to be a constant, which indicates the simple linear relationship between the change in temperature, $d\theta$, and the anemometer voltage, dE. It is worth mentioning that the ratio between the velocity and temperature sensitivity can be expressed (see e.g. Bruun 1995, chap. 7) as

$$\frac{e_U^{\mathrm{CCA}}}{e_\theta^{\mathrm{CCA}}} \propto -\frac{I^2}{d^2}\,, \tag{4.14}$$

which explains the need for extremely small wire diameters for temperature measurements.[14]

The temperature calibration took place in the centre of the pipe exit at the bulk velocity and the cold-wire was calibrated against thermocouples with a measurement resolution of 0.1 K. Due to the small diameter and the low

[14]Nowadays *Wollaston* wires down to 0.5 micron are commonly facilitated in temperature measurements. Here however due to the large length-to-diameter ratio given by the probe configuration a diameter of 1.27 micron was chosen to increase the robustness of the probe.

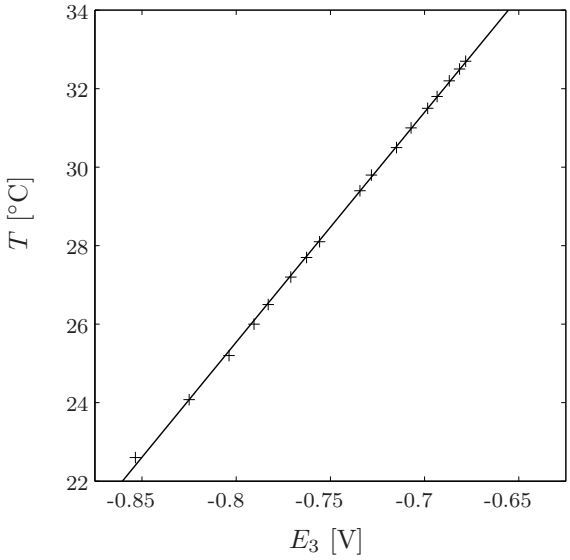

FIGURE 4.8. Example of a calibration plot for the cold-wire.

current through the cold-wire the anemometer output becomes a linear function of the fluid temperature as evident from relation (4.13) as well as one of the calibration curves shown in figure 4.8 and gains a high resistance against velocity variations. To check the validity of the velocity insensitivity of the cold-wire the velocity was changed and the measured temperature was compared against the thermocouples. The consistency was within the accuracy of the thermocouples. However at extremely low velocities, i.e. in the tail of the jet, the voltage from the CCA channel increases with decreasing velocity thus giving rise to an increase of the apparent temperature. This undesirable effect caused by the hot-wires placed downstream of the cold-wire could not be compensated for, so that the range of reliable measurements in the outer edge region, which inherently is effected by high *local* turbulence intensities, had to be shortened.[15]

[15]Preliminary measurements with a similar triple-wire probe with a resistance overheat ratio of 0.5 showed that for a large parts of the outer region of the jet the cold-wire was highly effected by the presence of the hot-wires. It should be noted that in the outer region of the jet a too high overheat ratio or a too close distance between the hot-wire and cold-wire can cause the appearance of spikes on the temperature signal due to the thermal wake of the hot-wire (Chevray & Tutu 1972). Instead of placing the cold-wire further upstream the resistance overheat ratio, a_R, was decreased to 0.3 in order to extend the region of applicability.

4.2.4. *Application to swirling jets*

The present measurements were conducted from the immediate vicinity of the pipe outlet up to 6 diameters downstream, with radial profiles consisting of up to 40 measurement points at every pipe diameter. Despite the fact that the investigated free jets are axisymmetric their full radial profiles were measured on both sides, to check the measurement accuracy especially for higher statistical moments and to have sufficient data to correct the physical centre of the jet, which might deviate from the geometrical centre at axial positions further downstream.

The signals from the CTA and CCA channels of an *AN-1003 hot-wire anemometry* system (AA lab systems) were offset and amplified through the circuits to match the fluctuating signal components to the voltage range of the analog/digital unit used, and then digitised on a personal computer using a 16-bit A/D converter at a sampling frequency of 4 kHz and an amount of 80000 to 200000 samples depending on the downstream position of the probe were collected. Besides the three voltage signals from the *hot-wire anemometer*, the voltage from the pressure transducer was recorded as well. This was done in order to check the constancy of the mass flow and leave open the possibility of analysing suspected time series, which by recalling that the swirling jet is extremely sensitive to disturbances might become important.

The *Reynolds* number of the isothermal jets (non-swirling and swirling) were set constant to 24000 by fixing the flow at the supply pipe checked by the orifice flow meter, whereas the swirl number was set either to zero or to 0.5 by adjusting the rotational speed of the pipe. In the case of both heated jets the flow rate through the supply pipe was not changed, and the pipe was rotated with the same rotational speed in order to keep the inlet conditions as similar as possible to the isothermal jets. Even though the fluid density, ρ, and dynamic viscosity, μ, changes slightly within 4 % and 3 %, respectively for the maximum local increase in temperature, the momentum flux remains nearly constant, due to the constant mass flux. The maximum decrease in the *Reynolds* number due to the addition of heat is restricted to 3 %, whereas the swirl number could maximally be 4 % lower. These slight variations are nevertheless within an acceptable tolerance, so that the *Reynolds* number as well as the swirl number will henceforth be stated as 24000 and 0.5, respectively.

The advantage of the combined X-wire/cold-wire probe in this type of flows is that it allows simultaneous measurements of instantaneous signals from the velocity components of interest and the temperature, thus providing *Reynolds* stresses and fluxes. Among others Rose (1962), Pratte & Keffer (1972), Mehta *et al.* (1991) and Elsner & Kurzak (1987) used *hot-wire anemometry* to measure all three velocity components as well as the corresponding *Reynolds* stresses. The latter provides also the temperature and the *Reynolds* fluxes. Here, however, only streamwise as well as azimuthal velocity components were measured

beside the temperature and thus only the corresponding *Reynolds* stresses and fluxes were accessed. The reason for this shortcoming is conditional due to the violation of the underlying assumptions for the *hot-wire anemometer* relations addressed in sections 4.2.2 and 4.2.3 applied in the complex flow field of a free swirling jet. During the calibration and subsequent signal analysis, it is necessary to demonstrate that there exists a unique relationship between the two voltages from the X-probe and the two velocity components or its velocity magnitude and flow angle, i.e. the ratio between the azimuthal and axial velocity component. Regardless the calibration method used to extract the velocity components from the voltage signals (including the *look-up inversion method* used here) it is normally assumed that the mean velocity component perpendicular to the axial and azimuthal velocity components is zero ($W = 0$) and its fluctuation is negligible ($w/U \ll 1$) (see Bruun 1995, chap. 5). Thus very accurate results can be obtained for a purely two-dimensional flow situation, which unfortunately does not exist in reality, unless the flow is laminar. Tutu & Chevray (1975) for instance demonstrated that errors in the measured *Reynolds* stresses can be as high as 28 % when the *local* turbulence intensity is 35 %.[16] However for many flow situations the first assumption of a zero mean velocity component is acceptable and thus for *local* turbulence intensities below 20 % the maximal error is below 2 % and 5 % for the (overestimated) mean streamwise velocity component and the (underestimated) *Reynolds* stress, respectively (Ovink *et al.* 2001). It is worth noting that these values are the maximum ones and do not necessarily occur. Ovink *et al.* (2001) presents a modified *look-up inversion method*, which includes the effect of the normally neglected third velocity component.

The aforementioned paragraph reveals that an X-probe can be used to compute all the velocity components and their *Reynolds* stresses *if* a certain tolerable error induced by neglecting the third velocity component is accepted. *Laser-Doppler velocimetry* measurements by Facciolo (2006) indicate that the mean radial velocity component in a swirling jet is always below 4 % of the bulk velocity, whereas its root mean square value is comparable with the azimuthal turbulence intensity and hence does not exceed a maximum of approximately 18 % of the bulk velocity. It becomes clear that for a swirling jet, where not only the turbulence intensity of the azimuthal velocity component is of the same order as the streamwise turbulence intensity, but also the mean azimuthal velocity is comparable with the streamwise velocity component, the rotation

[16] The term *local* turbulence intensity is used to emphasise that the root mean square velocity components are scaled with the local mean axial velocity component, rather then with the bulk or centreline velocity as it is usually done. The same is valid for the r.m.s. value of the *passive scalar*, where the excess temperature (above ambient temperature) is scaled with its local mean temperature difference, rather then centreline temperature difference. If not explicitly stated *turbulence intensity* refers to the r.m.s. values normalised by the bulk velocity and centreline temperature difference, respectively.

of an X-probe to acquire the instantaneous radial velocity component is highly impaired.

Furthermore it is worth mentioning that the edge region of a free jet emanating into air at rest is one of the worst cases to apply *hot-wire anemometry*, mainly due to the high *local* turbulence intensities with values above 100 % and the occurrence of instantaneous flow reversal. The former makes the instantaneous velocity components lie outside the probe acceptance angle with a high probability as reported in chapter 5 of Piquet (2001), whereas the latter falsifies the hot-wire signal due to the inability of the hot-wire to sense the flow direction.[17] Figure 4.9 and 4.10 shows hot-wire calibration plots for the X-wire with 2000 instantaneous sampled voltage pairs for different downstream and radial positions for the heated non-swirling and swirling jet, respectively. Following the evolution in streamwise or radial direction the evolution of the cloud of voltage pairs can be followed. Comparing the calibration plots from the non-swirling jet with those of the swirling jet indicates the shift towards higher velocities around the centreline at the pipe outlet as well as the increase in the covered region for the swirling case indicating a higher turbulence intensity. In spite of the aforementioned problems it is not unusual to find data from hot-wire measurements from the edge region of free jets issuing into quiescent air presented without mentioning their unreliability or alluding to *how* the large errors inherent in the measured values were avoided.

Using the acquired number of samples the fraction of data points outside the calibration map can easily be assessed. Table 2 presents the radial positions where approximately 1 % and 4 % of the voltage pairs are outside the calibration domain. The radial positions can be utilised to assess the reliability of the results presented in the next chapter, especially for the higher moments.

Before *laser-Doppler velocimetry* was available[18] or suitable for measurements in turbulent flow it was common to rotate the X-probe (or a single slanted wire if no simultaneous acquisition of velocity correlations were aimed) 90 degrees about the x-axis as done by Rose (1962) or Pratte & Keffer (1972) in order to access the third velocity component, even though the assumption for a zero mean velocity for the third velocity component was violated. Therefore radial velocity components and associated *Reynolds* stresses measured in swirling jets with hot-wire probes consisting of one or two sensing elements as

[17] A reliable exception is the pulsed wire technique (thoroughly explained in Bradbury & Castro 1971).

[18] The first laser-Doppler measurements were performed by Yeh & Cummins (1964).

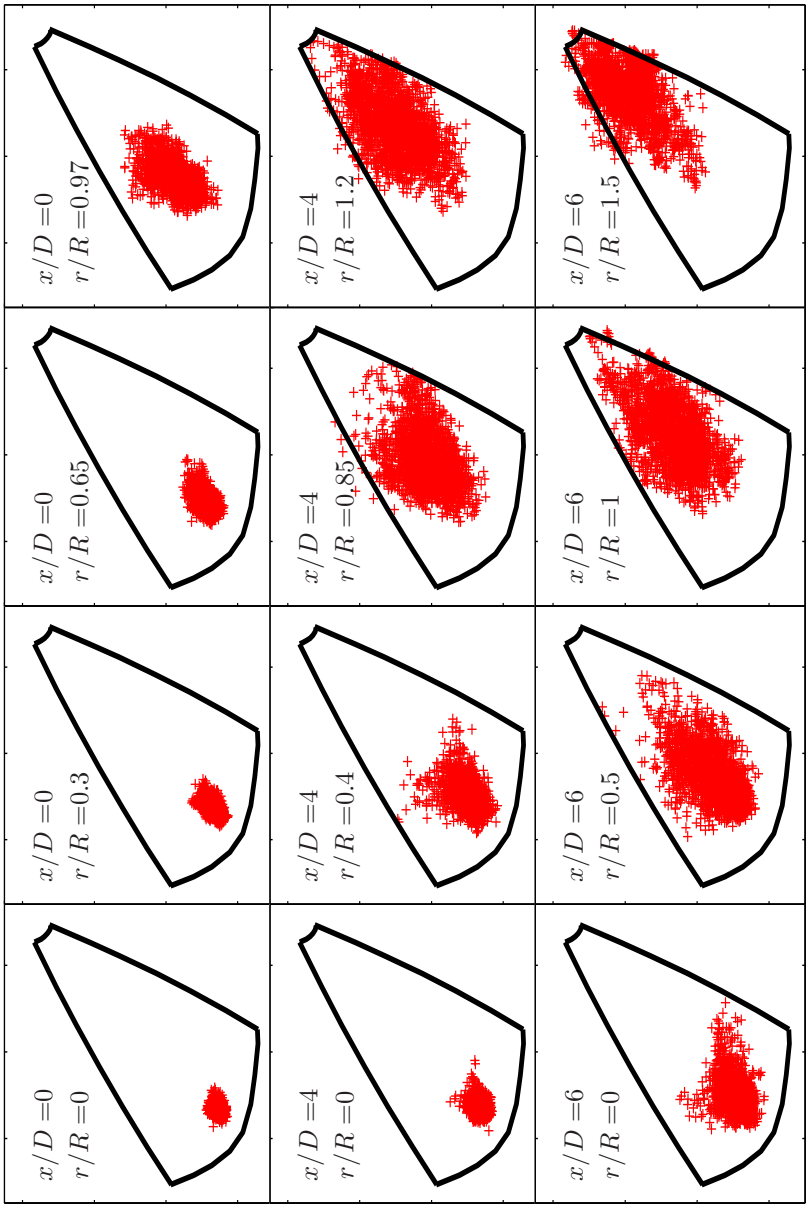

FIGURE 4.9. Hot-wire calibration plot for the X-wire with instantaneous measurement data for the heated non-swirling jet for different axial and radial positions.

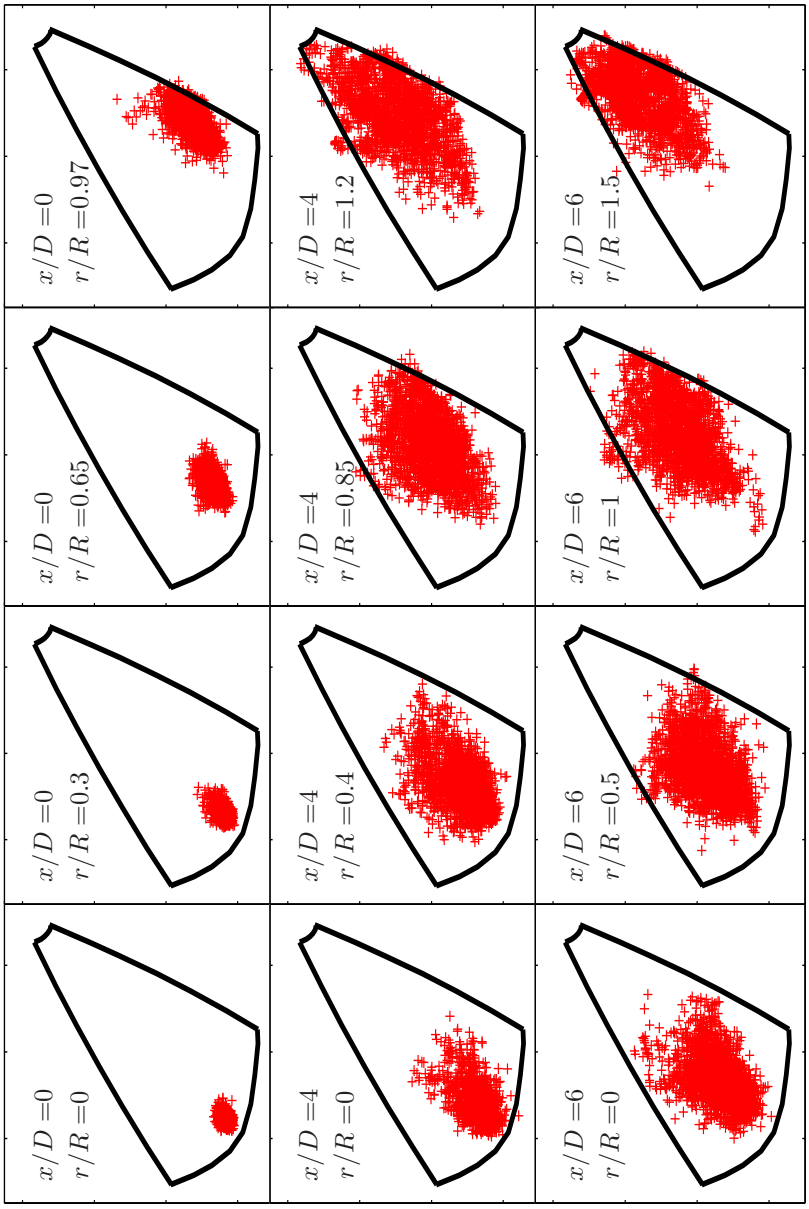

FIGURE 4.10. Hot-wire calibration plot for the X-wire with instantaneous measurement data for the heated swirling jet for different axial and radial positions.

	r/R			
	$S = 0$		$S = 0.5$	
x/D	1 %	4 %	1 %	4 %
2	1.00	1.20	0.90	1.25
3	0.90	1.30	0.90	1.25
4	1.10	1.30	0.95	1.35
5	0.90	1.40	1.00	1.30
6	1.10	1.40	0.90	1.55

TABLE 2. Radial positions where 1 % and 4 % of the measured voltage pairs are outside the calibration map for the heated non-swirling and swirling jet.

done by Mehta *et al.* (1991) and Elsner & Kurzak (1987) are questionable, unless the method used to overcome the uniqueness problem is made clear.[19] Here only the instantaneous axial and azimuthal velocity components were measured simultaneously besides the temperature signals.

[19] Even a three-wire probe could be insufficient and therefore it has been suggested that a four-wire probe can increase the uniqueness domain of the velocity-vector solution in comparison (Bruun 1995, chap. 6). This would extend the region of capability in the free swirling jet to measure the radial velocity component at the same time as the axial and azimuthal velocity components.

CHAPTER 5

Results and discussion

"If you torture data sufficiently,
it will confess to almost anything."

Fred Menger (1937–)

"The idea is to try to give all the information to help others to judge the value of your contribution; not just the information that leads to judgment in one particular direction or another."

Richard Phillips Feynman (1918–1988)

Having presented the theoretical background of swirling jets in chapter 2 the experimental results obtained from the combined X-wire and cold-wire probe are now illustrated and discussed in light of the previous works and the restrictions of the measurement technique reviewed in the previous chapter. Following the quotes above we will "torture" the obtained measurement data as much as possible in order to assess the effect of rotation on the dynamic and thermal flow fields and leave over what we have not been able to interpret at this stage.

The experiments were conducted at a *Reynolds* number of 24000 based on the cross-sectional mean velocity (or bulk velocity) of 6.0 m/s and the pipe diameter, meaning that the flow rate was maintained at a constant value for all of the non-swirling and swirling cold and heated jets. The swirl number was fixed for both the cold and heated jet at $S = 0.5$, i.e. the wall azimuthal velocity, V_w, was set equal to half the bulk velocity. This corresponds to a rotational speed of the pipe of about 16 revolutions per second. The measurements were started at $x/D = 0$ with an increment of one diameter up to $x/D = 6$. Full radial profiles of the axial and azimuthal velocity components as well as the temperature were acquired. Results from the tail of the jet with streamwise mean velocities below 0.5 m/s are not presented here, due to their inherent errors.

The results from the cold jet are not presented here, but were used to verify the heated jet measurements, i.e. to check the reliability of the temperature compensation method and the influence of the *passive scalar* on the dynamics of the flow. The results showed that the temperature compensation method

was accurate and that no influence on the velocity field by the *passive scalar* could be detected.

Also in "cold" jets there is often a temperature difference between the jet air and the ambient air due to heating of the air through the fan, the supply pipes or channels or by means of dissipative effects inherent in the flow. In the present work the mean temperature of the non-swirling jet was about 1 °C above the ambient air and in the case of the swirling jet about 2 °C. Especially in studies where one is interested in the gross effects of rotation on the mean quantities, such as time-averaged velocity components or their turbulence intensities it is crucial to take precautions that the effect of temperature variations on the velocity sensors are compensated for. The present measurements in the cold jet indicate that mean velocity components as well as their root mean square values may be underestimated up to 12 % and 8 %, respectively, when neglecting the temperature changes across the jet for the measurement position with the highest temperature difference in the swirling jet.[1] Thus it is important to report not only the probe configuration and its calibration method, but also *if* and *how* temperature drifts where taken into consideration.

Hereby we close the excursus concerning temperature variations in hot-wire measurements outside temperature controlled environments and lead over to the results from the heated jet. The following sections deal with the mean flow development as well as that for the passive contaminant. To elucidate the structure of the flow in more detail an account on higher moments and integral time scales conclude this chapter.

Finally it should be noted that although the measurements at the pipe outlet represent a fully developed turbulent (rotating) pipe flow it is not the aim of the present study to investigate this deeply, rather it provides accurate and well-defined exit conditions for the jet to be analysed. For an account on fully developed turbulent (rotating) pipe flow the reader is referred to Facciolo (2006), who provides an extensive study by means of *hot-wire anemometry*, *laser-Doppler velocimetry* as well as *direct numerical simulations* (DNS).

In the following we present results from both the non-swirling and swirling jets in all figures where appropriate in order to facilitate comparisons between the two cases.

[1] The observed high underestimation is mainly due to the low resistance overheat ratio, a_R, selected for the triple-wire measurement probe. X-wires with their common value of $a_R = 1.5$ and single-wires with even higher wire temperatures can reduce the underestimation drastically. However, for measurements in the outer region of the jet, i.e. outside the jet half-width or far downstream in the developing or far-field region, the discrepancy between the measured and real velocity components increases giving rise for misinterpretations of the effect of rotation.

5.1. Mean flow development

5.1.1. *Velocity and temperature profiles*

Mean axial velocity and temperature profiles for the pipe outlet, four diameters downstream and the farthest measured downstream position, $x/D = 6$, are shown in figure 5.1 and 5.2. The time-averaged values were normalised using the bulk velocity, U_b, and the centreline mean temperature (relative to ambient) at the pipe outlet of the non-swirled jet, $\theta_{0,S=0}$, in order to emphasise the effect of the rotation on both the flow dynamics as well as the passive contaminant. In the following T and θ will be used to denote the actual temperature and the temperature excess above ambient, respectively, whereas the subscript 0 stands for the centreline value at the pipe outlet. The radius is non-dimensionalised by the pipe radius, R, rather than the velocity or temperature half-widths as usually done in investigations concerning jets in the self-preserving region.

The left side of figure 5.1 presents the mean axial velocity component for the non-swirling jet, whereas the right side of the figure shows the values for its swirling counterpart. The streamwise velocity component at the pipe outlet (or more precisely: 1 mm from the exit in order to prevent probe damage for the rotating pipe where slight vibrations are unavoidable) coincide very well with the empirical power-law profile $U/U_{0,S=0} = (1 - r/R)^{1/7}$ (see e.g. Schlichting 1979, chap. 20), confirming that the flow upstream from the pipe exit resembles a fully developed turbulent pipe flow (Xu & Antonia 2002*a*). Further downstream the streamwise centreline velocity decays, whereas in the outer region, i.e. the region beyond the pipe radius ($|r/R| > 1$), it increases. The addition of swirl to the pipe flow clearly shows an increase of the velocity in a core region as large as $0.75 \leqslant |R|$ while the velocity close to the wall decreases. This effect results in a decrease of the shear stresses at the wall as can be evidenced by experimental studies (see e.g. Kikuyama *et al.* 1983) as well as *direct numerical simulations* (see e.g. Satake & Kunugi 2002) on axially rotating pipe flows with stronger rotations and leads to an overall decrease of the pressure-drop.

Moving downstream the additional rotation decreases the streamwise velocity at the jet axis and conversely increases the one in the outer part of the mixing layer, i.e. for radial distances larger than the pipe radius. As evident from the streamwise velocity profiles the increased velocity is sustained up to 4 pipe diameters downstream when compared to the non-swirling jet and decays then rather quickly loosing up to 30 % of its initial centreline value at 6 diameters downstream. A common crossing point around the pipe radius is observable for both the jet with and without rotation for all downstream positions measured. Additionally results from *laser-Doppler velocimetry* measurements performed by Facciolo (2006) in the same facility and under the same conditions (but for the cold jet) are illustrated through dashed lines for the pipe outlet as

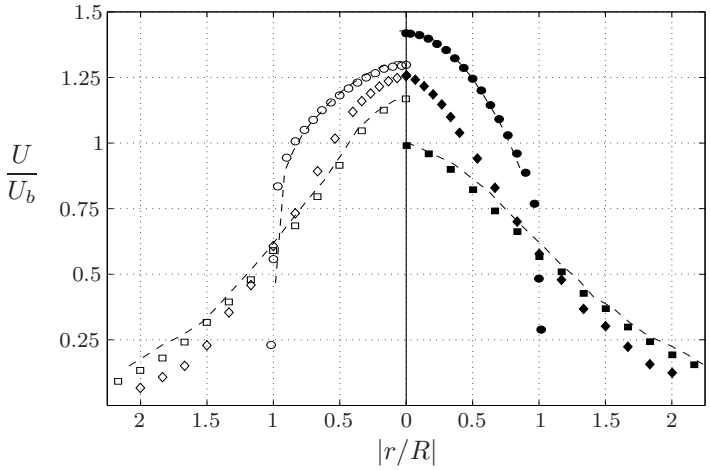

FIGURE 5.1. Mean axial velocity across the heated non-swirled (left side, open symbols) and swirled (right side, filled symbols) jet for three downstream positions: ○: $x/D = 0$, ◇: $x/D = 4$, □: $x/D = 6$. LDV results for a non-heated jet at the same Re from Facciolo (2006) for $x/D = 0$ and 6 are illustrated through dashed lines.

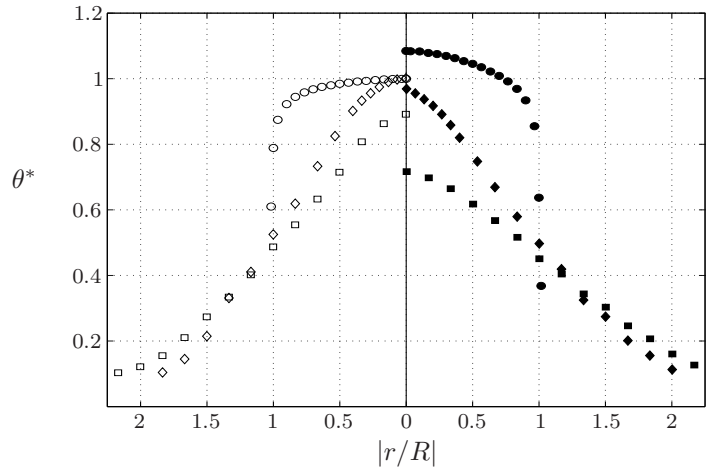

FIGURE 5.2. Mean temperature across the heated non-swirled (left side, open symbols) and swirled (right side, filled symbols) jet for three downstream positions: ○: $x/D = 0$, ◇: $x/D = 4$, □: $x/D = 6$.

well as 6 diameters downstream for comparison and indicate the quality of the used measurement technique for the entire region of the present investigation.

The mean temperature profiles for the same downstream positions as selected for the axial velocity component are presented in figure 5.2. Similar to the streamwise velocity component a non-dimensionalised temperature,

$$\theta^* = \frac{T - T_\infty}{T_{0,S=0} - T_\infty} \tag{5.1}$$

was introduced, where $T_{0,S=0}$ denotes the centreline mean temperature at the pipe outlet for the non-swirling case and T_∞ denotes the ambient temperature. The uniformity of the radial mean temperature profile at the pipe outlet is a result of the insulation along the entire pipe length. For $|r/R| < 0.7$ the maximum deviation from the centreline value is 0.03. By insulating the pipe to reduce the heat losses two objectives are reached; a more uniform temperature distribution and a shorter time needed to reach thermal steady state conditions. Furthermore the cold-wire probe is calibrated for temperature at the pipe exit and a uniform temperature across the probe is thereby ensured.

The addition of rotation shows the same effect on the *passive scalar* as it shows on the streamwise velocity component, i.e. especially the increase of temperature in a central core region and the faster axial decay of its centreline value. In contrast to the streamwise velocity component the centreline mean temperature for the swirling jet falls below the value of its non-swirling counterpart before 4 diameters downstream.

The observed increase in the temperature across a wide central region of the cross-sectional area of the pipe can be ascribed to the *Reynolds analogy*[2], which relates the heat transfer towards the wall to the wall shear stress. By rotating the pipe the streamwise velocity component in the central region increases and hence it has to decrease in the near-wall region in order to fulfil mass conservation. As a consequence the skin friction decreases. *Reynolds analogy* demands a proportional decrease in the convective heat transfer at the wall, i.e. the radial temperature gradient at the wall decreases. Thermocouple measurements at the pipe inlet ensured that the incoming flow remained at a constant temperature regardless of any change in rotational speed of the pipe. Hence the reduction of the heat transfer towards the pipe wall has to result in an increase of the axial flux of heat. The evaluation of the integral relation governing the *passive scalar* (as will be done in section 5.1.2) can be utilised to confirm this conclusion. The same effect, but not as clear, was also observed by Komori & Ueda (1985) in their axially rotating pipe with a divergent pipe

[2]Although the correct derivation of the *Reynolds analogy* is based on a zero pressure gradient as well as a *Prandtl* number of unity, we are rather interested in qualitative trends then in qualitative figures. Furthermore in turbulent flow the requirement of a zero pressure gradient is not as important as in laminar flow.

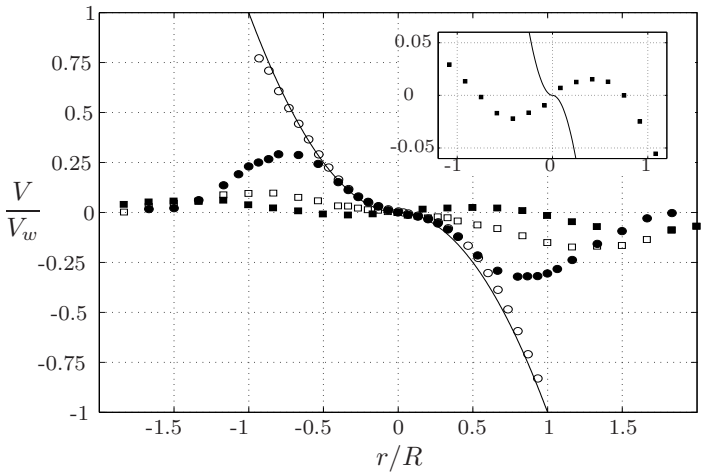

FIGURE 5.3. Mean azimuthal velocity across the heated swirled jet for four downstream positions: ○: $x/D = 0$, ●: $x/D = 2$, □: $x/D = 4$, ■: $x/D = 6$. Solid line represents a parabola $(r/R)^2$. Counter-rotating core is enlarged in the close-up.

exit for moderate swirl numbers.[3] It should be pointed out that the change in the temperature distribution when rotation is induced is almost observed immediately, which shows that this is an effect of the changing flow and not an effect of changed initial and boundary conditions.

It is interesting to mention the *vortex tube*[4] in this context and distinguish it from the observed aforementioned change in temperature. A *vortex tube* is a device without any moving parts which separates compressed gas into a stream of hot (warmer then the incoming air) and cold (colder then the incoming air) gas simultaneously. Highly compressed air is introduced tangentially into a tube open at one or both ends generating a swirl velocity approaching sonic velocity. Contrary to what is observed in the rotating pipe flow the outer region is found to be warmer and the central region to be colder then the incoming air. However in swirling jets generated by tangential injection of compressed air as done for instance by Naughton, Cattafesta & Settles (1997) (with a maximal azimuthal velocity component around 100 m/s) the *vortex tube* effect can be observed at the outlet of the orifice.

[3]For the case of strong swirl with reverse flow at the pipe outlet the temperature excess above ambient is decreasing and falls below the value of the non-swirling case.

[4]G. J. Ranque, a French physics student, invented the *vortex tube* while experimenting on a vortex pump in 1928 and R. Hilsch, a German physicist, rediscovered it in 1945. To gain an insight into the so-called *Ranque-Hilsch vortex tube* the reader is referred to *Universe of Atoms, an Atom in the Universe*, by M. P. Silverman.

Figure 5.3 shows the downstream evolution of the mean azimuthal velocity component scaled with the rotational speed of the pipe, V_w, for the present swirl number of 0.5. A parabola, $V/V_w = (r/R)^2$, is plotted in the figure to show that the azimuthal velocity component in the case of a rotating pipe flow is close to parabolic and, as mentioned in the review in section 3.4, is not in solid body rotation. Moving downstream the azimuthal velocity component in the outer part deviates from the parabolic shape in order to fulfil the boundary conditions enforced by the ambient air at rest. The figure shows the rapid decay of the swirl strength: only 30 % of the maximum azimuthal velocity component are retained after two diameters downstream. The position of the maximum of the azimuthal velocity component moves with increasing distance from the pipe exit first slightly towards the centreline and then radially outwards.

Another feature of a swirling turbulent jet issuing from a rotating pipe flow is evident from the close-up in figure 5.3, namely the counter-rotating core, which was first reported by Facciolo & Alfredsson (2004), who observed this unexpected characteristic of the flow through HWA and LDV as well as by means of DNS. The amplitude of the maximal azimuthal velocity component in the counter-rotating core should be considered with caution, due to the extreme low velocities associated with it. Indeed the mean radial velocity component in the region of occurrence of the counter-rotating core is of comparable magnitude: its maximum is geometrically around 1–1.5 pipe radii at 6 diameters downstream (Facciolo 2006). Nevertheless it is clear that the core rotates opposite to the rotational direction of the pipe.

Three-dimensional profiles of the mean axial velocity component and mean temperature are visualised in figures 5.4 and 5.5, thus making it possible to follow the evolution of the mean quantities along their radial and axial directions at the same time. Solid lines expressing *Gaussian*[5] distributions fitted through the measurement points are plotted for visual aid. Thick dashed lines are drawn through the centreline values (U^*_{CL} and θ^*_{CL}) as well as through the half-widths (R_U and R_θ) of the streamwise velocity component and temperature, representing the position where the considered quantity reaches half the value of its centreline value. The former depicts the axial decay rate and is hence an indication of the mixedness[6] while the latter facilitates the presentation of the spreading of the jet and hence visualises the entrainment rates for both the momentum (black lines) and heat (grey lines), respectively. Black lines in the radial direction correspond to the jet with swirl, while grey lines visualise the quantities for the non-swirling jet.

[5] Carl Friedrich Gauss (Gauß) (1777–1855), German polymath.

[6] It is important to note however that a faster axial decay does not necessarily indicate mixing enhancement. A faster axial decay might also be brought about by engulfing more unmixed fluid (e.g. ambient air at rest, colder air or a fluid with a low concentration) appearing or crossing the centreline (Mastorakos, Shibasaki & Hishida 1996). Hence additional indications from flow visualisations or higher order statistics have to be consulted.

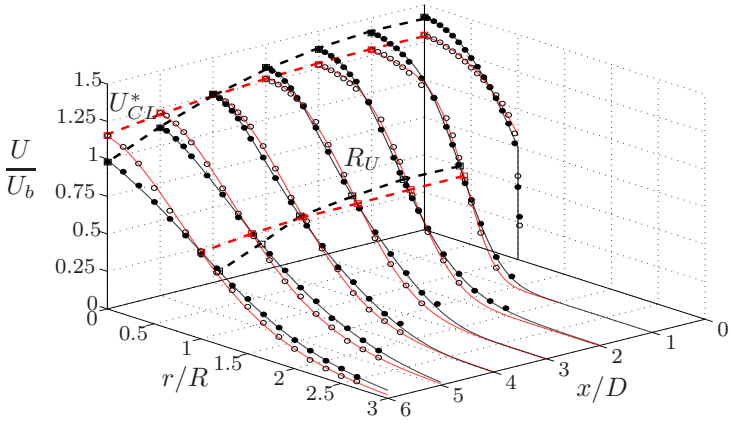

FIGURE 5.4. Three-dimensional profile of the mean axial velocity for the non-swirled (open markers) and swirled (filled markers) jet. Axial decays (U^*_{CL}) and mean velocity half-widths (R_U) are illustrated through the dashed lines. Full lines are for visual aid only.

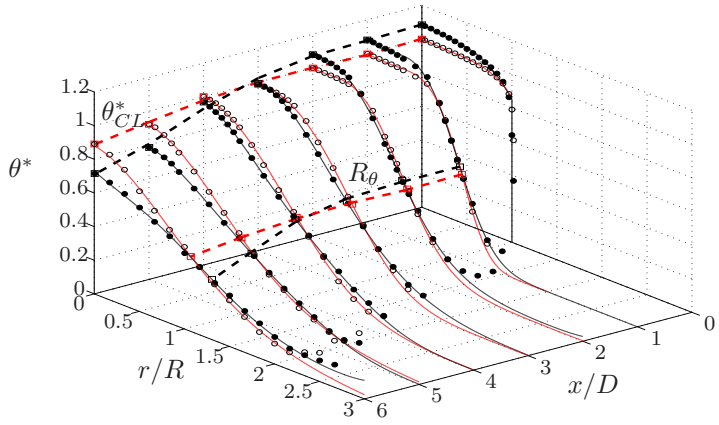

FIGURE 5.5. Three-dimensional profile of the mean temperature for the non-swirled (open markers) and swirled (filled markers) jet. Axial decays (θ^*_{CL}) and mean temperature half-widths (R_θ) are illustrated through the dashed lines. Full lines are for visual aid only.

A recognisable feature of the thermal field, observed in figures 5.2 and 5.5, is that its centreline value remains almost constant for downstream positions up to four pipe diameters, whereas the centreline streamwise velocity component decreases (weakly) continuously right from the beginning of the pipe outlet. Therefore one could define a *thermal* 'potential core' extending to four pipe diameters, whereas no *dynamic* 'potential core' exists by definition.[7] The different boundary conditions for the temperature (as evident from its mean and turbulence intensity profiles: almost uniform mean temperature profile and very low fluctuation level) and velocity (zero velocity at the wall, fully developed pipe flow axial velocity profile and a higher fluctuation level) can be used to explain this behaviour. Recalling that the initial thermal field resembles an almost uniform velocity profile, which exists for streamwise velocity components at nozzle outlets, the existence of a 'potential core' region becomes apparent.

Returning to the three-dimensional mean axial and temperature profiles it is clearly recognisable that the addition of swirl increases the mean streamwise velocity as well as the mean temperature for the first diameters downstream of the pipe outlet while in regions beyond three and four diameters downstream the axial velocity component and temperature are overtaken by the non-swirling centreline values, thus indicating the faster axial decay rates through the addition of swirl. It is an established experimental fact that rotation increases the spreading rates for both momentum and heat, as is clear from the strong curvature of the lines representing the half-width velocity and temperature values starting from approximately four pipe diameters downstream.

No difference between the spreading rates for momentum and heat can be detected for the first diameters. One may however assume from the position of the mean velocity and mean temperature half-width values (by drawing a vertical line from the half-width value down to the corresponding downstream position and reading off the radial position) that the *passive scalar* spreads faster than its corresponding streamwise velocity component. These differences are hard to recognise, but are detectable. Similar observations have been made in the near- and far-field of a free jet in the experimental study and *direct numerical simulation* of Drobniak, Elsner & El-Kassem (1998) and Lubbers, Brethouwer & Boersma (2001), respectively. The former reports a 20 % higher value for the temperature half-width value when compared to its dynamic counterpart at $x/D = 4$ in a jet issuing from a nozzle. This is in accordance with

[7] The term 'potential core' or 'potential cone' is quite frequently used in the literature concerning jets and denotes the region at the exit of the nozzle, which comprises a potential region of laminar or irrotational flow. The shear layer initiating from the nozzle edge in this region has not yet expanded to the centre of the jet, thus giving rise to a region of a uniform mean streamwise velocity component, which is independent of the streamwise coordinate, x. Hence it would be inappropriate to use the term for turbulent flows, which is present for instance at the outlet of a fully developed turbulent pipe flow, or for swirling jets in general except they exhibit a free vortex.

the experimental fact that, for both the *passive scalar* and the streamwise velocity component, the jet emanating from a nozzle spreads faster than the one emanating from a pipe (see e.g. Mi, Nobes & Nathan 2001 for the *passive scalar* and Xu & Antonia 2002*a* for the streamwise velocity component).

However a new observation is that for the case of rotation the half-width for both the mean streamwise velocity component and temperature experience a slight decrease compared to their non-swirling counterparts reaching a minimum around $x/D = 2$. Hence the swirling jet emanating from a fully developed turbulent pipe flow seems to bundle before it spreads in a larger angle.

5.1.2. *Flow entrainment and conservation of momentum and heat*

One of the features, which make the addition of swirl to a turbulent jet profitable, is its enhanced *entrainment*. The turbulent and thus rotational (vortical) motion convected from the pipe flow into the still ambient surroundings is restricted to a limited region within a large non-turbulent and hence irrotational reservoir. This limiting boundary is sharp and irregular (and not steady and regular as one would extract from figure 2.1) and plays a major role in the entrainment process, contrary to the laminar jet where viscous diffusion is the cause (see e.g. Tritton (1988), chap. 21 or Townsend (1976), chap. 6). The convoluted boundary of the turbulent jet is radially spreading with downstream evolution and continually engulfs irrotational fluid, which explains the increased mass flux. The entrainment is usually expressed through the ratio of volume or mass flux normalised with its initial value at the orifice. Integration of the streamwise velocity component times its radial position across the azimuthal-radial plane yields the volume flux, Q, (or its mass flux if multiplied with its density) at a certain downstream position.

The entrainment coefficient, Q/Q_0, for the non-swirled and swirled jet is shown in figure 5.6. The volume flux coming from the pipe is hereby denoted with Q_0. The jet without rotation reaches twice its mass flow after 6 pipe diameters for the *Reynolds* number of 24000. This trend agrees very well with the results by Boguslawski & Popiel (1979) from a stationary pipe with a length of 50 D presented through a dashed line in figure 5.6. Results from jets emanating from the stationary and rotating pipe in the experiments by Rose (1962) show however deviations from the present experiments. Unfortunately, neither of the authors mentioned their *Reynolds* number for which they computed the entrainment coefficients.[8]

[8]The *Reynolds* number of the mentioned jets emanating from pipes can however be estimated to be less than half as large and at least twice as large as the present *Reynolds* number for Rose (1962) and Boguslawski & Popiel (1979), respectively. Facciolo (2006) reports a decrease in the entrainment coefficient with increasing *Reynolds* number, whereas Pitts (1991) reports a threshold value of approximately 25000 to remove the effect of *Reynolds* number dependence on the entrainment behaviour. This might explain the good agreement with the data of Boguslawski & Popiel, but not the deviation with those of Rose. Nevertheless the swirling

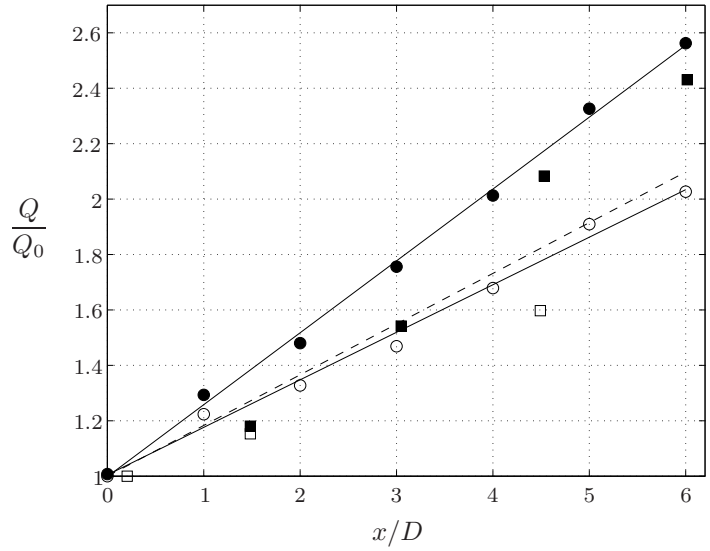

FIGURE 5.6. Downstream development of the entrainment coefficient for the non-swirled (open symbols) and swirled jet (filled symbols). ○: Present data (full lines are for visual aid only), □: Rose (1962), −−: Boguslawski & Popiel (1979).

As indicated in section 3.1 pressure gradients play a minor role in the near-field of a non-swirling jet. The addition of swirl however intensifies the radial and axial pressure gradients, which in turn influences the dynamics of the flow. This gave up to five times higher entrainment rates in the case of Park & Shin (1993) for strong swirl. Hence it is not surprising that the swirl strength is directly related to the rate of entrained air. This is in good agreement with other unbounded and wall-bounded free shear flows, where flow deceleration or an axial adverse pressure gradient increases entrainment as well as mixing (Sreenivas & Prasad 2000).

The differences in the entrainment rates in figure 5.6 may be due to the difficulties in acquiring reliable data in the region of low velocity and/or high *local* turbulence intensity. Another uncertainty arises when integrating over discrete mean streamwise velocity components in the tail region of the jet, which are weighted by the radius. The scatter in the computed entrainment rate was reduced by fitting *Gaussian* curves through the points in the outer region of the jet. Despite this problems the downstream evolution of the entrainment

jet results by Rose (1962), beyond $x/D = 4$, agree better than those in the vicinity of the pipe outlet.

	M_x [N]		M_θ [kW]	
x/D	$S = 0$	$S = 0.5$	$S = 0$	$S = 0.5$
0	0.138	0.138	0.230	0.244
2	0.135	0.135	0.220	0.224
4	0.141	0.139	0.226	0.218
6	0.131	0.141	0.205	0.211
mean	0.134	0.139	0.214	0.220
std	0.005	0.003	0.012	0.016

TABLE 3. Axial fluxes of the first-order approximation of the integral expressions of momentum conservation as expressed through equation (2.26) and (2.30).

coefficient clearly depicts the increased rate of mass in the case of the swirling jet, doubling its mass flow already at four diameters downstream.

Another important check of the reliability of the measurement technique is to verify whether the obtained time-averaged quantities fulfil the governing equations. The integral relations expressing the conservation of axial fluxes of momenta and heat were deduced in section 2.3 and they are used to explore the consistency of the results. However one is confronted with the same problems as for the entrainment rate in the low streamwise velocity range for both the axial and azimuthal velocity component as well as the temperature. Their radial mean profiles had to be extrapolated to enable the integration from the centre of the jet into the irrotational surrounding.[9] Only small variations were observed in the conservation equations of (2.26) and (2.30) by including their second-order terms.[10] The integral expressions of momentum conservation as expressed through equation (2.26) and (2.30) including their mean and standard deviations is given in table 3. Considering the axial fluxes at the pipe outlet it can be deduced that the axial flux of heat increases with the addition of swirl as anticipated in the previous section. On the contrary the integral relation for M_x remains unchanged for a change in swirl intensity. As evident from figure 5.3 the azimuthal velocity component decreases very rapidly making it

[9] *Gaussian* curves were used for the tails of the streamwise velocity and temperature profiles, whereas third order polynomials were fitted through the outer part of the azimuthal velocity components as well as through the tails of the first two downstream positions of the streamwise velocity component and temperature.

[10] The turbulence intensity of the radial velocity component was estimated to be equal to its azimuthal counterpart. Their axial and radial developments were shown to be comparable to each other (Facciolo 2006).

impossible to obtain a meaningful estimate of the angular momentum for the last three downstream positions. Hence the axial flux of angular momentum is not presented. Furthermore the integrand in equations (2.27) is weighted with the square of the radius, which introduces an even higher dependence on the extrapolated tail compared to the previous cases. Nevertheless, from the angular momentum at the pipe outlet, M_ϕ, the swirl number in terms of the integral relations introduced in equation (2.26) and (2.27) can be computed to $S_{\phi x} = 0.15$. This might help to range the present investigation into the series of previous works reviewed in section 3.4.

5.2. Turbulence development

5.2.1. *Velocity and temperature fluctuations*

As emphasised in the previous chapters the main advantage of the present measurement technique is its ability to obtain simultaneous time signals from two velocity components and the temperature. The simultaneous acquisition especially of longitudinal velocity and temperature opens the possibility to study the mixing process in a more detailed way than for instance through *laser-Doppler velocimetry* combined with a cold-wire for temperature measurements.[11]

A simultaneous record of 1000 samples of the normalised streamwise velocity and temperature fluctuations corresponding to 0.25 s is shown in figure 5.7 taken at $x/D = 6$.[12] Both time records are taken from a region of high turbulence intensity corresponding to $|r/R| \simeq 1$. The upper two plots are from the non-swirled jet indicating the turbulent nature of the velocity and temperature fluctuations. The corresponding plot for the swirling jet is given in the bottom side from which one could anticipate that the turbulence intensities for the streamwise velocity as well as the temperature are increased due to the addition of swirl. However what is more striking is the observable ramp-like temperature signal with repeating structures. A defined length and amplitude for the upper temperature signal is observable, whereas it seems to have no prevailing length and amplitude if swirl is added to the jet. It would of course be naive to relate this change from an ordered to a destroyed pattern to the addition of swirl just by examining a trace of samples picked out of a long

[11] The problem with combined cold-wire and LDV measurements, as for instance used by Pietri, Amielh & Anselmet (2000), is due to the necessity to seed the flow with particles, e.g. with small droplets of condensed smoke. These particles however deposit on the cold-wire increasing the effective diameter of the sensor and hence its thermal inertia. Consequently the cold-wire response is progressively modified and the wire might even break. Pietri *et al.* reports that they had to clean the wire every 90 seconds at a downstream position of 5 pipe diameters. Measurements closer to the pipe outlet might need even shorter time intervals making measurements cumbersome.

[12] The upstream displacement of the cold-wire in relation to the position of the X-wire is negligible for all measured values. A fluid particle covers the distance between both positions (0.5 mm) for most of the measured positions within the time interval to record two samples.

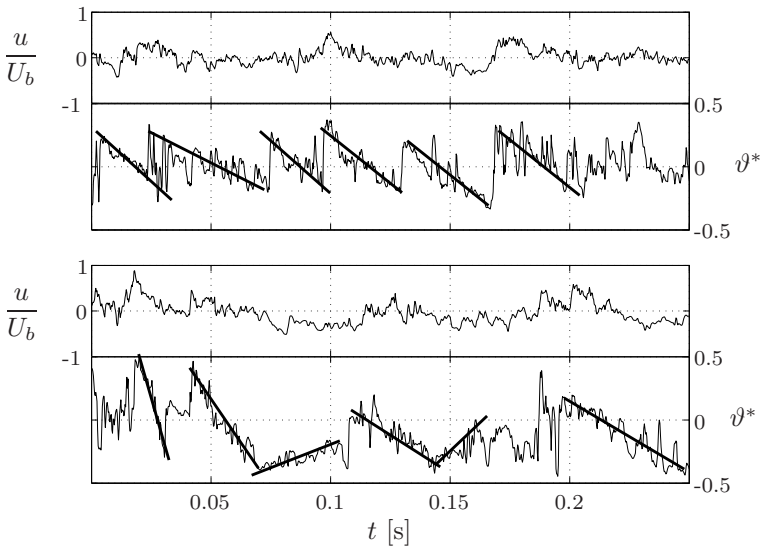

FIGURE 5.7. Simultaneous records of the normalised streamwise velocity and temperature fluctuations at $x/D = 6$ for the non-swirled (top side) and swirled (bottom side) jet at radial position around $r/R = 1$.

record of signals. Statistical tools will be necessary to analyse the fluctuating components of velocity and temperature in a more comprehensive manner, which will be applied throughout the following sections.

5.2.2. *Turbulence intensities*

The radial distribution of the root mean square value for the fluctuations in the axial velocity component, u_{rms}, is shown in figure 5.8, where it is normalised with the bulk velocity.[13] Even though the gross effects of the rotation on the mean streamwise velocity component at the pipe outlet is quite large, the streamwise turbulence intensity is almost unaffected (although there is a slight decrease in the centre of the pipe). Moving downstream the effect of rotation shows its impact by increasing the centreline turbulence intensity more than 3.5 times at four diameters downstream. Again the LDV data of Facciolo (2006) for $x/D = 0$ and 6 is illustrated through dashed lines for comparison and shows good agreement.

[13]The notation u_{rms} and u' as well as their corresponding expressions for the azimuthal velocity component and temperature will be used synonymously.

The root mean square values of the temperature fluctuations are shown in figure 5.10. As for the mean temperature also here the values were non-dimensionalised by dividing the temperature r.m.s. by the maximum temperature difference above ambient for the non-swirling jet. Hence the non-dimensionalised root mean square value of the temperature fluctuations is given through

$$\vartheta'^{*} = \frac{\vartheta'}{T_{0,S=0} - T_{\infty}} \,. \tag{5.2}$$

The low fluctuating level observed at the pipe outlet is due to the flat mean temperature profile.[14] In fact the fluctuating level should be equal to zero within a central part of the pipe if the temperature distribution was homogenous over the pipe cross-sectional area. This can be assessed by considering the transport equation for the temperature variance, equation (B.1), for the case of a fully developed turbulent pipe flow,

$$0 = -2\overline{w\vartheta}\frac{\partial\theta}{\partial r} - \frac{1}{r}\frac{\partial r\overline{w\vartheta\vartheta}}{\partial r} \,, \tag{5.3}$$

which represents a balance between the production term and the turbulent diffusion term. It should be noted, however, that the terms representing the diffusion and thermal dissipation, which may be neglected for the free jet flow, are not negligible within the pipe. As shown in figure 5.11 the root mean square value of the temperature fluctuations, ϑ'^{*}, follows quite well the distribution given by the radial mean temperature gradient, $\partial\theta/\partial r$, of the production term. Especially in the central region of the pipe, where the radial mean temperature is almost constant, the ratio between both quantities is also nearly constant.

The $\cup$-shaped profile of the temperature fluctuations intensity, which resembles the turbulence intensity profiles for the streamwise velocity fluctuations of jets emanating from nozzles (having 'top-hat' mean streamwise velocity profiles) diminishes rather quickly adapting the shape of the turbulence intensity profiles for the velocity components in the developing free jet, figures 5.8 and 5.9. This indicates the transition from the 'top-hat' profile to one which is more likely to be presented by a *Gaussian* distribution. The measurement results for the root mean square value of the temperature for the non-swirling jet at a downstream position of 3 pipe diameters agrees very well with the data presented by Xu & Antonia (2002*b*) from an over 100 pipe diameters long pipe at a *Reynolds* number of 86000 and the same excess temperature as in the present case. Xu & Antonia (2002*a*) studied the effect of initial conditions

[14] It is interesting to note that temperature root mean square values as low as 0.1 % (Drobniak *et al.* 1998) and as high as 1.2 % (Burattini & Djenidi 2004) of $\theta_{0,S=0}$ are reported at the centreline of nozzle exits. The mean radial temperature profile of the latter corresponds quite well to the one obtained in the present study.

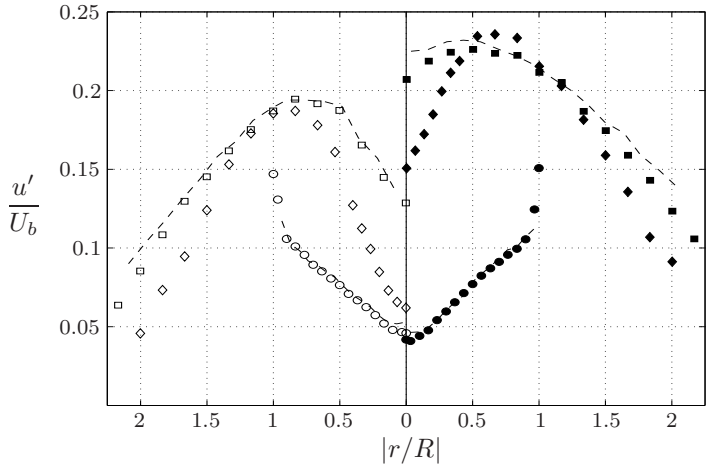

FIGURE 5.8. Root mean square value of the axial velocity fluctuations across the heated non-swirled (left side, open symbols) and swirled (right side, filled symbols) jet for three downstream positions: ○: $x/D = 0$, ◇: $x/D = 4$, □: $x/D = 6$. LDV results for a non-heated jet at the same Re from Facciolo (2006) for $x/D = 0$ and 6 are illustrated through dashed lines.

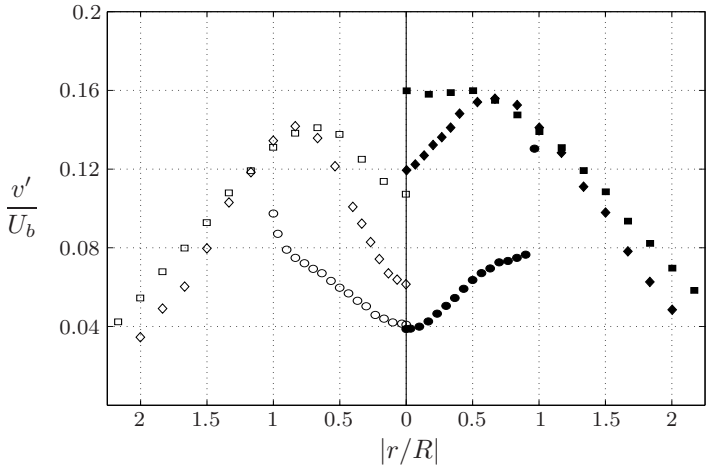

FIGURE 5.9. Root mean square value of the azimuthal velocity fluctuations across the heated non-swirled (left side, open symbols) and swirled (right side, filled symbols) jet for three downstream positions: ○: $x/D = 0$, ◇: $x/D = 4$, □: $x/D = 6$.

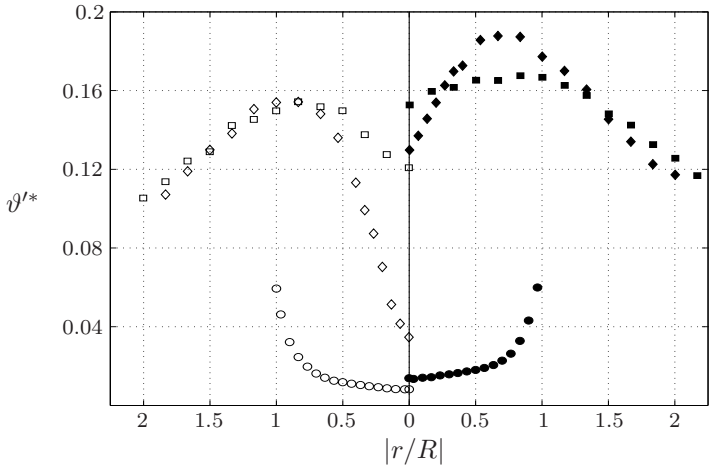

FIGURE 5.10. Root mean square value of the temperature fluctuations across the heated non-swirled (left side, open symbols) and swirled (right side, filled symbols) jet for three downstream positions: ○: $x/D = 0$, ◇: $x/D = 4$, □: $x/D = 6$.

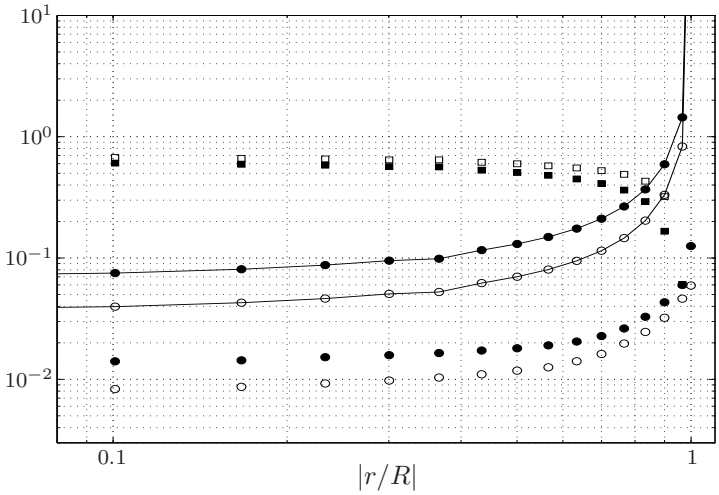

FIGURE 5.11. Comparison between the r.m.s. value of the temperature fluctuations and the radial mean temperature gradient across the non-rotating (open symbols) and rotating (filled symbols) heated pipe flow. ○: ϑ'^*, ⊖: $-\partial\theta^*/\partial r^*$ ($r^* = r/R$), □: ratio of the latter to the former.

on the temperature field as well as on the velocity field of turbulent jets emanating from both a circular nozzle and a long stationary pipe. It should be noted that previous works showed that the scalar decay rate in the self-similar far-field depends on the initial *Reynolds* number when the jet issues from a smooth contraction. However, the *Reynolds* number dependence of the scalar field for jets originating from a long pipe is much weaker and may be negligible as reported by Pitts (1991). This is similar to what was reported for the mean velocity field in section 5.1.2.

The azimuthal turbulence intensity exhibits a similar behaviour as the streamwise component, except its intensity is smaller as evident from figure 5.9. Radial profiles of the turbulence intensity for the streamwise velocity component in jets as well as in wakes are known to exhibit off-axis peaks in the developed region at radial locations representing a region of high shear and mixing corresponding to high turbulence production. The turbulence intensity of *passive scalar* fluctuations exhibit similar profiles, whereas velocity fluctuations in the radial and azimuthal directions are known to have a plateau with the highest values occurring around the centreline.[15] The off-axis peaks in the root mean square fluctuations are mainly attributed to unmixed regions of jet fluid and the entrained air leading to large-scale variations in the mixing region, whereas the contributions along the centreline are primarily attributed to the small-scale fluctuations (Schefer & Kerstein 1994).

The three turbulence intensities summarised in the three-dimensional profiles in figures 5.12–5.14 provide another possibility to analyse the mixing behaviour in the near-field of the jet. As evident from the off-axis peaks and the strong valleys around the centreline for all measured fluctuating components the heated jet fluid is not well mixed with the entrained cold air. However with increasing downstream position the valley looses its extreme difference to the maximum value indicating the transition towards the well mixed and developed jet. The addition of swirl clearly enhances the centreline values (dashed lines) for all turbulence intensities starting from 2–3 pipe diameters having their largest difference to the non-swirled jet at 4–5 exit diameters. This confirms the global effect of swirl to enhance mixing. The axial decays of the non-swirling (grey dashed lines) and swirling (black dashed line) jet visualises this enhancement through their parted trends which seem to converge further downstream due to the restriction of full mixedness.

Pietri *et al.* (2000) reports that the temperature field develops earlier than the velocity field based on the earlier increase of ϑ_{rms} compared to u_{rms} and w_{rms}, which remains almost unchanged up to 5 pipe diameters, whereas ϑ_{rms}

[15] The axisymmetry of the flow requires that v_{rms} and w_{rms} are equal, which can be observed in the data of Hussein *et al.* (1994) from measurements in the far-field of jets emanating from round nozzles, but also in the case of the swirling jet starting from about 8 pipe diameters downstream in the data of Facciolo (2006).

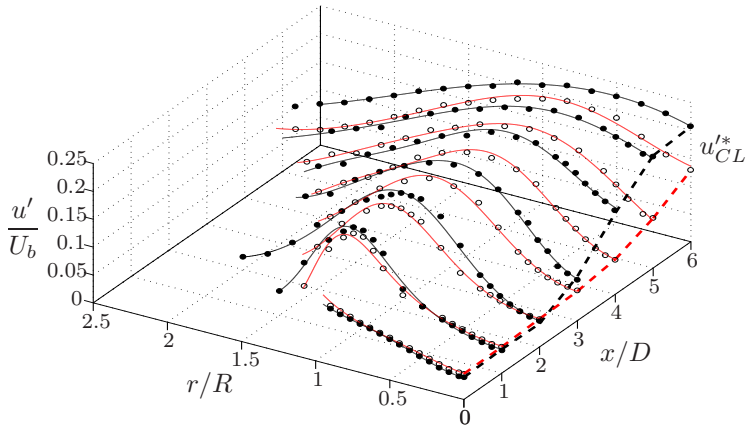

FIGURE 5.12. Three-dimensional profile of the root mean square value of the axial velocity fluctuations for the non-swirled (open markers) and swirled (filled markers) jet. Their centreline developments (u'^*_{CL}) are illustrated through the dashed lines. Full lines are for visual aid only.

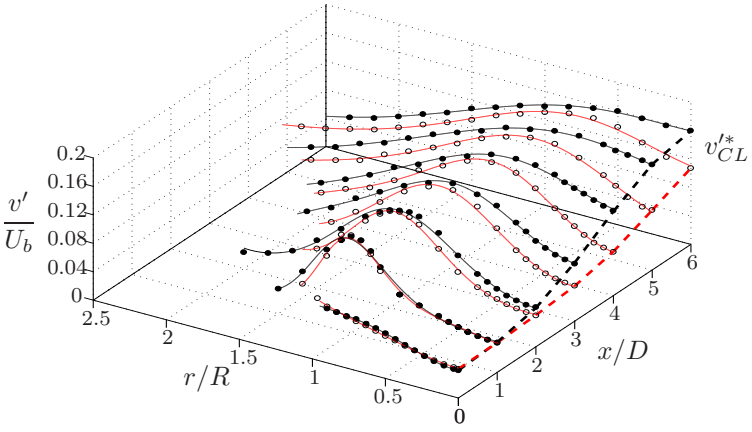

FIGURE 5.13. Three-dimensional profile of the root mean square value of the azimuthal velocity fluctuations for the non-swirled (open markers) and swirled (filled markers) jet. Their centreline developments (v'^*_{CL}) are illustrated through the dashed lines. Full lines are for visual aid only.

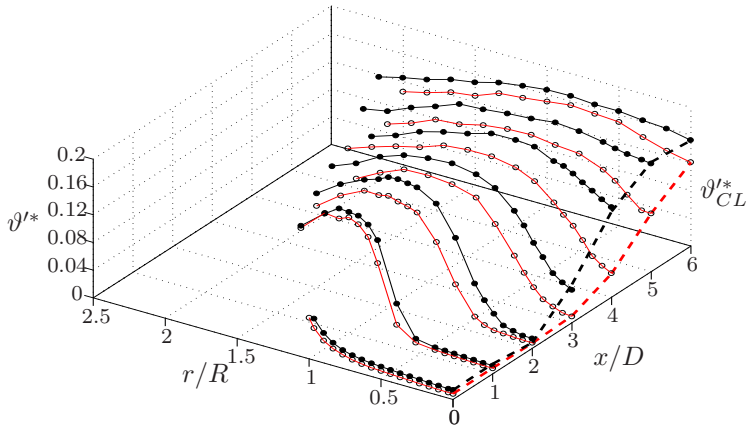

FIGURE 5.14. Three-dimensional profile of the root mean square value of the temperature fluctuations for the non-swirled (open markers) and swirled (filled markers) jet. Their centreline developments (ϑ'^*_{CL}) are illustrated through the dashed lines. Full lines are for visual aid only.

starts to increase from stations about $x/D = 3$.[16] This can be confirmed at least qualitatively by comparing the centreline development of ϑ_{rms} with the root mean square values of the measured velocity components.

It is worth mentioning that the temperature variance for the near-field of the jet emanating from a long pipe does not exhibit a double peak within the first three diameters downstream. Such double peaks were for instance observed by Drobniak *et al.* (1998) and Burattini & Djenidi (2004) within the first three nozzle diameters, where the two peaks were equidistantly displaced from a minimum located at the nozzle radius.

5.2.3. *Reynolds shear stress and heat fluxes*

Another indication of the effect of rotation on the free jet is apparent from the correlation coefficients, i.e. the cross-variances of the fluctuating components normalised by their appropriate variances. Hence, per definition, they are bounded by $\pm$ 1, representing perfect correlation or perfect anti-correlation, respectively. The cross-variances are related to the turbulent momentum flux, $\rho\,\overline{uv}$, as well as the turbulent heat fluxes, $\rho\,c_p\,\overline{u\vartheta}$ and $\rho\,c_p\,\overline{v\vartheta}$, in the streamwise and azimuthal directions.

[16] This is however not clear from the evolution of the root mean square values of u_{rms} and ϑ_{rms} presented in their figure 2b.

The longitudinal heat flux, expressed in form of $\rho_{u\vartheta}$, is visualised for different downstream positions in figure 5.15. No differences are detectable between the non-swirling and swirling jet for the fully developed pipe flow as well as the farthest measured downstream position, while only marginal differences are observable at $x/D = 2$. The near-wall peak for the pipe flow indicates the strong correlation of axial velocity and temperature fluctuations as observed in the DNS of Satake & Kunugi (2002).

In contrast a distinct difference can be found four pipe diameters downstream, where the addition of swirl increases the correlation between the instantaneous axial velocity component and the temperature remarkably, which could be anticipated through the increase of the root mean square value of both fluctuating variables as shown in figures 5.8 and 5.10. Clearly a change in the turbulence structure has occured keeping in mind that the mean axial velocity component and temperature at this downstream position is rather unchanged as evident from figures 5.4 and 5.5. Hence swirl strongly promotes the longitudinal heat flux in a central region of the jet between $3 \leqslant x/D \leqslant 5$. Pietri *et al.* (2000) explains the observed behaviour in relation to the end of the *dynamic* 'potential core' region around $x/D = 4.5$ by linking it to the axisymmetric mixing layer which develops from the nozzle and reaches the jet axis at this downstream position.

One can follow the maximum values of the axial *Reynolds* fluxes from the pipe outlet to 6 diameters downstream travelling from the pipe wall ($|r/R| = 1$) to the jet centreline. In contrast for the swirling jet the maximum value reaches the centreline 1–2 pipe diameters earlier. The centreline development shows that for the non-swirling case a minimum is reached around $x/D = 4$ while no minimum is observed for the swirling case. The centreline value remains rather constant right from the pipe outlet up to three pipe diameters downstream. A similar trend is found by Xu & Antonia (2002*b*) where the same correlation coefficient reaches its minimum and maximum value around $x/D = 3$ and 10, respectively.

The low values of the correlation coefficient of axial velocity and temperature fluctuations, as e.g. observed around the centreline at 4 pipe diameters downstream in the case of the non-swirling jet, are an indication for the unmixedness of the flow at that particular local position and it will be shown in the next section 5.3.1 that these regions correspond to highly thermal intermittent regions, meaning that cold air 'blobs' are probably reaching or crossing the centreline of the warm air stream.

The remaining correlation coefficients corresponding to the azimuthal heat flux and the axial-azimuthal *Reynolds* shear stress are shown in figure 5.16 and

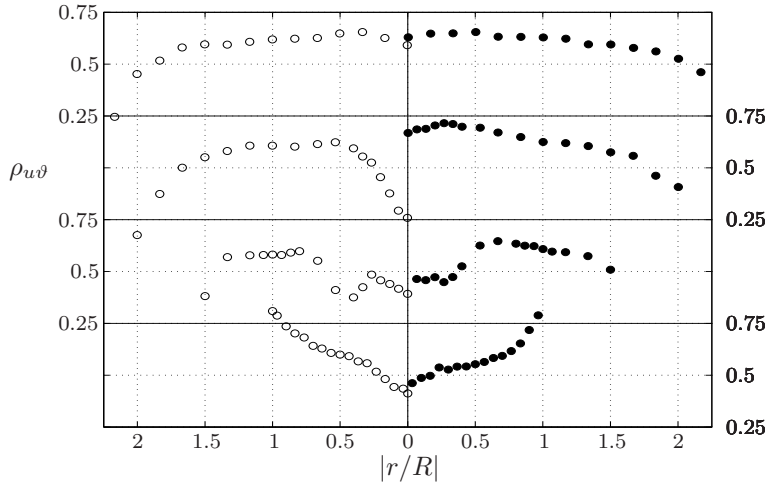

FIGURE 5.15. Correlation coefficient of axial velocity and temperature fluctuations across the heated non-swirled (left side, open symbols) and swirled (right side, filled symbols) jet for four downstream positions: from bottom to top corresponding to $x/D = 0$, 2, 4 and 6.

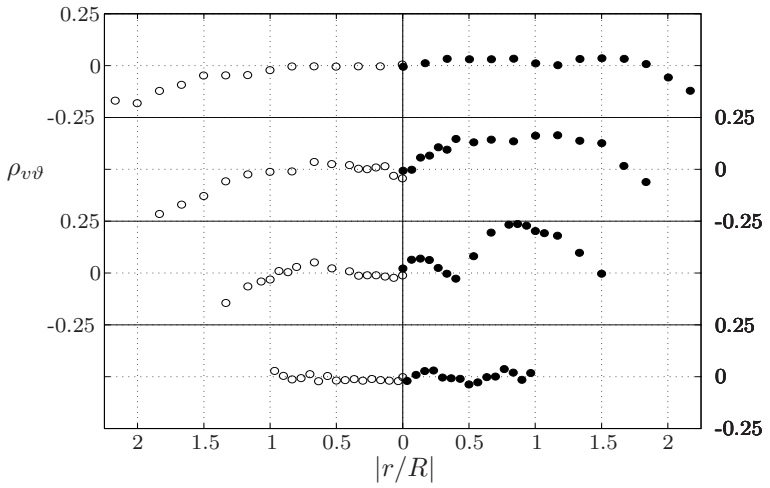

FIGURE 5.16. Correlation coefficient of azimuthal velocity and temperature fluctuations across the heated non-swirled (left side, open symbols) and swirled (right side, filled symbols) jet for four downstream positions: from bottom to top corresponding to $x/D = 0$, 2, 4 and 6.

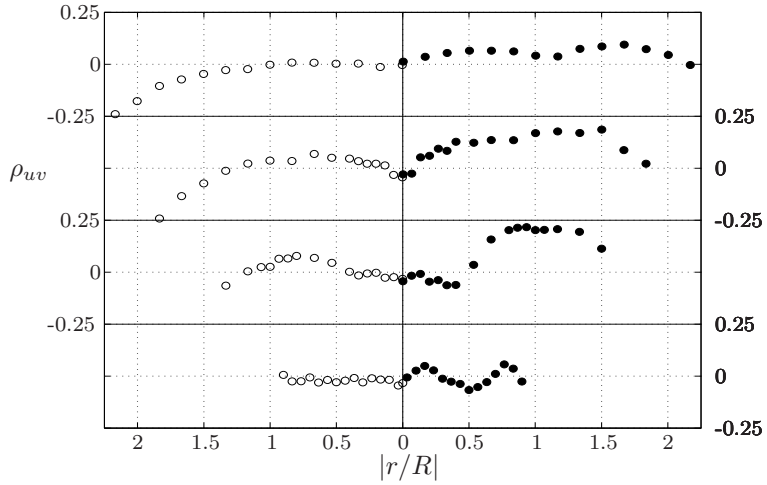

FIGURE 5.17. Correlation coefficient of axial and azimuthal velocity fluctuations across the heated non-swirled (left side, open symbols) and swirled (right side, filled symbols) jet for four downstream positions: from bottom to top corresponding to $x/D = 0$, 2, 4 and 6.

5.17, respectively.[17] As expected there is no correlation between the fluctuating axial and azimuthal velocity component as well as the fluctuating azimuthal velocity component and the *passive scalar* for the non-swirling pipe flow. The strong correlation between the fluctuating axial velocity component and the temperature suggests a strong similarity between the two other correlation coefficients containing the fluctuating azimuthal velocity component, which can be confirmed by comparing figures 5.16 and 5.17. For both of them the correlation coefficient remains zero along the centreline and varies slightly outwards in the developing free jet. For the axially rotating pipe flow two slight peaks in the correlation coefficients involving the fluctuating azimuthal velocity component are observable, one near the pipe wall and the other near the centreline. The *direct numerical simulation* results of Orlandi & Fatica (1997) confirms the shape of the distribution for ρ_{uv}.

Comparison of the three correlation coefficients clearly indicates the strong connection between the streamwise velocity component and the *passive scalar*. To access this high correlation in a more quantitative manner, which is directly related to its physical transport mechanism, i.e. the turbulent heat

[17]It should be noted that only one side of the axisymmetric pipe and jet flow is presented here and that the other half, due to the change of sign in the azimuthal velocity component, exhibits an antisymmetric profile.

fluxes in the streamwise and azimuthal direction, $\rho\, c_p\, \overline{u\vartheta}$ and $\rho\, c_p\, \overline{v\vartheta}$, respectively, as well as the axial-azimuthal *Reynolds* shear stress, $\rho\, \overline{uv}$, are presented non-dimensionalised in figures 5.18–5.20. Here the *Reynolds* fluxes were non-dimensionalised by $U_b\theta_{0,S=0}$ and the *Reynolds* stress by U_b^2.

As anticipated from the strong correlation coefficient between the fluctuating axial velocity component and the temperature, the streamwise *passive scalar* flux is almost an order of magnitude higher then the other two presented fluxes. The addition of rotation shows a drastic increase in the streamwise heat flux, especially 3–5 diameters downstream along and around the centreline, and remains also over the whole cross-section larger than its non-swirling counterpart. Hence swirl strongly promotes the longitudinal heat flux.

In the case of jets emanating from rotating nozzles the sudden increase of the longitudinal heat flux is related to the end of the *dynamic* 'potential core' (see e.g. Komori & Ueda 1985). Although there is no *dynamic* 'potential core' in the present case (recall its definition given in footnote 7 on page 62) the free shear flow emanating from the pipe exit maintains its low turbulence intensity along and around the centreline until the strong conical shear layer initiating from the pipe edge reaches the centreline. From there on all root mean square values of the velocity and temperature fluctuations are increasing rapidly as is clearly evident from figures 5.12–5.14. The increased entrainment, due to the addition of swirl, shortens the distance for the strong conical shear layer to reach the centreline and hence shortens the distance needed for transition from fully developed turbulent pipe flow to developing jet flow.

The azimuthal *passive scalar* flux and axial-azimuthal *Reynolds* shear stress, figures 5.19 and 5.20, should be zero for the non-swirling case, due to symmetry reasons. Even though there is a slight increase in the outer region for increasing downstream positions the maximum amplitude is still an order of magnitude smaller than the longitudinal heat flux term. Similar difficulties were reported by Mehta *et al.* (1991) and Nayeri (2000).[18]

The addition of swirl to the developing jet shows a drastic increase in the secondary *Reynolds* shear stresses as well as the azimuthal *passive scalar* flux. As pointed out by Launder & Morse (1979) and Gibson & Younis (1986) the secondary (in magnitude) *Reynolds* shear stress, $\overline{uv}$ (as evident from equation (A.4), where $2V\overline{uv}/r$ becomes effective for $V \neq 0$), exerts a strong influence on the primary *Reynolds* shear stress, $\overline{uw}$, which in turn influences the rate of spread as well as the decay of the axial mean centreline velocity.

[18] Nayeri argues that the nonzero values for the secondary *Reynolds* stresses, present in his experiment, are caused by a small offset of the vane angle of the swirl generator. It remains however unclear how much the resulting weak azimuthal velocity component (2 % of the mean streamwise velocity component) is responsible for a secondary *Reynolds* shear stress, $\overline{uv}$, as high as 27 % of the primary *Reynolds* shear stress, $\overline{uw}$. Mehta *et al.* observes for the same quantity a value around one fifth of the primary *Reynolds* shear stress in the case of a stationary pipe.

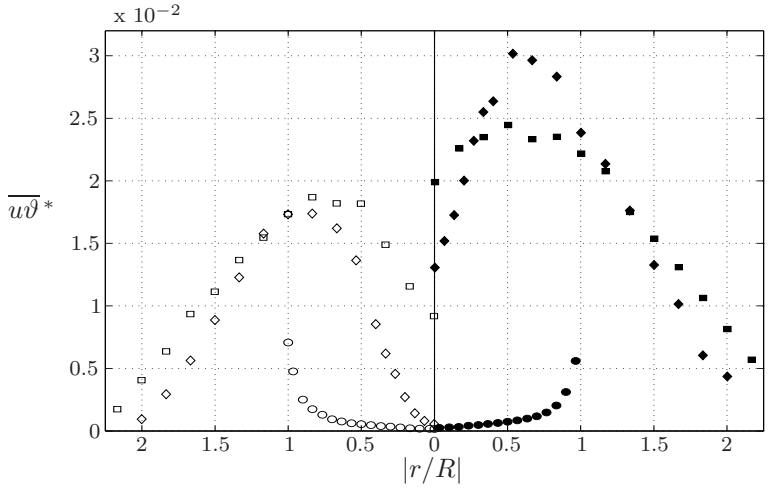

FIGURE 5.18. Streamwise *passive scalar* flux across the heated non-swirled (left side, open symbols) and swirled (right side, filled symbols) jet for three downstream positions: ○: $x/D = 0$, ◇: $x/D = 4$, □: $x/D = 6$.

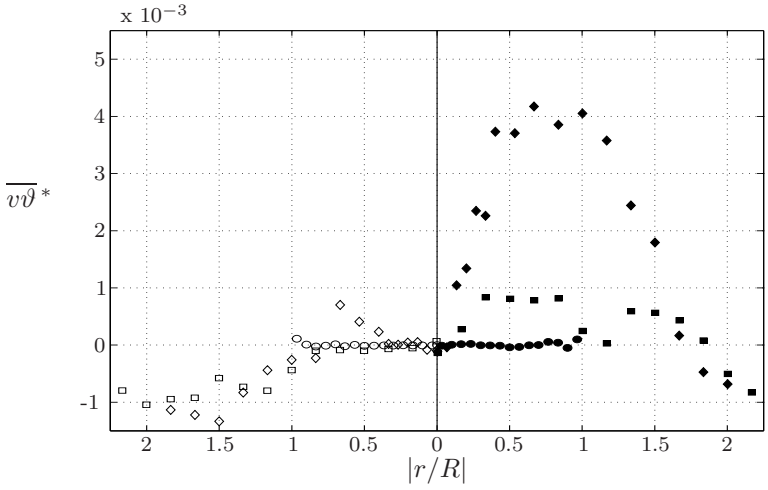

FIGURE 5.19. Azimuthal *passive scalar* flux across the heated non-swirled (left side, open symbols) and swirled (right side, filled symbols) jet for three downstream positions: ○: $x/D = 0$, ◇: $x/D = 4$, □: $x/D = 6$.

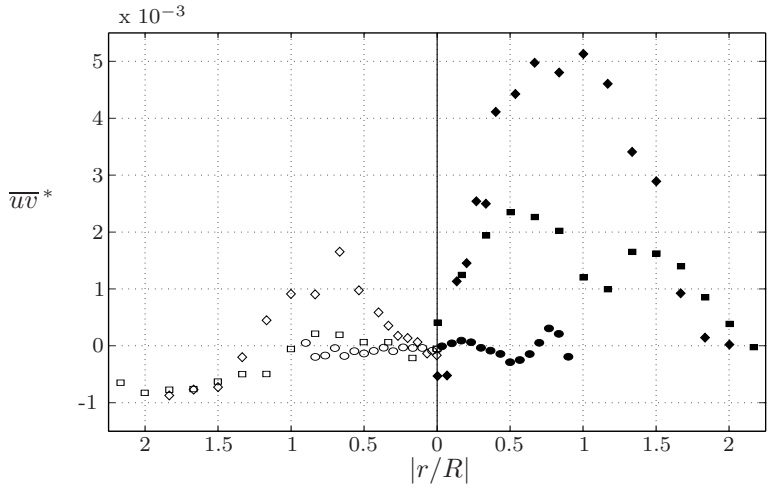

FIGURE 5.20. Axial-azimuthal *Reynolds* shear stress across the heated non-swirled (left side, open symbols) and swirled (right side, filled symbols) jet for three downstream positions: ○: $x/D = 0$, ◇: $x/D = 4$, □: $x/D = 6$.

We already mentioned a series of problems in section 4.2.4 regarding the use of *hot-wire anemometry* related to the highly intermittent outer region of the free jet. Before concluding this section the observed rapid decay of all measured correlation coefficients in the outer region of the jet should be discussed: Due to the entrainment of ambient air, which is initially at rest, local turbulence intensities of the order of unity in the outer region of the jet can easily occur. Furthermore the time-averaged streamwise velocity component is slowed down and instantaneous flow reversal can occur. Hence the forward-reverse ambiguity and sensitivity to the third velocity component causes errors, especially for the *Reynolds* shear stresses and fluxes. A quantification of the errors in the *Reynolds* stresses was investigated by Tutu & Chevray (1975) and more recently by Ovink *et al.* (2001) as mentioned in section 4.2.4. They showed that the *Reynolds* stresses are underestimated whereas the mean streamwise velocity component is overestimated with increasing *local* turbulence intensity, i.e. with increasing radial distance from the centreline. The former deficiency can be evinced from the correlation coefficients in the outer jet region with increasing distance from the centreline as shown in figures 5.15–5.17. Consequently, it should be avoided to normalise the *Reynolds* stresses by the measured local mean velocity components, because it would even more increase the underestimation of the *Reynolds* stresses.

5.3. Higher statistical moments

Higher statistical moments, e.g. the skewness and flatness factor, can be used to describe the shape of the *probability density function* (p.d.f.) of a fluctuating signal. We have already investigated the root mean square value, the square root of the second central moment, of the velocity and temperature fluctuations, which is a measure of the departure from the mean value. However, it is not affected by any lack of symmetry in the p.d.f. about the origin and hence the normalised third central moment, the skewness factor, is an important indicator for deviations from symmetry; it is entirely dependent on the lack of symmetry. The normalised fourth central moment, the flatness factor[19], is also used to illustrate the the shape of the p.d.f.s of the measured variables.

5.3.1. *Probability density distributions*

The probability density functions of the streamwise and azimuthal velocity fluctuations, $p(u)$ and $p(v)$, as well as that for the temperature fluctuations, $p(\vartheta)$, at a downstream position of 6 D are shown in figures 5.21–5.23, respectively. The quantities on the abscissa were normalised by their root mean square values, whereas the probability density functions were scaled in such a way that the area under each curve is equal to one. The p.d.f.s of three distinct radial positions, corresponding to the centreline ($|r/R| \simeq 0$), a region of high turbulence intensity ($|r/R| \simeq 0.6$) and a highly intermittent region ($|r/R| \simeq 1.9$), are presented for the fluctuating components of both the non-swirling (dash-dotted line) and swirling (solid line) jet. *Gaussian* distributions are also included as dotted lines for each p.d.f. for comparison.

Let us consider the p.d.f. of the streamwise velocity fluctuations of the non-swirling jet around its axis. The shape of the curve contains the information that small positive values of u are more likely than small negative ones, however large negative values of u are more likely than large positive values of u giving rise to a negative skewness factor. A physical interpretation could be, that the entrained air (which is initially colder and slower) is not fully mixed with the warm jet emanating from the pipe. The measurement probe consequently would experience occasionally air 'blobs' with lower and colder instantaneous streamwise velocities and temperatures, respectively.

The position of the mean axial centreline velocity at the pipe outlet for the non-swirling case, $U_{0,S=0}$, is drawn into the figure to emphasise that instantaneous axial velocities as high as $U_{0,S=0}$ still occur with a high probability.

[19] The literature is not consistent regarding the definition of the flatness factor and the kurtosis. Pope (2000) for instance uses both terms synonymously while Piquet (2001) introduces the normalised fourth central moment as the flatness factor and its deviation from the *Gaussian* value of 3 as the excess factor or the kurtosis.

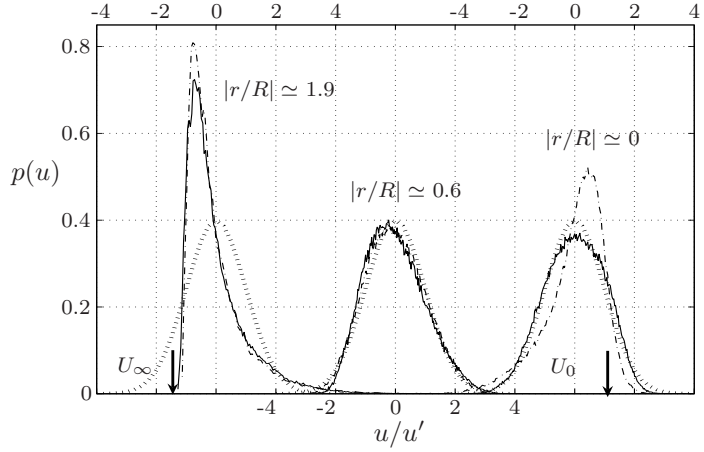

FIGURE 5.21. Probability density function of the streamwise velocity fluctuations for the non-swirled (dash-dotted line) and swirled jet (solid line) at radial positions corresponding to high intermittency (left), high turbulence intensity (middle) and the centreline (right) at $x/D = 6$. *Gaussian* distributions are plotted for comparison (dotted).

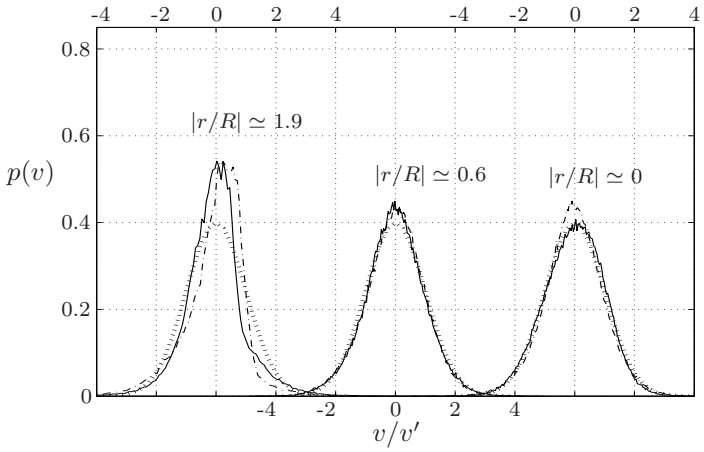

FIGURE 5.22. Probability density function of the azimuthal velocity fluctuations for the non-swirled (dash-dotted line) and swirled jet (solid line) at radial positions corresponding to high intermittency (left), high turbulence intensity (middle) and the centreline (right) at $x/D = 6$. *Gaussian* distributions are plotted for comparison (dotted).

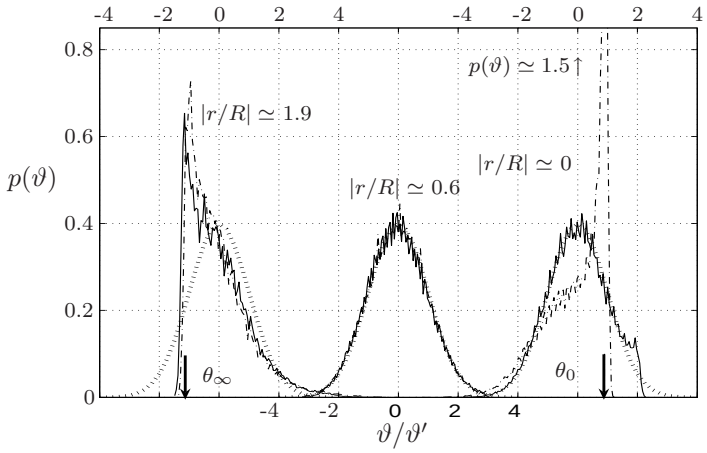

FIGURE 5.23. Probability density function of the temperature fluctuations for the non-swirled (dash-dotted line) and swirled jet (solid line) at radial positions corresponding to high intermittency (left), high turbulence intensity (middle) and the centreline (right) at $x/D = 6$. *Gaussian* distributions are plotted for comparison (dotted).

Moving radially outwards, towards the position of high turbulence intensity (see figure 5.8), the shape of the p.d.f. resembles an almost *Gaussian* distribution indicating the good mixing between the heated jet and the newly entrained cold air. The tail of the jet illustrated in the leftmost side of the figure shows a highly positively skewed and peaked p.d.f. indicating the occurrence of large-scale intermittent structures of high velocity air.[20] The p.d.f. at this radial position is bounded by the velocity of the ambient air ($U_\infty = 0$ m/s), i.e. air at rest. The inspection of the shape of the p.d.f. leads us to infer that back flow, instantaneous flow in the negative x-direction, might be present for a certain fraction of the time-series of the axial velocity component.[21] Thus we reach the limits of the applied measurement technique, at least for the velocity components.

The addition of swirl clearly changes the scenario for the jet around its centreline: the initially negatively skewed and peaked p.d.f. follows nearly a *Gaussian* distribution. On the contrary, no large changes are observable for

[20]The large-scale intermittency or so-called external intermittency at the edge of a heated free round jet was probably first encountered by Corrsin (1943), by investigating traces of temperature signals.

[21]The associated instantaneous axial velocities at this outer radial position are however for approximately 90 % within the region of the X-wire calibration plot (compare with figures 4.9 and 4.10 as well as table 2 in section 4.2.4).

the other two radial positions. Both radial positions experience approximately the same mean streamwise velocity component as well as turbulence intensity for the non-swirling as well as swirling jet. The fluid at the local position corresponding to the region with high turbulence intensity is furthermore already well-mixed with the entrained air, so that the addition of rotation does not show any further detectable contribution to the mixing process. The faster axial velocity decay and the higher turbulence intensity at the centreline in comparison with its non-swirling counterpart reduces the probability that streamwise velocity fluctuations as high as the initial centreline velocity occur. This indicates that the kinetic energy of the mean flow has mainly been utilised to entrain more irrotational air at ambient temperature and to mix it with the warm and faster mean stream.[22]

The probability density function of the fluctuating azimuthal velocity component is plotted for the sake of completeness, but does not show any significant effect of rotation on the histograms[23].

A similar interpretation as for the fluctuating streamwise velocity component can be gained from the histograms of the temperature signals for the same radial positions at $x/D = 6$. Here again the non-swirled jet exhibits an even more negatively skewed and highly peaked p.d.f. pointing out the coexistence of 'blobs' of almost unmixed fluid at a temperature close to the initial centreline temperature, θ_0, with 'blobs' of well-mixed fluid. Pietri *et al.* (2000) relates the presence of regions of 'hot' fluid at a temperature very close to θ_0 to the limited effect of molecular diffusivity on the temperature field. At the edge of the jet the opposite scenario is present, namely 'blobs' of 'cold' air close to (and even below[24]) the ambient temperature coexist with well mixed warmer air associated with a more or less *Gaussian* part along the positive abscissa. The slight undershooting below the mean ambient temperature observed in the leftmost p.d.f. can be attributed to a slight drift in the ambient temperature of the order of the measurement resolution of the thermocouples used to monitor

[22]The position of U_∞ and U_0 as well as θ_∞ and θ_0 for the swirling jet is of course different from that of the non-swirling jet, nevertheless its actual position is not drawn into the figure, due to space restrictions. Their ambient values are almost at the same position as for their non-swirling counterparts, while their centreline values move slightly towards the positive tail of the p.d.f.s.

[23]Here we loosely use the term histogram synonymously for the p.d.f., even though the first is actually the measured and computed quantity, whereas the latter is the quantity we wish to represent in the limit of infinitely long sample records.

[24]The cold-wire, contrary to the hot-wires, is not bounded at its 'lower side'. Nevertheless care should be paid to the contamination from the hot-wires *if* the cooling velocity falls below a certain velocity at which forced convection is not anymore much larger than free convection or conduction to the prongs, as mentioned in section 4.2. Besides this unrestrainedness for the temperature measurement it is however important to note, that a conserved *passive scalar* is characterised though its *boundedness*, i.e. if $\tilde{\vartheta}(\mathbf{x}, t)$ is the instantaneous passive scalar quantity, then $\tilde{\vartheta}$ for all $(\mathbf{x}, t)$ also lies within the range given by its initial and boundary conditions (see e.g. Pope 2000, chap. 2).

the ambient temperature, i.e. 0.1 K, and/or to the choice of setting θ_∞ at the mean ambient temperature. A similar explanation was given by Chevray & Tutu (1977), who observed the same effect on the temperature p.d.f.s in the highly intermittent region of a heated free jet.

The addition of swirl to the jet clearly shows that the highly frequent 'hot' fluid regions in the non-swirling jet do hardly occur in the well mixed swirling jet along the centreline.[25] Hence the probability of intermediate temperatures and consequently mixed fluid increases for the swirling jet when compared with the non-swirling jet.

As evident from the aforementioned analysis the probability density function makes it possible to assess the mixing properties of the flow as well as the passive contaminant.[26] However the amount of p.d.f.s needed to analyse the local positions along the radial and axial direction for both the non-swirling and swirling jet thoroughly would unnecessarily overfill the present monograph with a vast amount of plots. Instead, in the following, we will investigate the velocity and temperature distribution by examining the radial profiles of the skewness and flatness factor.

The skewness and flatness factors get large contributions from fluctuations with large deviations from the mean value. For a *Gaussian* distribution the value of the skewness factor is zero (due to its symmetric properties) and the value of the flatness factor is three. Large negative deviations of the signal would result in a negative value of the skewness factor (and vice versa for large positive deviations) and a flatness factor which will be larger than three. Such values may indicate an intermittent character of the fluctuations.[27]

---

[25] As mentioned in footnote 22 the position of θ_0 for the swirling jet moves outwards along the abscissa towards $\vartheta/\vartheta' \simeq 2$.

[26] This clearly emphasises the advantage of the present measurement technique compared to its non-intrusive alternatives. LDV and PIV are both highly restricted if the mixing properties in intermittent flows are aimed to be studied. As pointed out by Staicu (2002) the problem with LDV in highly intermittent flows is, that in high velocity regions more particles will probably pass the measurement volume in a given time interval than in low velocity regions. This will especially weight the higher order statistics differently strong. For the PIV on the other hand another problem occurs. In the processing of the images of the PIV one normally filters out any 'improbable' velocity vectors. However in large-scale intermittent flow regions these rejected velocity vectors might be a result of the intermittency itself. Hence special care has to be given to distinguish conspicuous velocity vectors caused by intermittency as well as particles from another interrogation area.

[27] Even though a small value of the intermittency factor, the fraction of volume (time) where the variable is 'active', yields a large value of the flatness factor, a large value of the flatness factor does not necessarily imply intermittency as reasoned by Kennedy & Corrsin (1961). However this should not hinder one to facilitate the radial distribution of the flatness factor to get an estimate of the intermittency factor, γ, defined as the flatness factor of a *Gaussian* distribution to that in the intermittent region (Klebanoff 1954), as long as the turbulent part of the intermittent signal is roughly *Gaussian*.

5.3.2. *Skewness factor*

The radial profiles of the skewness factor for the axial and azimuthal velocity fluctuations, S_u and S_v, as well as the temperature fluctuations, S_ϑ, for both the non-swirling and swirling jet, are presented in figure 5.24–5.26. Horizontal lines corresponding to the *Gaussian* values are drawn in the figures to both have a reference value and to separate radial profiles for different downstream positions from one another.

Considering the skewness factor for the streamwise velocity fluctuations across the heated non-swirling and swirling jet, figure 5.24, clearly illustrates that the addition of swirl to the jet has a modifying effect on the symmetry of the probability density function. Only very small changes are apparent at the pipe outlet and the near outlet region as well as the outer part of the developing jet, whereas drastic changes are found at the jet axis for $x/D = 4$ and 6 with different consequences. The profile for S_u for the non-swirling jet follows quite well the DNS performed by Eggels (1994), at least for the range of radial measurement points, which were accessible with the present measurement technique. The DNS results by Eggels show that within the buffer layer the skewness factor starts to increase and reaches a positive skewness value around unity at the pipe wall. Furthermore our measurements follow closely the LDV measurements of Facciolo (2006) for both the non-swirling and swirling jet.[28] The radial and axial distribution of the skewness factor for the azimuthal velocity fluctuations on the other hand shows marginal effects around the jet centreline and more pronounced differences in the outer region of the jet as well as at the near-wall region of the pipe flow, where the azimuthal mean velocity component is profoundly nonzero.

The distribution of the skewness factor for the azimuthal velocity fluctuations shows remarkable alterations in regions where the mean azimuthal velocity component deviates from zero. Here, as for the correlations involving the azimuthal velocity component, the profiles are antisymmetric around the centreline.

By going over to the skewness factor of the *passive scalar* fluctuations it becomes immediately apparent that the temperature field exhibits more anomalies than the velocity field and that it is a very sensitive detector for changes in the turbulent flow itself.[29] This is however not surprising if one recalls that the advection-diffusion relation, equation (2.14), governing the *passive scalar* does not contain a pressure term. It is known that pressure acts non-local and thus implies for turbulent flows that pressure (which is directly coupled to the velocity field) fluctuations induce far-field pressure forces, which in turn

[28] Recalling the problems encountered in LDV measurements (see footnote 26) it should be emphasised that the pipe flow does not contain large-scale intermittency associated with entrained flow and hence the compared LDV measurements can be considered unbiased.
[29] Note the different scale for the ordinate for $x/D = 2$ and 4.

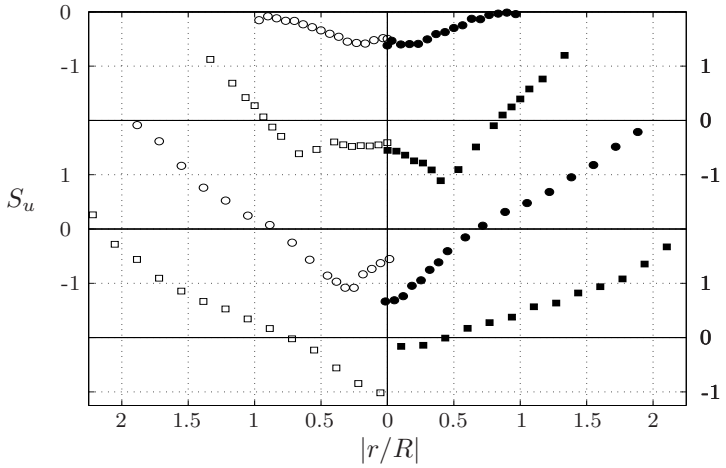

FIGURE 5.24. Skewness factor of the streamwise velocity fluctuations across the heated non-swirled (left side, open symbols) and swirled (right side, filled symbols) jet for four downstream positions: from top to bottom corresponding to $x/D = 0$, 2, 4 and 6.

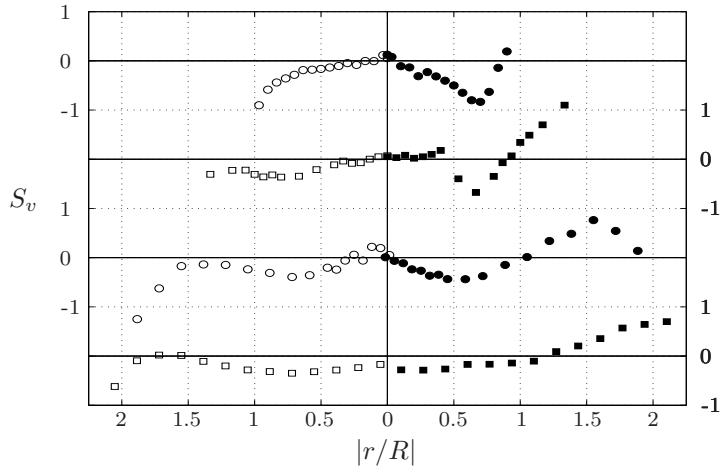

FIGURE 5.25. Skewness factor of the azimuthal velocity fluctuations across the heated non-swirled (left side, open symbols) and swirled (right side, filled symbols) jet for four downstream positions: from top to bottom corresponding to $x/D = 0$, 2, 4 and 6.

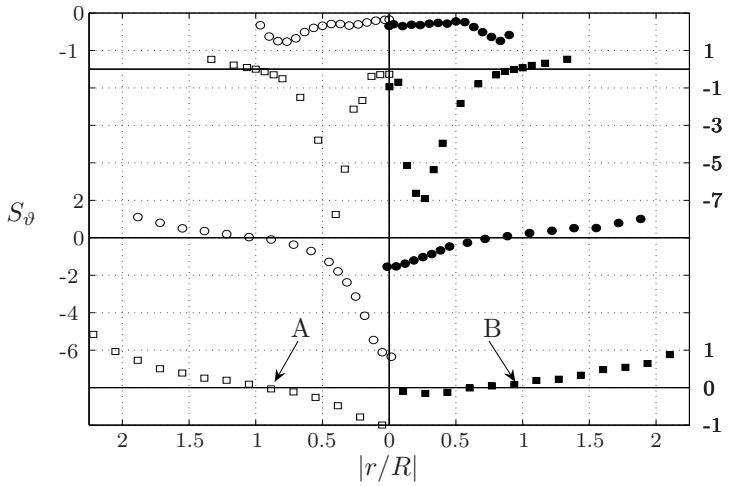

FIGURE 5.26. Skewness factor of the temperature fluctuations across the heated non-swirled (left side, open symbols) and swirled (right side, filled symbols) jet for four downstream positions: from top to bottom corresponding to $x/D = 0$, 2, 4 and 6.

has the consequence that every part of a turbulent flow feels every other part (Davidson 2004).[30] Consequently the pressure field acts as a redistribution process within the velocity field smoothing out much of the intermittent structures. This redistribution process, however, is absent for the *passive scalar* field, which explains the possibility of occurrence of sharp peaked p.d.f.s or relatively high values of the flatness factor.

Another feature, already mentioned in section 5.2.1, is the formation of ramps and cliffs on which the *passive scalar* fluctuations are carried on.[31] Both of these features are utilised to explain the strong deviations of the skewness

[30]This explains why low amplitude velocity fluctuations can also occur in the irrotational ambient air near the interface of the free turbulent jet.

[31]These ramp-like structures apparent more or less in the time records of passive contaminants were first observed in high *Reynolds* number scalar measurements in the atmospheric boundary layer during the late sixties. Since then much effort has been spent to the more fundamental question whether or not the *passive scalar* becomes isotropic for the small scales at the limit of infinitely high *Reynolds* numbers. Until grid turbulence measurements of the *passive scalar*—performed mostly during the eighties—were available, it was believed that the local isotropy theory could also be utilised to describe the small scales of the scalar field. This was mainly a result of the fact that most experiments were performed in external flows containing large-scale intermittency (as is the case in free jets, due to excursions of ambient air entraining the jet) as well as internal intermittency. However since results from grid turbulence measurements (in the absence of entrainment and large-scale anisotropy) as well as *direct numerical simulations* are available no doubt remains that local isotropy does not

factor of the temperature fluctuations. For instance Danaila *et al.* (1999) experimentally analysed higher order moments of temperature fluctuations created in the gap between two counter-rotating disks, one heated and the other cooled. They observed left-running "ramps with cliffs" at the beginning of the ramps near the hot disk and right-running "ramps with cliffs" at the end of the ramps near the cold disk. The signals associated with the hot disk showed negative skewness values while those associated with the cold disk positive ones. In the central region the ramps of opposite slopes cancelled one another out on average indicating "symmetric mixing", a stage of statistical "quasi-isotropic" mixing, with almost *Gaussian* values for the skewness and flatness factor.

Chevray & Tutu (1977) relate the observed occurrence of highly negative skewness factors of the temperature fluctuations along the centreline in the near-field of the jet to the result of the entrainment process. By utilising a rather abstract physical reasoning they argue as follows: Considering the near-field of the jet in the absence of thermal diffusivity the temperature can adopt either the value at the exit, θ_0, or the one in the ambient air, θ_∞. If Q_0 is the volume flux at the pipe outlet and Q_e the total volume flux entrained up to x/D, then the p.d.f. of the temperature fluctuations can be expressed as the superposition of two delta functions,

$$p(\vartheta) = \frac{Q_e}{Q}\,\delta(\vartheta) + \frac{Q_0}{Q}\,\delta(\vartheta - \theta_0)\,, \tag{5.4}$$

where Q is the total volume flux ($= Q_0 + Q_e$). From this expression the skewness factor as a function of the ratio of entrained to the initial volume flux,

$$S_\vartheta = \frac{Q_e/Q_0 - 1}{\sqrt{Q_e/Q_0}}\,, \tag{5.5}$$

can be derived. Facilitating the entrainment coefficient depicted in figure 5.6 on page 64 a negative skewness factor along the centreline can be found for $Q_e/Q_0 < 1$, i.e. $x/D < 4$ and 6 for the swirling and non-swirling jet, respectively. Although the assumption that the entrained air occupies all radial positions and the omission of the thermal diffusivity are crude assumptions, the analyses illustrates the reason for the asymmetry of the p.d.f. for the *passive scalar* fluctuations along the centreline.

Besides the highly negative values for the skewness factor of the temperature fluctuations (and streamwise velocity fluctuations) along the centreline between $x/D = 3$ and 5, the region of high turbulence intensity at $x/D = 2$ exhibits also highly negatively skewed p.d.f.s. Corrsin & Uberoi (1950) and more recently Burattini & Djenidi (2004) observed a similar trend along the

apply to small-scale scalar turbulence. These and other features of *passive scalars* in turbulence are reviewed in Warhaft (2000) to whom we refer for further information on *passive scalar* mixing.

centreline in a heated round jet emanating from a round nozzle. Corrsin & Uberoi report an almost one-sided (negatively skewed) temperature signal on the jet axis, roughly between $x/D = 3$ and 5, whereas the streamwise velocity fluctuations in that region did not show such a strong skewness.

The addition of swirl clearly shows its effect on the skewness factors for $x/D = 4$ and 6, whereas only slight changes occur for the region near the pipe outlet. The radial positions marked with A and B correspond to the traces of the streamwise velocity fluctuations and temperature fluctuations presented in figure 5.7 on page 67. The centreline evolution of S_u and S_v for the non-swirling jet agrees fairly well with results from round jet experiments without co-flow (Xu & Antonia 2002*b* and Mi *et al.* 2001) as well as with co-flow (Pietri *et al.* 2000).

5.3.3. *Flatness factor*

The normalised fourth central moment for both components of the velocity fluctuations as well as the *passive scalar*[32] fluctuations are shown in figures 5.27–5.29. The high excess above the *Gaussian* value in the tail region of the jet especially for the velocity fluctuations in combination with the positive skewness observed at these radial positions indicates that the measurement probe is sensing 'blobs' of 'cold' air for a remarkable fraction of time. Hence the region is highly intermittent. At regions corresponding to high streamwise turbulence intensity values close to the *Gaussian* value of three are observable.

The profiles for the flatness factor of the *passive scalar* magnifies the intermittent signals much stronger than its counterpart for the fluctuating velocity components with values up to 150 ($\approx e^5$). Such high values were for instance observed by Pietri *et al.* (2000) ($F_\vartheta \simeq 200$ for $x/D = 3$), whereas Mi *et al.* (2001)[33] and Xu & Antonia (2002*b*) only observed values up to 6–7.

Comparison of the flatness factor for the streamwise velocity fluctuations across the heated jet reveals that the distribution for the swirling jet, e.g. $x/D = 2$ and 4, resembles that for the non-swirling jet at a later downstream position, e.g. $x/D = 4$ and 6. A similar shift in upstream direction by addition of rotation can be observed for the azimuthal velocity component as well as the temperature, whereas for the latter it is not as clear as for the former. This behaviour is also weakly noticeable in the plots for the skewness factor. Hence, swirl reduces the downstream distance needed to mix the jet with the ambient air.[34] It is furthermore worth mentioning that swirl does not have a significant

[32] Note the different scale for the ordinate for $x/D = 2$ and 4.

[33] There is however an inconsistency between their presented p.d.f.s and the axial evolution of the skewness and flatness factor (shown in their figures 18 and 21), which does however not explain these drastic differences.

[34] A similar shift in upstream direction of the p.d.f.s can also be found by periodic forcing as for instance done by Mastorakos *et al.* (1996) in a free jet emanating from a fully developed turbulent pipe flow.

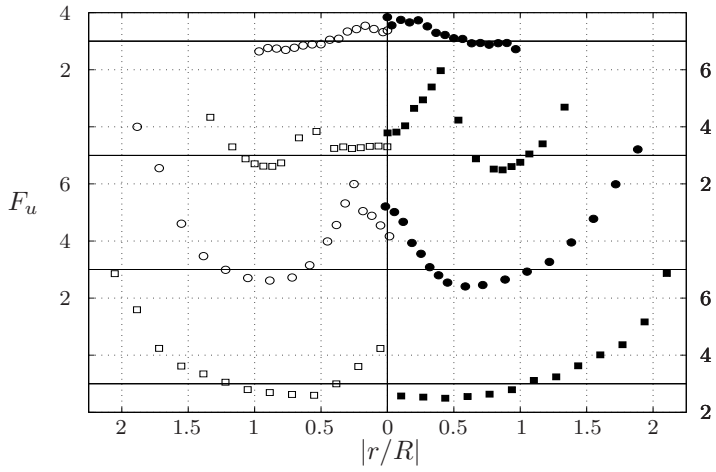

FIGURE 5.27. Flatness factor of the streamwise velocity fluctuations across the heated non-swirled (left side, open symbols) and swirled (right side, filled symbols) jet for four downstream positions: from top to bottom corresponding to $x/D = 0$, 2, 4 and 6.

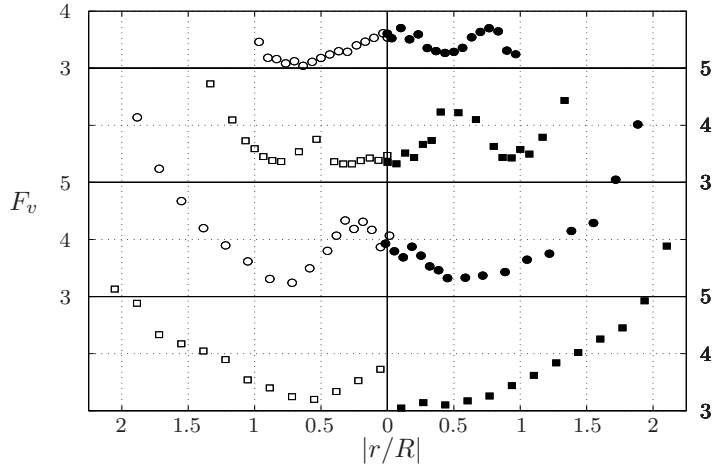

FIGURE 5.28. Flatness factor of the azimuthal velocity fluctuations across the heated non-swirled (left side, open symbols) and swirled (right side, filled symbols) jet for four downstream positions: from top to bottom corresponding to $x/D = 0$, 2, 4 and 6.

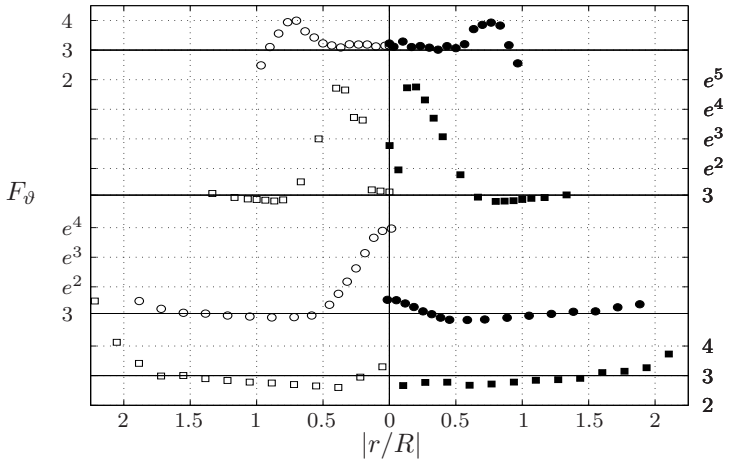

FIGURE 5.29. Flatness factor of the temperature fluctuations across the heated non-swirled (left side, open symbols) and swirled (right side, filled symbols) jet for four downstream positions: from top to bottom corresponding to $x/D = 0$, 2, 4 and 6.

effect on the mixing within the first two pipe diameters downstream. This was already anticipated through the unchanged turbulence development around the centreline in this downstream region through figures 5.12–5.14 on pages 72 and 73.[35]

5.4. Integral time scales

The higher statistical moments, presented and discussed in the previous section, gave an insight into the flow structures of the jet. Another way of looking into the structure is to compute the integral time and length scales of the turbulent flow. In the present study a single probe was used, hence only the time-correlations could be obtained.

The autocorrelation coefficient of a time signal for instance the fluctuating streanwise velocity fluctuation $u(\tau;\mathbf{x})$ at a given position, $\mathbf{x}$, is defined as

$$R_{uu}(\tau;\mathbf{x}) = \frac{\overline{u(t;\mathbf{x})\,u(t+\tau;\mathbf{x})}}{\overline{u(t;\mathbf{x})^2}}\,, \tag{5.6}$$

where the numerator is the autocorrelation function and τ denotes the time

[35] A similar conclusion was reasoned by McIlwain (2000) from particle pathlines obtained from *large eddy simulations* of a swirling round jet, which did not show a significant influence on mixing within $0 < x/D < 2.5$.

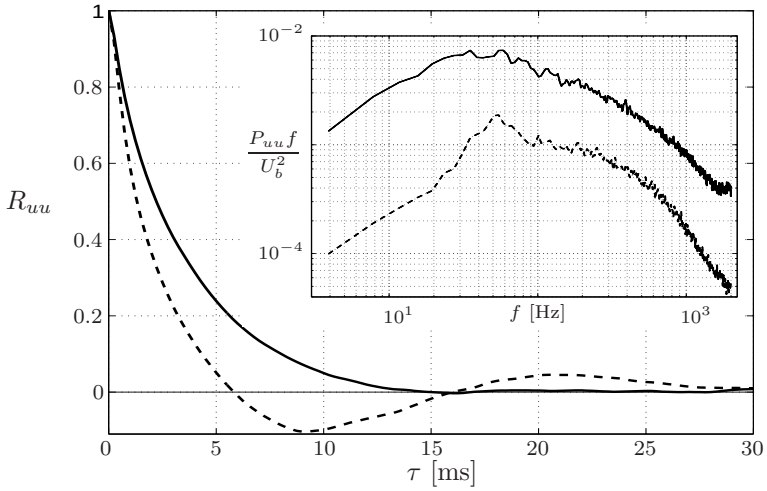

FIGURE 5.30. Autocorrelation coefficient of the streamwise velocity fluctuations at the jet centreline for the non-swirled (dashed line) and swirled jet (solid line) as well as its corresponding power spectral density for $x/D = 4$.

difference between the two times where the product of the random variables is evaluated. Hence R_{uu}, which is an even function and has the properties of $R_{uu}(0;\mathbf{x}) = 1$ and $|R_{uu}| < 1$, gives information about the time over which the signal is correlated with itself.

As an example the autocorrelation coefficient of the streamwise velocity fluctuations at the centreline for the non-swirling and swirling jet at $x/D = 4$ are plotted in figure 5.30. There is quite a large difference in both the qualitative and quantitative behaviour of the autocorrelation for these two cases. For the non-swirling case the correlation drops rapidly to zero and then reaches a negative minimum after which it becomes positive again. The swirling jet on the other hand approaches zero more slowly and does not show a significant minimum. The time for which the autocorrelation reaches zero is related to the size of the energetic eddy scales in the flow which shows that the turbulence scales in the swirling jet are larger than in the non-swirling jet. The distinct negative minimum and a second positive maximum for the non-swirling case may correspond to a periodic flow structure, which is completely absent for the swirling case. The time delay corresponding to the minum (≈ 9 ms) can be converted to a length scale by multiplying it with the local centreline velocity which gives approximately 68 mm, i.e. a length of the order of the jet

diameter. These differences indicate that the flow structures are significantly different for the two cases.

If we further take the *Fourier* transform of the autocorrelation functions given in figure 5.30 the *power spectral density* (PSD or spectrum) for the streamwise velocity fluctuations can be obtained. The estimate for the power spectral density functions shown in the same figure were smoothed by averaging overlapped spectra for discrete blocks (*Welch*'s method). [36] The so obtained spectra are multiplied with the frequency, f, so that the area under each spectrum corresponds to the energy content of the fluctuating signal, i.e. the square of the root mean square value of the fluctuating component. In accordance with figure 5.8 the energy content of the swirling jet is drastically higher (15 % instead of 6.3 % for the streamwise turbulence intensity) and instead of a distinct peak as in the case of the non-swirling jet a broader peak, shifted towards lower frequencies and hence larger scales, can be observed.

By integrating the autocorrelation coefficient over the time delay a integral time scale of the streamwise velocity fluctuations can be defined as

$$\mathcal{T}_u = \int_0^{t_0} R_{uu}(\tau;\mathbf{x})\, d\tau \,. \tag{5.7}$$

There are different integration upper limits, t_0, for the determination of integral scales (see e.g. O'Neill *et al.* 2004, for a comparison between the different integration domains), however here the first zero-crossing of $R_{uu}(\tau;\mathbf{x})$ was selected due to its well-defined nature. Application of equation (5.7) to the autocorrelation coefficients shown in figure 5.30 computes a integral time scale of 1.8 and 3.7 ms for the non-swirling and swirling jet, respectively. If one furthermore assumes the applicability of the usual form of *Taylor's*[37] *hypothesis*,

$$\frac{\partial}{\partial t} = U_c \frac{\partial}{\partial x} \,, \tag{5.8}$$

the so-called frozen-turbulence approximation, which provides a link between temporal and spatial correlations, the integral time scale can be transformed into an integral length scale, Λ_u, by multiplying it with the local convection velocity, U_c, i.e. the local streamwise velocity component. Although the *Taylor hypothesis* was derived in the limit of low turbulence intensity Mi & Antonia (1994) showed that it could be applied in circular jets in regions near the jet axis. Consequently the integral time scales can be transformed into integral length scales, yielding 13.8 and 28.2 mm for the non-swirling and swirling jet, which is of the order of the pipe radius. Hence a doubling in the time and length

[36] A block size of 1024 was chosen in combination with a '*Hanning* window' to avoid aliasing, whereas 50 % overlap was applied.

[37] Sir Geoffrey Ingram Taylor (1886–1975), British physicist.

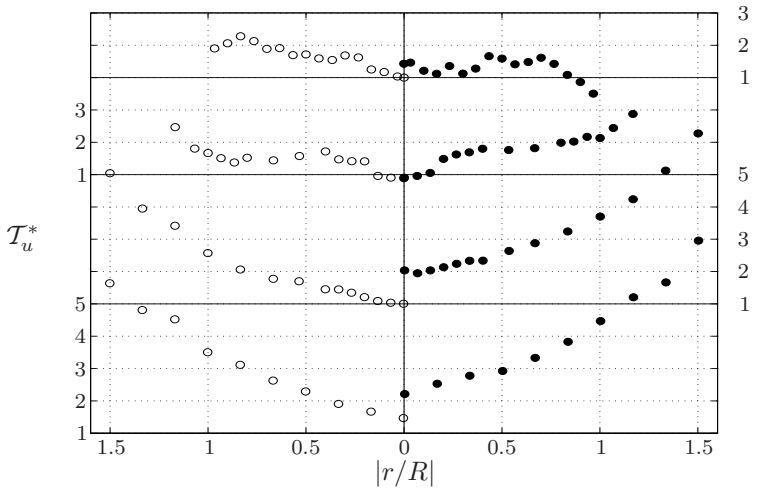

FIGURE 5.31. Integral time scale across the heated non-swirled (left side, open symbols) and swirled jet (right side, filled symbols) for four downstream positions: from top to bottom corresponding to $x/D = 0$, 2, 4 and 6.

scale due to the addition of rotation to the jet indicates a clear alteration in the turbulence structure.

To further investigate the effect of swirl on the integral scales figure 5.31 shows the radial and downstream evolution of the normalised integral time scale, $\mathcal{T}_u^*$. The integral time scale is here normalised by the integral time scale at the centreline of the non-rotating pipe flow. For the non-swirling jet $\mathcal{T}_u^*$ remains nearly unchanged up to $x/D = 4$, whereas the addition of rotation doubles the integral time scale at $x/D = 4$. The expected increase with radial distance from the centreline for free jets can be observed starting from 4 pipe diameters downstream, whereas for the swirling jet, this seems to occur slightly earlier.

Analogous the autocorrelation coefficient and integral time scale for the *passive scalar* can be computed (results are not shown here). As anticipated through the strong correlation between the streamwise velocity and temperature fluctuations the downstream and radial evolution of the integral time scale of the temperature fluctuations is similar to the one in figure 5.31 for the streamwise velocity fluctuations.

If we combine the results from the analysis of the shapes of probability density functions of the temperature fluctuations one could imply that an increase in the integral time (and hence length) scale of the turbulence leads to enhanced mixing in jets within a shorter downstream evolution. Mastorakos

et al. (1996), who decreased the integral time scale of the jet by fitting different perforated plates upstream of the exit of a pipe (such that the measured mean streamwise velocity and turbulence intensity at the exit were unchanged in comparison with the simple pipe flow) found that mixing was delayed and concluded likewise that an increase in the integral length scale of the turbulence causes faster mixing.

CHAPTER 6

Summary

This work focusses on the effect of rotation on the mixing of a *passive scalar* in the near field of a free jet. The jet emanates from a fully developed turbulent pipe flow and is slightly heated above the ambient temperature, making the temperature act as a passive contaminant. The effect of rotation is studied by rotating the pipe axially which gives rise to a swirling jet at the pipe outlet. In both the non-rotating and rotating cases the pipe flow is fully developed.

Several experimental studies concerning the effect of swirl on the mixing characteristics in swirling jets have been reported. A comprehensive and detailed "blueprint" of the near-field of swirling jets has however been hindered due to secondary disturbances and traces induced by swirl generating methods. This also limits the usefulness of previous studies for comparisons with numerical simulations and computations. Here however, due to the generation of a swirling jet by a axially rotating pipe (100 pipe diameters long) flow, the observed alterations in the well-defined dynamically and thermally axisymmetric flow field could solely be ascribed to the effect of swirl. In this sense there are no comparable studies concerning the *passive scalar* mixing.

A considerable part of the experimental work was to design and build a combined measurement probe for velocity and temperature as well as to develop the signal processing techniques to calibrate, analyse and compensate the output signals from the probe. By means of an in-house designed combined X-wire and cold-wire probe the axial and azimuthal velocity components as well as the temperature were acquired simultaneously making it possible to compensate the hot-wire signals against variations in the temperature. This made it possible to simultaneously access instantaneous velocity and temperature signals. Also the validity of the velocity measurements in the outer parts of the jet where the velocities are small was analysed.

Extensive measurements across the jet from the pipe outlet to 6 pipe diameters downstream for all combinations of unheated, heated, non-swirled and swirled jets at a *Reynolds* number of 24000 were performed, thus providing a large amount of data to study the effect of rotation on the dynamic and thermal flow field, the turbulence (joint) statistics, the turbulence structure as well as the mixing of a *passive scalar* in the near-field of the jet.

The results for the dynamic (velocity) field are in very good agreement with the LDV measurements by Facciolo (2006) conducted in the same facility under the same conditions and extend them towards the thermal field. The addition of a moderate degree of swirl (angular velocity of the pipe wall half as high as the bulk velocity in the pipe, which is well below the occurrence of vortex breakdown) highly modifies the dynamic and thermal flow field of the jet in its near-field region to that effect that the swirling jet in comparison to its non-swirling counterpart spreads and mixes faster as well as increases momentum and heat transfer rates.

An interesting observation was that the centreline mean temperature at the pipe outlet was increased for the rotating pipe in comparison to the non-rotating pipe flow. This could be explained by utilising *Reynolds analogy*, linking the decrease in the skin friction and hence convective heat transfer towards the wall to a increase in the axial flux of heat, demonstrating the validity of *Reynolds analogy* also for this case.

Whereas no significant change in the turbulence structure is detectable within the first two pipe diameters, a considerable change around four pipe diameters downstream is found, which shortens the downstream distance and hence time needed to mix the jet with the ambient air. Connected to this the integral time and hence length scale of the turbulence is found to increase with the addition of swirl indicating that an increase of the integral scale is related to faster mixing.

Acknowledgements

This work is sponsored by the *Swedish Energy Agency* (STEM), within its energy related fluid dynamics program, which is gratefully acknowledged. It has been carried out within the research environment that recently has formed the *Linné Flow Centre*.

First of all I wish to thank my supervisor Prof. Henrik Alfredsson for accepting me as his graduate student, for guiding me into the field of experimental fluid dynamics and to share his physical understanding of fluids in general.

I am thankful for having Dr. Nils Tillmark as my second supervisor for bringing order in my hectic being and for helping me with all non-technical and technical issues during my first 2 years in the lab. Thanks to Prof. Alessandro Talamelli for showing great interest in my work, spending nights with me in the basement to solve hot-wire and *LabView* related problems and also for the delicious tiramisùs you provided at Henriks' place and in the lab.

Professors Bengt Sundén and Laszlo Fuchs as well as all the other group participants at the *Lund Institute of Technology* are acknowledged for their collaboration within the main project.

Our toolmakers, Marcus Gällstedt and Ulf Landén, deserve a special thank for being there, whenever I had problems.

To my former room mates Dr. Davide M. and Dr. Luca F.: Thank you for cheering me up whenever I fell into despair and for making our office more then just a second home. Special thanks to my new office mate Michael T. for your endless will to correct my English and for making our office an oasis of fun and productivity.

Thank you Veronica E. not only for your endless desire to teach me Swedish. Special thanks to Allan C., Gabriele B., Dr. Fredrik L. and Dr. Jens F. and all the other employees at *KTH Mechanics*.

I thank my family for supporting me over the years and letting me always know that they are satisfied with me. Last but not least I express my gratefulness for having the most understanding wife, who since the last ten years had to share me with my studies. Thank you Wera!

APPENDIX A

Reynolds stress transport equations

The transport equations for the *Reynolds* stresses in cylindrical polar coordinates are derived from the *Navier-Stokes* equations, equations (2.4)–(2.6), in the usual way (see e.g. Libby 1996, chap. 4). For turbulence at high *Reynolds* numbers away from surfaces viscous diffusion or dissipation is negligible and the transport equations for the *Reynolds* stresses under steady state and axisymmetric mean flow conditions are found to (see e.g. Traugott 1958 or chapter 5 of Piquet 2001): [1]

$$\begin{aligned} W\frac{\partial\overline{ww}}{\partial r} + U\frac{\partial\overline{ww}}{\partial x} = &-\frac{2}{\rho}\overline{w\frac{\partial p}{\partial r}} \\ &- 2\overline{ww}\frac{\partial W}{\partial r} - 2\overline{uw}\frac{\partial W}{\partial x} + \frac{4}{r}V\overline{vw} \\ &- \frac{1}{r}\frac{\partial r\overline{www}}{\partial r} - \frac{\partial\overline{uww}}{\partial x} + \frac{2}{r}\overline{vvw} \end{aligned} \tag{A.1}$$

$$\begin{aligned} W\frac{\partial\overline{vv}}{\partial r} + U\frac{\partial\overline{vv}}{\partial x} = &\\ &- 2\overline{vw}\frac{1}{r}\frac{\partial rV}{\partial r} - 2\overline{uv}\frac{\partial V}{\partial x} - \frac{2}{r}W\overline{vv} \\ &- \frac{1}{r}\frac{\partial r\overline{vvw}}{\partial r} - \frac{\partial\overline{vvw}}{\partial x} - \frac{2}{r}\overline{vvw} \end{aligned} \tag{A.2}$$

[1] It should be noted that the terms containing the extra strain V/r are not true production terms, but rather represent the effect of rotation on the coordinate axis (see e.g. Nayeri 2000).

$$
\begin{aligned}
W\frac{\partial\overline{uu}}{\partial r} + U\frac{\partial\overline{uu}}{\partial x} = &-\frac{2}{\rho}\overline{u\frac{\partial p}{\partial x}} \\
&- 2\overline{uu}\frac{\partial U}{\partial x} - 2\overline{uw}\frac{\partial U}{\partial r} \\
&- \frac{1}{r}\frac{\partial r\overline{uuw}}{\partial r} - \frac{\partial\overline{uuu}}{\partial x}
\end{aligned}
\tag{A.3}
$$

$$
\begin{aligned}
W\frac{\partial\overline{uw}}{\partial r} + U\frac{\partial\overline{uw}}{\partial x} = &-\frac{1}{\rho}\overline{w\frac{\partial p}{\partial x}} - \frac{1}{\rho}\overline{u\frac{\partial p}{\partial r}} = \\
&- \overline{uu}\frac{\partial W}{\partial x} - \overline{ww}\frac{\partial U}{\partial r} + \overline{uw}\frac{W}{r} + \frac{2}{r}V\overline{uv} \\
&- \frac{1}{r}\frac{\partial r\overline{uww}}{\partial r} - \frac{\partial\overline{uuw}}{\partial x} + \frac{1}{r}\overline{uvv}
\end{aligned}
\tag{A.4}
$$

$$
\begin{aligned}
W\frac{\partial\overline{uv}}{\partial r} + U\frac{\partial\overline{uv}}{\partial x} = &-\frac{1}{\rho}\overline{v\frac{\partial p}{\partial x}} \\
&- \overline{uw}\frac{1}{r}\frac{\partial rV}{\partial r} - \overline{uu}\frac{\partial V}{\partial x} - \overline{vw}\frac{\partial U}{\partial r} + \overline{uv}\frac{\partial W}{\partial r} \\
&- \frac{1}{r^2}\frac{\partial r^2\overline{uvw}}{\partial r} - \frac{\partial\overline{uuv}}{\partial x}
\end{aligned}
\tag{A.5}
$$

$$
\begin{aligned}
W\frac{\partial\overline{vw}}{\partial r} + U\frac{\partial\overline{vw}}{\partial x} = &-\frac{1}{\rho}\overline{v\frac{\partial p}{\partial r}} \\
&- \overline{ww}\frac{1}{r}\frac{\partial rV}{\partial r} - \overline{uv}\frac{\partial W}{\partial x} - \overline{uw}\frac{\partial V}{\partial x} + \overline{vw}\frac{\partial U}{\partial x} + \frac{2}{r}V\overline{vv} = \\
&- \frac{1}{r^2}\frac{\partial r^2\overline{vww}}{\partial r} - \frac{\partial\overline{uvw}}{\partial x} + \frac{1}{r}\overline{vvv}
\end{aligned}
\tag{A.6}
$$

APPENDIX B

Reynolds flux transport equations

The transport equations for the *Reynolds* fluxes in cylindrical polar coordinates are derived from the *Navier-Stokes* equations, equations (2.4)–(2.6) and the advection-diffusion equation for the *passive scalar*, equation (2.15), analogous to the transport equations for the *Reynolds* stresses. For turbulence at high *Reynolds* numbers and hence high *Peclet* numbers away from surfaces viscous and thermal diffusion dissipation is negligible and the transport equations for the *Reynolds* fluxes under steady state and axisymmetric mean flow conditions are found to:

$$\begin{aligned} W\frac{\partial\overline{\vartheta\vartheta}}{\partial r} + U\frac{\partial\overline{\vartheta\vartheta}}{\partial x} = & \\ & - 2\overline{w\vartheta}\frac{\partial\theta}{\partial r} - 2\overline{u\vartheta}\frac{\partial\theta}{\partial x} \\ & - \frac{1}{r}\frac{\partial r\overline{w\vartheta\vartheta}}{\partial r} - \frac{\partial\overline{u\vartheta\vartheta}}{\partial x} \end{aligned} \tag{B.1}$$

$$\begin{aligned} W\frac{\partial\overline{w\vartheta}}{\partial r} + U\frac{\partial\overline{w\vartheta}}{\partial x} = & -\frac{1}{\rho}\vartheta\overline{\frac{\partial p}{\partial r}} \\ & - \overline{ww}\frac{\partial\theta}{\partial r} - \overline{uw}\frac{\partial\theta}{\partial x} - \overline{w\vartheta}\frac{\partial W}{\partial r} - \overline{u\vartheta}\frac{\partial W}{\partial x} \\ & - \frac{1}{r}\frac{\partial r\overline{ww\vartheta}}{\partial r} - \frac{\partial\overline{uw\vartheta}}{\partial x} + \frac{1}{r}\left(2V\overline{v\vartheta} + \overline{vv\vartheta}\right) \end{aligned} \tag{B.2}$$

$$\begin{aligned}\frac{1}{r}W\frac{\partial r\overline{v\vartheta}}{\partial r}+U\frac{\partial\overline{v\vartheta}}{\partial x}=&\\ -\overline{w\vartheta}\left(\frac{\partial\theta}{\partial r}+\frac{1}{r}\frac{\partial rV}{\partial r}\right)-\overline{uv}\frac{\partial\theta}{\partial x}-\overline{u\vartheta}\frac{\partial V}{\partial x}&\\ -\frac{1}{r^2}\frac{\partial r^2\overline{vw\vartheta}}{\partial r}-\frac{\partial\overline{uv\vartheta}}{\partial x}&\end{aligned}\tag{B.3}$$

$$\begin{aligned}W\frac{\partial\overline{u\vartheta}}{\partial r}+U\frac{\partial\overline{u\vartheta}}{\partial x}=-\frac{1}{\rho}\overline{\vartheta\frac{\partial p}{\partial x}}&\\ -\overline{uu}\frac{\partial\theta}{\partial x}-\overline{u\vartheta}\frac{\partial U}{\partial x}-\overline{uw}\frac{\partial\theta}{\partial r}-\overline{w\vartheta}\frac{\partial U}{\partial r}=&\\ -\frac{1}{r}\frac{\partial r\overline{uw\vartheta}}{\partial r}-\frac{\partial\overline{uu\vartheta}}{\partial x}&\end{aligned}\tag{B.4}$$

References

Abramovich, G. N. 1963 *The theory of turbulent jets*. MIT Press, Cambridge, Massachusetts, USA.

Alfredsson, P. H. & Tillmark, N. 2005 A beginners guide to fluid mechanics measurements. Book manuscript.

Antonia, R. A. & Mi, J. 1993 Temperature dissipation in a turbulent round jet. *J. Fluid Mech.* **250**, 531–551.

Antonia, R. A. & Zhao, Q. 2001 Effect of initial conditions on a circular jet. *Exp. Fluids* **31**, 319–323.

Bilen, K., Bakirci, K., Yapici, S. & Yavuz, T. 2002 Heat transfer from a plate impinging swirl jet. *Int. J. Energy Res.* **26**, 305–320.

Billant, P., Chomaz, J. M. & Huerre, P. 1998 Experimental study of vortex breakdown in swirling jets. *J. Fluid Mech.* **376**, 183–219.

Boguslawski, L. & Popiel, C. O. 1979 Flow structure of the free round turbulent jet in the initial region. *J. Fluid Mech.* **90**, 531–539.

Bourke, P. J. & Pulling, D. J. 1970 A turbulent heat flux meter and some measurements of turbulence in air flow through a heated pipe. *Int. J. Heat Mass Transfer* **13**, 1331–1338.

Bradbury, L. J. S. & Castro, I. P. 1971 A pulsed wire technique for velocity measurements in highly turbulent flows. *J. Fluid Mech.* **49**, 657–691.

Bradbury, L. J. S. & Castro, I. P. 1972 Some comments on heat-transfer laws for fine wires. *J. Fluid Mech.* **51**, 487–495.

Bradshaw, P., Launder, B. E. & Lumley, J. L. 1996 Collaborative testing of turbulence models. *J. Fluid Eng-T ASME* **118**, 243–247.

Bremhorst, K. & Bullock, K. J. 1970 Spectral measurements of temperature and longitudinal velocity fluctuations in fully developed pipe flow. *Int. J. Heat Mass Transfer* **13**, 1313–1329.

Bruun, H. H. 1995 *Hot-wire anemometry: Principles and signal analysis*. Oxford University Press Inc., New York, USA.

Burattini, P., Antonia, R. A., Rajagopalan, S. & Stephens, M. 2004 Effect of initial conditions on the near-field development of a round jet. *Exp. Fluids* **37**, 56–64.

Burattini, P. & Djenidi, L. 2004 Velocity and passive scalar characteristics in a round jet with grids at the nozzle exit. *Flow Turbul. Combust.* **72**, 199–218.

Buresti, G., Talamelli, A. & Petagna, P. 1994 Experimental characterization of the velocity field of a coaxial jet configuration. *Exp. Thermal Fluid Sci.* **9**, 135–146.

Cheesewright, R. 1972 The application of digital techniques to hot-wire anemometry in highly turbulent flows. In *Proc. DISA Conf. on Fluid Dyn. Meas. in the Indust. and Medical Env.*, pp. 145–151. Leicester University: University Press.

Chevray, R. & Tutu, N. K. 1972 Simultaneous measurements of temperature and velocity in heated flows. *Rev. Sci. Instrum.* **43**, 1417–1421.

Chevray, R. & Tutu, N. K. 1977 Conditional measurements in a heated turbulent jet. In *Structure and mechanisms of turbulence II* (ed. H. Fiedler), *Lecture Notes in Physics*, vol. 76, pp. 73–84. Springer-Verlag, Berlin, Germany.

Chew, Y. T., Khoo, B. C. & Li, G. L. 1998 An investigation of wall effects on hot-wire measurements using a bent sublayer probe. *Meas. Sci. Technol.* **9**, 67–85.

Chigier, N. A. & Beér, J. M. 1964 Velocity and static pressure distributions in swirling air jets issuing from annular and divergent nozzles. *J. Basic Eng.* **86**, 788–798.

Chigier, N. A. & Chervinsky, A. 1967 Experimental investigation of swirling vortex motion in jets. *J. Appl. Mech.* **34**, 443–451.

Collis, D. & Williams, M. 1959 Two-dimensional convection from heated wires at low Reynolds numbers. *J. Fluid Mech.* **6**, 357–389.

Comte-Bellot, G. 1976 Hot-wire anemometry. *Annu. Rev. Fluid Mech.* **8**, 209–231.

Corrsin, S. 1943 Investigation of flow in an axially symmetrical heated jet of air. *Tech. Rep.*. NACA, Wartime Rep. W-94.

Corrsin, S. & Uberoi, M. S. 1950 Further experiments on the flow and heat transfer in a heated turbulent air jet. *Tech. Rep.*. NACA, TN 998.

Craya, A. & Darrigol, M. 1967 Turbulent swirling jet. *Phys. Fluids* **34**, S197–S199.

Danaila, L., Le Gal, P., Anselmet, F., Plaza, F. & Pinton, J. F. 1999 Some new features of the passive scalar mixing in a turbulent flow. *Phys. Fluids* **11**, 636–646.

Davidson, P. A. 2004 *Turbulence. An introduction for scientists and engineers*. Oxford University Press, Oxford, UK.

van Dijk, A. 1999 Aliasing in one-point turbulence measurements - Theory, DNS and hotwire experiments. PhD thesis, Delft University of Technology, The Netherlands.

van Dijk, A. & Nieuwstadt, F. T. M. 2004*a* The calibration of (multi-) hot-wire probes. 1. Temperature calibration. *Exp. Fluids* **36**, 540–549.

van Dijk, A. & Nieuwstadt, F. T. M. 2004*b* The calibration of (multi-) hot-wire probes. 2. Velocity-calibration. *Exp. Fluids* **36**, 550–564.

Drobniak, S., Elsner, J. W. & El-Kassem, E.-S. A. 1998 The relation between coherent structures and heat transfer processes in the initial region of a round jet. *Exp. Fluids* **24**, 225–237.

Durst, F., Zanaoun, E.-S. & Pashtrapanska, M. 2001 In situ calibration of hot-wires close to highly heat-conducting walls. *Exp. Fluids* **31**, 103–110.

Eggels, J. G. M. 1994 Direct and large eddy simulation of turbulent flow in a cylindrical pipe geometry. PhD thesis, Delft University of Technology, The Netherlands.

Eisner, T. & Aneshansley, D. J. 1999 Spray aiming in the bombadier beetle: photographic evidence. *Proc. Natl. Acad. Sci. USA* **96**, 9705–9709.

Elsner, J. W. & Kurzak, L. 1987 Characteristics of turbulent flow in slightly heated free swirling jets. *J. Fluid Mech.* **180**, 147–160.

Elsner, J. W. & Kurzak, L. 1989 Semi-preserving development of a slightly heated free swirling jet. *J. Fluid Mech.* **199**, 237–255.

Facciolo, L. 2006 A study on axially rotating pipe and swirling jet flows. PhD thesis, KTH Mechanics, Stockholm, Sweden, TRITA-MEK Tech. Rep. 2006:02.

Facciolo, L. & Alfredsson, P. H. 2004 The counter-rotating core of a swirling turbulent jet issuing from a rotating pipe flow. *Phys. Fluids* **16**, L71–L73.

Facciolo, L., Orlandi, P. & Alfredsson, P. H. 2005 Swirling jet issued form fully developed rotating pipe flow - experiments and numerics. In *Proc. 4th Int. Symp. Turbulence Shear Flow Phenomena*, pp. 1243–1248.

Farokhi, S. & Taghavi, R. 1990 Modern developments in shear flow control with swirl. *Tech. Rep.*. Kansas Univ. Center for Research, USA, KU-FRL-724-4.

Farokhi, S., Taghavi, R. & Rice, E. J. 1989 Effect of initial swirl distribution on the evolution of a turbulent jet. *AIAA J.* **27**, 700–706.

Feyedelem, M. S. & Sarpkaya, T. 1998 Free- and near-free-surface swirling turbulent jets. *AIAA J.* **36**, 359–364.

Fiedler, H. E. 1997 A note on secondary flow in bends and bend combinations. *Exp. Fluids* **23**, 262–264.

Fingerson, L. M. & Freymuth, P. 1996 Thermal anemometers. In *Fluid mechanics measurements*, 2nd edn. (ed. R. J. Goldstein), chap. 3, pp. 115–173. Taylor & Francis, Washington, DC, USA.

Fujii, S., Eguchi, K. & Gomi, M. 1981 Swirling jets with and without combustion. *AIAA J.* **19**, 1438–1442.

Gallaire, F. & Chomaz, J.-M. 2003 Mode selection in swirling jet experiments: A linear stability analysis. *J. Fluid Mech.* **494**, 223–253.

George, W. K. 1990 Governing equations, experiments, and the experimentalist. *Expl. Thermal Fluid Sci.* **3**, 557–566.

Gibson, M. M. & Younis, B. A. 1986 Calculation of swirling jets with a Reynolds stress closure. *Phys. Fluids* **29**, 38–48.

Gilchrist, R. T. & Naughton, J. W. 2005 An experimental study of incompressible jets with different initial swirl profiles: Mean results. *AIAA J.* **43**, 741–751.

Gómez, J.-L., Marscher, A. P., Alberdi, A., Jorstad, S. G. & García-Miró, C. 2000 Flashing superluminal components in the jet of the radio galaxy 3c120. *Science* **289**, 2317–2320.

Gore, R. W. & Ranz, W. E. 1964 Back flows in rotating fluids moving axially through expanding cross sections. *AIChE J.* **10**, 83–88.

Grandmaison, E. W. & Becker, H. A. 1982 Turbulent mixing in free swirling jets. *Can. J. Chem. Eng.* **60**, 76–82.

Gupta, A. K., Lilley, D. G. & Syred, N. 1985 *Swirl flows*. ABACUS Press, Cambridge, USA.

Hinze, J. O. 1975 *Turbulence*, 2nd edn. McGraw-Hill, New York, USA.

Hishida, M. & Nagano, Y. 1978 Simultaneous measurements of velocity and temperature in nonisothermal flows. *J. Heat Transfer* **100**, 340–345.

Hussein, H. J., Capp, S. P. & George, W. K. 1994 Velocity measurements in a high-Reynolds-number, momentum-conserving, axisymmetric, turbulent jet. *J. Fluid Mech.* **258**, 31–75.

Imao, S., Itoh, M. & Harada, T. 1996 Turbulent characteristics of the flow in an axially rotating pipe. *Int. J. Heat Fluid Flow* **17**, 444–451.

Kennedy, D. A. & Corrsin, S. 1961 Spectral flatness factor and 'intermittency' in turbulence and in non-linear noise. *J. Fluid Mech.* **10**, 366–370.

Kerr, N. M. & Fraser, D. 1965 Swirl. Part 1: Effect on axisymmetrical turbulent jets. *J. Inst. Fuel* **38**, 519–526.

Kikuyama, K., Murakami, M., Nishibori, K. & Maeda, K. 1983 Flow in an axially rotating pipe. *Bull. JSME* **26**, 506–513.

King, L. 1914 On the convection of heat from small cylinders in a stream of fluid: Determination of the convection constants of small platinum wires with applications to hot-wire anemometry. *Phil. Trans. Roy. Soc.* **214A**, 373–432.

Klebanoff, P. S. 1954 Characteristics of turbulence in a boundary layer with zero pressure gradient. *Tech. Rep.*. NACA, rep. 1247.

Komori, S. & Ueda, H. 1985 Turbulent flow structure in the near field of a swirling round free jet. *Phys. Fluids* **28**, 2075–2082.

Launder, B. E. & Morse, A. P. 1979 Numerical prediction of axisymmetric free shear flows with a Reynolds stress closure. In *Turbulent Shear Flows I* (ed. F. Durst, B. E. Launder, F. W. Schmidt & J. H. Whitelaw), pp. 279–294. Springer-Verlag, Berlin, Germany.

Lekakis, I. 1996 Calibration and signal interpretation for single and multiple hot-wire/hot-film probes. *Meas. Sci. Technol.* **7**, 1313–1333.

Libby, A. P. 1996 *Introduction to turbulence*. Taylor & Francis, Bristol, Pennsylvania, USA.

Lilley, D. G. 1977 Swirl flows in combustion: A review. *AIAA J.* **15**, 1063–1078.

Loiseleux, T. & Chomaz, J.-M. 2003 Breaking of rotational symmetry in a swirling jet experiment. *Phys. Fluids* **15**, 511–523.

Lomas, C. 1986 *Fundamentals of hot-wire anemometry*. Cambridge University Press, Cambridge, UK.

Lubbers, C. L., Brethouwer, G. & Boersma, B. J. 2001 Simulation of the mixing of a passive scalar in a round turbulent jet. *Fluid Dynam. Res.* **28**, 189–208.

Lucca-Negro, O. & O'Doherty, T. 2001 Vortex breakdown: A review. *Prog. Energy Combust. Sci.* **27**, 431–481.

Mastorakos, E., Shibasaki, M. & Hishida, K. 1996 Mixing enhancement in axisymmetric turbulent isothermal and buoyant jets. *Exp. Fluids* **20**, 279–290.

McIlwain, S. 2000 Large eddy simulation of the near field of round and coaxial jets with mild swirl. PhD thesis, Queen's University, Kingston, Ontario, Canada.

McIntosh, A. C. & Forman, M. 2004 The efficiency of the explosive discharge of the bombadier beetle, with possible biomimetic applications. In *19th Int. Colloquium on the Dynamics of Explosions and Reactive Systems* (ed. M. W. Collins & C. A. Brebbia), *Design & Nature*, vol. 6, pp. 227–236. WIT Press.

Mehta, R. D. 1991 Swirling mixing layer. ERCOFTAC database, http://www.cfd.me.umist.ac.uk/ercofold/database/test59/test59.html.

Mehta, R. D., Wood, D. H. & Clausen, P. D. 1991 Some effects of swirl on turbulent mixing layer development. *Phys. Fluids* **3**, 2716–2724.

Mi, J. & Antonia, R. A. 1994 Correction to taylor's hypothesis in a turbulent circulat jet. *Phys. Fluids* **6**, 1548–1552.

Mi, J., Nobes, D. S. & Nathan, G. J. 2001 Influence of jet exit conditions on the passive scalar field of an axisymmetric free jet. *J. Fluid Mech.* **432**, 91–125.

Moro, J. P., Vukoslavčević, P. V. & Blet, V. 2003 A method to calibrate a hot-wire X-probe for applications in low-speed, variable-temperature flow. *Meas. Sci. Technol.* **14**, 1054–1062.

Morse, A. P. 1980 Single-stream swirling jet in still air. ERCOFTAC database, http://www.cfd.me.umist.ac.uk/ercofold/database/test26/test26.html.

Naughton, J. W., Cattafesta, L. N. & Settles, G. S. 1997 An experimental study of compressible turbulent mixing enhancement in swirling jets. *J. Fluid Mech.* **330**, 271–305.

Nayeri, C. 2000 Investigation of the three-dimensional shear layer between confined coaxial jets with swirl. PhD thesis, Technical University of Berlin, Germany.

Oberbeck, A. 1895 Über die abkühlende Wirkung von Luftströmen. *Ann. Phys. Chem.* **56**, 397–411.

Oberlack, M. 1999 Similarity in non-rotating and rotating turbulent pipe flows. *J. Fluid Mech.* **379**, 1–22.

Ogawa, A. & Hatakeyama, H. 1979 Fluiddynamical characteristics of turbulent straight and rotational jets (1st report). *J. Coll. Engng. Nihon Univ.* **A-20**, 133–144.

Ogawa, A., Hatakeyama, H. & Fujita, Y. 1981 Fluiddynamical characteristics of turbulent straight and rotational jets (2nd report). *J. Coll. Engng. Nihon Univ.* **A-22**, 157–170.

Ogawa, A., Hatakeyama, H. & Fujita, Y. 1982 Fluiddynamical characteristics of turbulent straight and rotational jets (3rd report). *J. Coll. Engng. Nihon Univ.* **A-23**, 89–102.

Oljaca, M., Gu, X., Glezer, A., Baffico, M. & Lund, F. 1998 Ultrasound scattering by a swirling jet. *Phys. Fluids* **10**, 886–898.

O'Neill, P. L., Nicolaides, D., Honnery, D. & Soria, J. 2004 Autocorrelation functions and the determination of integral length with reference to experimental and numerical data. In *15th Australasian Fluid Mechanics Conference*. The University of Sydney, Sydney, Australia.

Orlandi, P. & Fatica, M. 1997 Direct simulations of turbulent flow in a pipe rotating about its axis. *J. Fluid Mech.* **343**, 43–72.

Österlund, J. M. 1999 Experimental study of zero pressure-gradient turbulent boundary layer flow. PhD thesis, KTH Mechanics, Stockholm, Sweden, TRITA-MEK Tech. Rep. 1999:16.

Ovink, R., Lamers, A. P. G. G., Steenhoven, A. A. & Hoeijmakers, H. W. M. 2001 A method of correction for the binormal velocity fluctuation using the look-up inversion method for hot-wire anemometry. *Meas. Sci. Technol.* **12**, 1208–1213.

Paranthoën, P., Petit, C. & Lecordier, J. C. 1982 The effect of the thermal prong wire interaction on the response of a cold wire in gaseous flows (air, argon, helium). *J. Fluid Mech.* **124**, 457–473.

Park, S. H. & Shin, H. D. 1993 Measurements of entrainment characteristics of swirling jets. *Int. J. Heat Mass Transfer* **36**, 4009–4020.

Perry, A. 1982 *Hot-wire anemometry*. Clarendon Press, Oxford, UK.

Pietri, L., Amielh, M. & Anselmet, F. 2000 Simultaneous measurements of temperature and velocity fluctuations in a slightly heated jet combining a cold wire and laser doppler anemometry. *Int. J. Heat Fluid Flow* **21**, 22–36.

Piquet, J. 2001 *Turbulent flows: Models and physics*, revised 2 edn. Springer-Verlag, Berlin Heidelberg, Germany.

Pitts, W. M. 1991 Reynolds number effects on the mixing behaviour of axisymmetric turbulent jets. *Exp. Fluids* **11**, 135–141.

Pope, S. B. 2000 *Turbulent flows*. Cambridge University Press, Cambridge, UK.

Pratte, B. & Keffer, J. F. 1972 The swirling turbulent jet. *J. Basic Eng.* **94**, 739–747.

Rahai, H. R. & Wong, T. W. 2002 Velocity field characteristics of turbulent jets from round tubes with coil inserts. *Appl. Thermal Eng.* **22**, 1037–1045.

Rajaratnam, N. 1976 *Turbulent jets*. Elsevier, Amsterdam, The Netherlands.

Reynolds, A. 1961 On the dynamics of turbulent vortical flow. *Z. Angew. Math. Phys.* **12**, 149–158.

Richards, C. D. & Pitts, W. M. 1993 Global density effects on the self-preservation behaviour of turbulent free jets. *J. Fluid Mech.* **245**, 415–435.

Ricou, F. P. & Spalding, D. B. 1961 Measurements of entrainment by axisymmetrical turbulent jets. *J. Fluid Mech.* **11**, 21–32.

Rose, W. G. 1962 A swirling round turbulent jet; 1 - Mean-flow measurements. *J. Appl. Mech.* **29**, 615–625.

Samet, M. & Einav, S. 1988 Mean value measurements of a turbulent swirling-jet. *AIAA J.* **26**, 619–620.

Sandborn, V. A. 1976 Effects of velocity gradients on measurements of turbulent shear stress. *AIAA J.* **14**, 400–402.

Satake, S. & Kunugi, T. 2002 Direct numerical simulation of turbulent heat transfer in an axially rotating pipe flow. Reynolds shear stress and scalar flux budgets. *Int. J. Num. Methods Heat Fluid Flow* **12**, 958–1008.

Schefer, R. W. & Kerstein, A. R. 1994 Role of large-scale structure in a nonreacting turbulent CH_4 jet. *Phys. Fluids* **6**, 652–661.

Schetz, J. A. 1980 *Injection and mixing in turbulent flow*. AIAA, New York, USA.

Schlichting, H. 1979 *Boundary-layer theory*, 7th edn. McGraw-Hill, New York, USA.

Sislian, J. P. & Cusworth, R. A. 1986 Measurements of mean velocity and turbulent intensities in a free isothermal swirling jet. *AIAA J.* **24**, 303–309.

Sreenivas, K. R. & Prasad, A. K. 2000 Vortex-dynamics model for entrainment in jets and plumes. *Phys. Fluids* **12**, 2101–2107.

Staicu, A. D. 2002 Intermittency in turbulence. PhD thesis, Eindhoven University of Technology, The Netherlands.

Syred, N. 2006 A review of oscillation mechanism and the role of the precessing vortex core (PVC) in swirl combustion systems. *Prog. Energy Combust. Sci.* **32**, 93–161.

Syred, N. & Beér, J. M. 1974 Combustion in swirling flows: A review. *Combust. Flame* **23**, 143–201.

Taghavi, R. & Farokhi, S. 1988 Turbulent swirling jets with excitation. *Tech. Rep.*. Kansas Univ. Center for Research, USA, NASA-CR-180895.

Toh, I. K., Honnery, D. & Soria, J. 2005 Velocity and scalar measurements of a low swirl jet. In *Proc. 4th Australian Conf. Laser Diagnostics Fluid Mech. Comb.*, pp. 129–132. The University of Adelaide, South Australia, Australia.

Townsend, A. A. 1976 *The structure of turbulent shear flow*, 2nd edn. Cambridge University Press, Cambridge, UK.

Traugott, S. C. 1958 Influence of solid-body rotation on screen-produced turbulence. *Tech. Rep.*. NACA, TN 4135.

Tritton, D. J. 1988 *Physical fluid dynamics*, 2nd edn. Oxford University Press, Oxford, UK.

Tutu, N. K. & Chevray, R. 1975 Cross wire anemometry in high intensity turbulence. *J. Fluid Mech.* **71**, 785–800.

Vukoslavčević, P. V. & Petrovic, D. V. 2000 *Multiple hot-wire probes: Measurements of turbulent velocity & vorticity vector fields*. Coronet Books Inc., Philadelphia, Pennsylvania, USA.

Vukoslavčević, P. V. & Wallace, J. M. 2002 The simultaneous measurement of velocity and temperature in heated turbulent air flow using thermal anemometry. *Meas. Sci. Technol.* **13**, 1615–1624.

Warhaft, Z. 2000 Passive scalars in turbulent flows. *Annu. Rev. Fluid Mech.* **32**, 203–240.

Wikström, P. M. 1998 Measurement, direct numerical simulation and modelling of passive scalar transport in turbulent flows. PhD thesis, KTH Mechanics, Stockholm, Sweden, TRITA-MEK Tech. Rep. 1998:11.

Wooten, D. C., Wooldridge, C. E. & Amaro, A. J. 1972 The structure of jet turbulence producing jet noise. *Tech. Rep.*. Stanford Research Institute, California, USA, SRI Project 8139.

Wygnanski, I. & Fiedler, H. E. 1969 Some measurements in the self-preserving jet. *J. Fluid Mech.* **38**, 577–612.

Xu, G. & Antonia, R. A. 2002*a* Effect of different initial conditions on a turbulent round free jet. *Exp. Fluids* **33**, 677–683.

Xu, G. & Antonia, R. A. 2002*b* Effect of initial conditions on the temperature field of a turbulent round free jet. *Int. Comm. Heat Mass Transfer* **29**, 1057–1068.

Yeh, Y. & Cummins, H. Z. 1964 Localized fluid flow measurements with an He-Ne laser spectrometer. *Appl. Phys. Lett.* **4**, 176–178.

Ziegler, M. 1934 The construction of a hot-wire anemometer with linear scale and negligible lag. *Proc. K. Ned. Acad. Wet.* **15**.